A Cross-Layer Communications Framework for THz Band Plant Monitoring Nanonetworks

Armita Afsharinejad

School of Science and Computing

Waterford Institute of Technology

This dissertation is submitted for the degree of

Doctor of Philosophy

Supervisors: Dr. Alan Davy and Dr. Brendan Jennings

September 2016

Dedication

I dedicate this thesis to my loving family

Declaration

I hereby certify that this material, which I now submit for assessment on the program of study leading to the award of Doctor of Philosophy, is entirely my own work and has not been taken from the work of others save to the extent that such work has been cited and acknowledged within the text of my work.

Student ID 20056265

Signed ....

Acknowledgment

I would like to express my sincere gratitude to my supervisors, Dr. Alan Davy and Dr. Brendan Jennings, for their continues support, patience and motivation towards the completion of this research project and my PhD study.

I would like to particularly thank Dr. Conor Brennan, for his guidance and immense knowledge, and also for providing me an opportunity to join his research team in Dublin City University (DCU). Also I highly appreciate the support from Dr. Tadashi Nakano from the University of Osaka, who invited and hosted me in his team for a short period. In addition, I feel grateful for all the advice and support provided by the other TSSG and Waterford Institute of Technology (WIT) research community and staff members, especially Dr. Willie Donnelly and Dr. Bernard Butler. I also thank and appreciate the help and support of my fellow labmates and friends at TSSG.

My sincere thanks goes to a long list of great people that I got to know through this tough journey among which stand Sven Naumann who encouraged me at various stages of my study, as well as Sabour-Pickett and Bulbulia families for their genuine support and also for treating me like a family member.

Last but not least, I wish to thank my wonderful parents, Mina and Khosrow, and also my dearest siblings, Armin, Azin and Arash, whose endless love and constant support gave me the strength and confidence to continue.

Publications

1. A. Afsharinejad, A. Davy, B. Jennings, and C. Brennan. Performance analysis of plant monitoring nanosensor networks at THz frequencies. *IEEE Internet of Things Journal*, 3(1):59–69, 2016.

2. A. Afsharinejad, A. Davy, and B. Jennings. Dynamic channel allocation in electromagnetic nanonetworks for high resolution monitoring of plants. *Nano Communication Networks*, 7:2–16, 2016.

3. A. Afsharinejad, A. Davy, B. Jennings, S. Rasmann, and C. Brennan. A path-loss model incorporating shadowing for THz band propagation in vegetation. In *IEEE International Conference on Global Communications (Globecom)*, pages 1–6, 2015.

4. A. Afsharinejad, A. Davy, B. Jennings, and C. Brennan. An initial path-loss model within vegetation in the THz band. In *European Conference on Antennas and Propagation (EuCAP)*, pages 1–5, 2015.

5. A. Afsharinejad, A.Davy, B. Jennings, and S. Balasubramaniam. GA-based frequency selection strategies for graphene-based nano-communication networks. In *IEEE International Conference on Communications (ICC)*, pages 3642–3647, 2014.

6. A. Afsharinejad, A.Davy, and B. Jennings. Frequency selection strategies under varying moisture levels in wireless nano-networks. In *ACM International Conference on Nanoscale Computing and Communication (Nanocom)*, pages 1–9, 2014.

7. A. Afsharinejad, A.Davy, and B. Jennings. THz band frequency selection strategies for Electromagnetic nano-devices. In *Irish Royal Academy Communications and Radio Science Research Colloquium*, 2014.

Abstract

For the realization of more efficient environmental monitoring applications, e.g., precision agriculture, the current technologies face many constraints in terms of observation precision and real-time capabilities. Nanotechnology promises new solutions to address such limitations through the fabrication of nano-scale devices which can be interconnected. The tiny size of these devices offers entirely new features that cannot be observed at larger scales, including the fine-grained detection of substances even at the molecular level. According to the existing literature, the predicted communication channel for nano-devices will be in the THz band, which has not been broadly studied yet. However, the limited research work already indicates numerous challenges for THz communications, mainly in terms of signal attenuation. These issues, which will be more prominent in the proximity of vegetation, can drastically affect the transmission range and channel capacity. As it is evident in the current literature, the traditional communication protocols cannot be deployed for nanonetworks, since they do not consider the specific constraints of such networks.

Through this thesis, we propose a framework for THz nanonetwork communications in vegetation environments, to address those challenges. This research work can be considered as an initial step towards the realization of such types of communications.

The proposed framework is composed of different components, including a cross-layer communication approach with specifications at the the physical and data link layers. It is also comprised of generic models of plants as well as models for approximation of the probability of success in transmissions. The performance of the proposed framework is analyzed based on the proposed theoretical models and by considering various communication scenarios.

Contents

List of Figures

List of Tables

Chapter 1

Introduction

Nanotechnology has enabled the manufacturing of new materials at nano-scale with novel properties. The specific attributes of such nanomaterials can lead to the design and fabrication of nano-scale devices which can evolve many of the existing applications as well as offer new types of applications. For example, a new generation of biomedical applications can be envisioned, which deploy bio-compatible nano-scale agents for early detection of diseases.

Due to their tiny size, nano-devices will be capable to perform very basic tasks while having a very limited functional range. Those limitations can be overcome through interconnecting a massive number of nano-devices and forming a nano-scale network, which in turn can extend their functionality. However, providing interconnections among such nodes is not trivial. Among the potential solutions, molecular and Electromagnetic (EM) communication paradigms are proposed as the most feasible techniques to enable nano-communications[1]. Molecular communications are based on biological chemical signaling, while EM communications refer to the traditional communication techniques via the transmission of EM waves.

Each of these approaches offers several properties which can be crucial/vital for the feasibility of nano-communications, meanwhile they include some shortcomings that can limit their applicability. In general, the preference for selecting either of these communication mechanisms depends mainly on the nature of the intended application. For example, EM waves travel at or near the speed of light, which makes them the ideal choice for real-time industrial applications. In contrast, molecular communications occur at an extremely slow speed. However, as such mechanisms are matching biological processes, they can be adopted as the best solutions in biomedical applications.

[1] In the rest of this document this term is used to refer to nanonetwork communications or communication among nano-devices.

Nanonetworking can benefit broad application categories, including military, industrial and environmental systems. Among such a wide range, we are interested in their environmental solutions, specifically for monitoring purposes. It is known that plants communicate by releasing various chemical compounds to share vital information with their neighboring plants, many of which are unknown or cannot be detected based on existing technologies. The precision and timely detection of these emissions can be beneficial in different aspects; for example, identifying the factors that threaten the health of crops above and below the ground as well as the timing of their occurrence. In this regard, we believe that nanonetworks can greatly improve current agricultural systems, through the provision of fine-grained and real-time data around vegetation chemical emissions. Because of the mentioned time constraints of such applications, EM nanonetworks will be the best suited communication solution. Therefore, in this thesis, we mainly focus on the deployment of EM nanonetworks in vegetation environments.

It is envisioned that the operational frequency of EM nano-devices will be in the THz channel, due to the constraints imposed by their tiny communication units [7]. EM communications at such an extremely high frequency can theoretically enable real-time and data-intensive applications. However, THz radiation are moisture-sensitive and prone to a very high degree of medium-specific attenuation and distortion, the scale of which cannot be observed in lower frequency regions. As a result, the practical transmission range for THz nano-communications will be in the order of a few centimeters, while providing a limited channel capacity. Such issues can severely affect the performance of EM nanonetworks in the proximity of vegetation, where the humidity level of the channel can be relatively high and can vary frequently. In addition, the energy limitations of nano-devices and also their rough deployment environments can be considered as other barriers, which can challenge the realization of the mentioned applications.

In conclusion, the specific properties of nanonetworks as well as the unique characteristics of their communication channel imply that the current communication protocols need radical modifications to accommodate their needs.

In this thesis, we aim to address some of those challenges through the introduction of efficient cross-layer[2] approaches for nano-communications, which are inspired from those deployed in cognitive radio [79]. The proposed strategies, which include specifications for the physical and data link layers, are attenuation- and medium-aware, while satisfying several objectives. In addition, we develop a framework to analyze performance of the proposed approaches across nanonetworks, in terms of the probability of successful transmissions. In

[2]The term cross-layer in this document refers to an approach which is implemented in more than one layer of the protocol stack.

the next section, we present our research hypothesis, which defines the general scope of this project.

1.1 Research Hypothesis

The main focus of this dissertation is the area of EM nano-scale communication networks operating in the proximity of plants. Considering that the concept of nanonetworking and the relevant research around this topic has only recently emerged, this work intends to investigate how novel communication strategies can lead to the feasibility of EM nanonetworks and their environmental applications. The proposed approaches need to take the communication constraints of nanonetworks into account. We introduce our research hypothesis that intends to summarize the overall objective of this thesis as:

A cross-layer communications framework, which includes frequency allocation strategies combined with medium-specific path-loss models will be viable for nanonetwork communications in a vegetation environment.

Next, we divide the above statement into separate questions. The validation of the mentioned hypothesis will be achieved by addressing each of the questions individually.

1.1.1 First Research Question (RQ1)

What is the actual signal attenuation pattern for short range THz radiation in a vegetation environment; and how can the different attributes of the transmission medium affect such a pattern?

The existing THz channel models for short range communications majorly consider propagation through a standard medium consisting of several gases. There is also a limited number of research works, which discuss THz communications through the human body.

However, to the best of our knowledge, the THz wave propagation behavior in the medium of plant foliage is not studied yet in literature. The provision of such models can offer a better understanding of the physical channel constraints, which is essential for the realization of environmental applications of EM nanonetworks.

In this regard, the introduction of basic THz path-loss models can be considered as the first step, with the simplifying assumption that the medium is mainly composed of air and plant leaves. The proposed models need to account for the most common types of loss in typical wireless links, e.g., spreading, absorption and shadowing. In addition, they need to be generic enough to be modified for various plant species; while being able to approximate the encountered loss as a function of different transmission parameters, including different compositions of the transmission medium as well as various attributes of vegetation.

1.1.2 Second Research Question (RQ2)

What is the effect of transmission frequency on the performance of THz nano-communication in the vicinity of vegetation; and how can the most efficient frequencies be allocated to nano-devices?

It is known that free-space transmissions in the THz band are exposed to a very high level of frequency-dependent attenuation and distortion. However, for communications through vegetation, the specific THz signal degradation pattern is unknown. Therefore, first, an investigation needs to be carried out to determine the attenuation behavior across the THz spectrum based on different specifications for the transmission link. Then, according to the observed results, their influence on different aspects of performance, e.g., the effective transmission distance, needs to be studied.

If it is evident that the frequency plays a significant role on reducing the performance, some mechanisms for efficient frequency assignment to nano-devices have to be discussed. In such a case, it should be examined if the traditional channel allocation solutions, deployed in wireless communications, can be used in nano-communications to compensate those effects. Any proposed approaches need to consider the optimization of several performance parameters through frequency tuning, while considering the specific characteristics/constraints of EM nanonetworks. The performance evaluation metrics can be considered in the areas of achievable channel capacity, spectrum utilization and power consumption. As the level of importance for optimization objectives can vary, the introduced methods also need to be able to prioritize them.

1.1.3 Third Research Question (RQ3)

For an EM nanonetwork which is operating in the proximity of plants, how can the performance of nano-communications be evaluated, specifically by differentiating between line of sight/ non-line of sight transmissions?

Traditionally, the performance evaluation of wireless communications can be carried out by considering specific transmission scenarios and the actual measurement of several performance metrics. However, as the EM nanonetworking is yet not realized and there are no fabricated nano-devices available, the performance measurements of nano-communications is not feasible.

As an initial step to address such a limitation, the performance analysis of nanonetwork communications can be performed based on modeling. The provided models need to include specifications for the structure of vegetation as the hosting environment for a nanonetwork, which can be modified based on the vegetation attributes. There is also a need for the introduction of novel performance analysis models, given the structural model of plants. One approach for the provision of such models can be based on considering the effect of plant foliage on the probability of failure/success in transmissions. In that case, the provided models need to account for LoS/ NLoS nano-communications and their effect on the total failure/success rate.

1.2 Main Contributions

This thesis contributes to the area of THz nano-scale communication networks. It specifically provides a cross-layer communications framework for vegetation monitoring nanonetworks. In this regard, it specifies THz channel models in vegetation environments for nano-communications, while investigating communication challenges at the physical channel. Then, through the definition of several channel allocation mechanisms, which are based on the relevant channel models, it aims to address those challenges. In addition, it provides a performance evaluation framework for an analysis of the efficiency of the proposed approaches. Table 1.1 maps each of the provided research questions to its relevant contributing chapter. The main contributions can be summarized as follows:

- **Initial THz path-loss models**: The definition of THz path-loss models in the vicinity of plants, for an analysis on the signal loss in nano-communications. The proposed models take the spreading, absorption and surface scattering loss into account; and they can approximate the total signal degradation level in a hybrid channel composed of air and plant leaves. These models can be categorized into the primary and log-distance based classes. The former defines the average loss as a function of transmission frequency, distance and channel conditions, e.g., attributes of leaves and medium composition. However, the log-distance model, which relies on Monte-Carlo simulations, is proposed for certain frequencies and it approximates the variation of loss from its mean value due to variable link conditions, e.g., variable number and attributes of the encountered leaves.

- **Performance evaluation framework**: The introduction of a framework for evaluating the performance of THz nano-communications in the proximity of a plant; which is composed of two components. The first component is based on abstract models of

Table 1.1 Mapping the research questions to their relevant contributing chapter.

Question ID	Relevant contribution	Addressed in
RQ1	Initial THz path-loss models	Chapter 3
RQ2	Initial THz path-loss models	Chapter 3
	Channel allocation methods	Chapter 5
RQ3	Performance evaluation framework	Chapter 4

a plant, in which a monitoring nanonetwork will be deployed. The introduced plant models can be modified according to generic attributes of a plant such as its height, leaf length and distribution. The second component specifies benchmarks for evaluating performance of the nanonetwork, in terms of successful transmission probability for LoS and NLoS nano-communications. Such a probability for LoS transmissions is defined based on the assumption that THz radiation cannot pass through leaves and also based on the THz channel absorption behavior for free-space propagation. The probability of success for NLoS transmissions is mainly defined by the limited ability of THz radiation to propagate through leaves and also by the high attenuation experienced by THz waves in air.

- **Channel allocation methods**: The definition of several frequency selection strategies for hierarchical vegetation monitoring nanonetworks, which include an initial mechanism for sink node selection. The main focus of the proposed approaches is allocating the most clear frequency channels, in terms of absorption and noise level, to nano-nodes in order to improve the overall performance in different contexts, including channel capacity, power consumption and spectrum utilization. These strategies, which can be implemented in the data link layer, deploy the previously mentioned THz channel models at the physical layer, and also the proposed performance evaluation framework.

Figure 1.1, demonstrates the introduced contributions in the form of a cross-layer framework for communications and its relevant position in the traditional protocol stack.

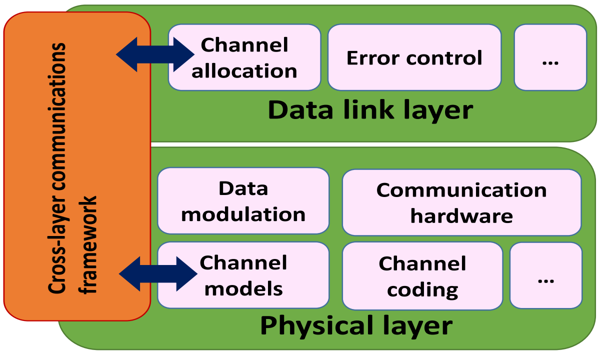

Fig. 1.1 The proposed communications framework.

1.3 Main Conclusions

The main conclusion of this thesis is that the future EM nano-scale networks can significantly improve the current agricultural system by providing real-time and high-resolution observations. It is predicted that EM nanonetworks will operate in the THz channel, which is the least explored frequency band and it demonstrates a very high level of frequency-selective signal loss. Therefore, a discussion of the THz channel constraints to pass the EM waves in vegetation environments can be considered as an initial step for the feasibility of such applications. Furthermore, efficient channel assignment strategies, which can deal with those constraints of the physical channel, will improve the performance of future nano-communications and their applications. As the research in this area is still at a very early stage, the efficiency of such approaches can be only determined based on abstract models of the deployment environment and also models for performance evaluation. In this thesis, through addressing the mentioned issues, the following general conclusions can be made:

- The attenuating behavior of the THz frequency band is highly medium- and distance-specific. It means that:
  - For free-space THz radiation in the presence of a variety of gases, several absorption peaks with different magnitudes at different frequencies can be observed. This frequency-selective behavior divides the entire THz spectrum into several transmission windows with relevant bandwidths. Furthermore, the magnitude of such an absorption directly depends on the medium composition, specifically the moisture levels, and the transmission distance.
  - Unlike free-space propagation, THz radiation through leaves undergoes a linear degradation, which is much higher in magnitude compared to radiation through a

gaseous medium. Such a loss depends on the chemical and physical attributes of leaves, including their thickness, distribution, surface roughness profile, constituent substances and so on.

  - These observations indicate that the effective transmission distance and also the channel capacity for nano-communications in the proximity of vegetation will be extremely limited.

- The total encountered attenuation can be approximated by means of THz path-loss models, given the properties of the communication channel, e.g., attributes of leaves, medium composition and so on. It was shown that the average path-loss can be approximated based on our proposed primary model and as a function of mean values of the transmission parameters, e.g., average number of the encountered leaves and their average thickness. Furthermore, it was shown that our introduced log-distance based model, which relies on simulation results, approximates the variations of path-loss around its mean value by taking the diversity of the properties of radio links into account, e.g., variable number of encountered leaves with different attributes. A comparison between the results of the two models reveals that they lead to identical approximations of path-loss. However, as the log-distance model is based on simulations, it is less suitable for real-time applications.

- The definition of precise THz path-loss models can be beneficial for nano- communications in different aspects, including:

  - According to the THz band attenuation behavior, transparent transmission windows can be located, in which the communications are exposed to the least loss. Then, higher level communication protocols can be deployed to assign such clear frequency channels to the nanonetwork components.

  - Based on the specifications of the communication channel, a path-loss threshold can be defined, which determines the maximum acceptable loss level at the receiver. Such a value can help the efficient design of transceivers.

- The high level of signal loss in THz nano-communications can be compensated by the deployment of absorption-aware channel allocation approaches, based on medium-specific path-loss models. Compared with transmissions at random frequencies, such mechanisms can significantly improve different aspects of nano-communication performance, especially in terms of achievable channel capacity, power consumption and spectrum utilization.

- The desired performance in nano-communications can be achieved based on the efficient design of nanonetworks and their components. For example, in this thesis it is shown that increasing the number of nano-nodes and also the network sink-nodes can improve the throughput. In this regard, the former helps with extending the observed data, while the latter helps with reducing the distance between nano-nodes and their respective data collection points. It is also demonstrated that an efficient selection of the path-loss threshold value can improve several performance metrics, including the loss probability and achievable transmission range.

1.4 Thesis Outline

The structure of this thesis is organized as follows:

- Chapter 2 provides a general overview of the concept of nano-scale networks. This overview defines the most fundamental components of such networks, namely as nano-devices/nano-machines, followed by their potential applications in different fields of science. Then, several proposed communication techniques across nanonetworks are introduced and the most feasible approaches, i.e., EM and molecular communications, are described in more detail. As the wave propagation velocity of EM nanonetworks and consequently their real-time nature is well suited for certain applications, specifically environmental monitoring systems, the communication challenges of such networks are investigated in the later discussion. These challenges include the limited power resources of nano-devices, high operational frequency in the THz channel and its resulting high signal loss and distortion, and also the rough environmental conditions for the deployment of EM nanonetworks. In the rest of the chapter, the existing literature to address these challenges are reviewed, which include several solutions in the physical and data link layers. Finally, this chapter concludes with highlighting the main motivations for this research work.

- Chapter 3 introduces theoretical models to measure the THz path-loss in free-space communications and also in the vicinity of the plant leaves. These models can approximate the mean value of the encountered signal attenuation, given the specifications of the transmission channel and physical characteristics of the plant. In order to approximate the variations of the path-loss from its mean value in such environments, a log-normal based path-loss model is proposed. Following, a channel capacity model for THz communications in vegetation environments is investigated. In the rest of the chapter, the proposed path-loss and also channel capacity models are evaluated by considering various channel conditions.

- Chapter 4 defines a framework for an analysis of the performance of THz nano-communications in the proximity of plants. The presented framework is composed of abstract models of a plant as the hosting environment for a nanonetwork, which can be modified according to the general attributes of the plant. It also defines performance evaluation metrics in terms of probability of successful transmissions for LoS and NLoS communications. The chapter finishes with an analysis of the proposed framework, and through the definition of the path-loss threshold boundaries it evaluates the effect of various parameters on the quality of transmissions.

- Chapter 5 focuses on the effects of dynamic channel assignment techniques to reduce the signal degradation level in THz nano-communications. In this regard, several frequency allocation strategies are proposed in this chapter, which are accompanied by an initial sink node selection algorithm. The proposed techniques tend to address the feasibility challenges of THz nanonetworks through optimizing several objectives, including channel capacity and power consumption. Following such a discussion, a multi-objective optimization technique based on GA is proposed to enhance the overall network performance according to the desired objectives. The proposed techniques can be implemented in the form of a data link layer protocol. Finally, by deploying the introduced framework in the previous chapter, the performance of these approaches is analyzed as a function of several transmission parameters.

- Chapter 6 summarizes this thesis and also highlights obtained outcomes. In addition, it reviews several potential research paths that are derived through this research work.

Chapter 2

Background and Literature Review

In this chapter, we provide an overview of the current state of the art in the general topic of nano-scale communications networks. This overview starts with the definition of nanonetworks and their relevant components, in §2.1. The section continues with a discussion on the potential applications and types of nanonetworks, in order to highlight their significance as the next generation of communication networks. Then, by focusing on specific types of nanonetworks, which are based on EM communication techniques, their potential communication challenges are investigated.

In §2.2, we present the published literature in the area of EM nanonetworks that aims to address those communication challenges. The major research work in this regard includes protocols and specifications for the physical and data link layers.

Finally, §2.3 concludes this chapter and highlights the main motivations for this dissertation.

2.1 Background

A general insight into the concept of nanonetworking is provided in this section, followed by potential applications in industrial, biomedical and environmental domains. Then, the most feasible communication approaches for nanonetworks, i.e., EM and molecular communications, are described and the relevant attributes of nano-scale components and the network structures in each category are discussed. Finally, with the main focus on EM nanonetworks, some of their communication challenges are reviewed, including the limited power resources, highly attenuative frequency channel and also the impact of harsh environmental conditions.

2.1.1 Nano-Devices and Nanonetworks

The concept of nanonetworking has recently emerged as a new communication paradigm that focuses on the interconnection of a large number of miniaturized devices, known as nano-devices/nano-machines. It is predicted that the size of a nano-device will fall into the range of 1 to a few hundred nanometres in each dimension.

According to the type of application, different approaches can be adopted for the fabrication of nano-devices. One approach is utilizing a variety of nanomaterials such as graphene, i.e., a two dimensional structure of tightly bonded Carbon atoms with peculiar quantum characteristics. Alternatively, engineered biological organisms, e.g., cells, can be deployed as biological nano-devices [7, 9]. Regardless of the fabrication approach, the functionality of nano-devices will be limited to only elementary sensing, actuating and processing, due to their size and consequently resource limitations.

The required building blocks of a nano-device will be application-specific. However, their most essential structural units can be summarized as memory, control, processing, communication, power, and actuation/sensing units [11].

One of the significant sub-categories of nanonetworks will be Wireless Nanosensor Networks (WNSNs). It is predicted that such networks can boost applications of traditional sensor networks. For example, highly sensitive nano-machines based on newly developed nanomaterials can be manufactured which will be capable to detect chemical compounds in concentrations as low as one part per billion as well as the presence of a variety of harmful entities such as viruses. By embedding such machines in various objects in our environment, particular monitoring WNSNs can be formed to obtain high-resolution data from hard-to-reach locations, e.g., under the ground or inside the human body.

2.1.2 Applications of Nanonetworks

The particular characteristics of nano-devices and nanonetworks not only rank them as the best candidates in certain scenarios, but such outstanding features can also establish new types of applications in different fields of science, including the emerging field of Internet of Things (IoT).

The idea of IoT has attracted the attention of the research community. This concept proposes the interconnection of a variety of objects with embedded components, e.g., sensors, controllers and so on, to the Internet in order to facilitate data exchange among them and ultimately enabling remote controlling. The developments in that area can lead to an increased demand for more precise control/observation levels, which can be addressed through the realization of nano-devices and consequently nanonetworks.

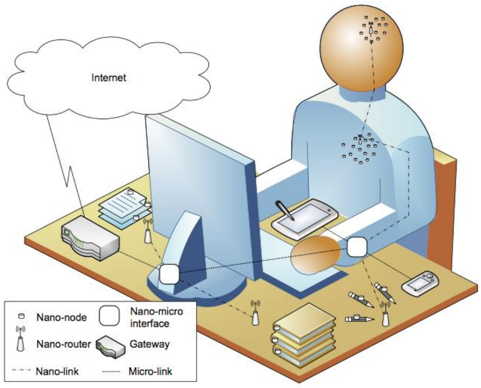

Fig. 2.1 An interconnected office as an application of the future IoNT [5].

The connection of future nanonetworks to the Internet will result in a hyper network structure referred to as the IoNT. It is predicted that IoNT will enable attractive applications, especially in the biomedical and industrial fields [5]. In the current literature a variety of IoNTs are proposed, depending on the type of their deployed components. Internet of Bio-NanoThings (IoBNT) is one of those proposals, which is composed of biological nano-machines. The deployment of biological components in nanonetworks can prevent any unpredicted effects, on health, pollution and so on, that can be caused by artificially fabricated nano-devices. Therefore, IoBNTs can be considered as the best fit for healthcare monitoring systems [11]. One of the interesting applications in this area can be envisioned through the interconnection of intrabody nanonetworks to Body Area Networks (BANs) and the Internet. The latter is deployed externally and it is capable to measure several health-related parameters from outside of the human body, such as heartbeat or temperature. However, the intrabody nanonetwork will be deployed internally to monitor other health-related factors which currently can be mainly examined via lab experiments, including blood composition [30]. The resulting interconnection can lead to more efficient biomedical systems.

Another subcategory of IoNTs is Internet of Multimedia-NanoThings (IoMNT), in which the nano-nodes are equipped with nano-scale multimedia units, e.g., highly-sensitive and precision nano-cameras or nano-phones. IoMNTs can be the best match for industrial applications, such as advanced holographic teleconferencing systems [56]. As another example for industrial applications, interconnected offices can be mentioned [5]. In an interconnected office, nano-transceivers, which are permanently connected to the Internet, will be embedded in every single item found in an office. Therefore, all such objects can be remotely tracked (Fig. 2.1).

In the following, we review a subset of the diverse range of applications that nanonetworks can offer in industrial, biomedical and environmental domains.

2.1.2.1 Industrial Applications

Nano-communications can transform a wide range of industrial applications by providing fundamental solutions for creating new materials as well as enabling new manufacturing and quality control procedures.

In this regard, one of the most practical applications will be in the area of consumer goods. For example, specific types of nanonetworks equipped with actuating nano-machines can be embedded in advanced fabrics and materials, to improve air-flow in the fabric. Such materials can be used in the textile industry, where the embedded nanonetwork can control different parameters, including the body temperature according to the external conditions. As another example in this area, we consider the deployment of nanosensors for creating ultra-high sensitivity touch surfaces or haptic interfaces.

Traditional monitoring and quality control mechanisms can also be significantly improved by means of nanonetworks. For example, the high-resolution sensing nature of WNSNs can help the real-time detection of toxic components in the water, which cannot be accomplished based on traditional alternatives. As another interesting application in this category, the real-time monitoring and controlling of chemical reactors can be mentioned [121].

A recent emerging concept in the area of multicore processing is the Network on Chip (NoC), which suggests the interconnection of processing cores and memory on a single chip for a higher communication performance [89]. In such applications, the processing units can be equipped with a graphene-based nano-antenna, graphenna, to enable wireless nano-communication as well as achieving very high data rates, i.e., in the order of a few Terabit per second (Tbps). In this case, the resulting nanonetwork is implemented in the form of a Wireless Network on Chip (WNoC) [1, 77].

2.1.2.2 Biomedical Applications

Some of the most attractive applications of nanonetworks are proposed in the biomedical fields. The tiny size, bio-compatibility and also the bio-stability of the nanonetwork components are considered the key factors to address many of the challenges and limitations which exist in the current medical systems. More efficient health monitoring and drug delivery systems, advanced immune system support and also genetic engineering are among the diverse biomedical solutions that such networks offer [9].

For example, a very large number of bio-nanosensor machines can be injected into the human body to monitor different chemicals and their concentrations, including Sodium, Cholesterol and Glucose. These applications will be crucial for people with chronic diseases, e.g., diabetics, where the blood components level can be constantly monitored by a healthcare provider.

The resulting nanonetwork in the previous scenario can also be utilized for high-resolution identification and localization of life threatening organisms, e.g., pathogens, infectious bacteria or cancer cells [87]. In such a case, certain types of nano-machines with actuation capabilities can be deployed to attack and destroy the malicious organisms by different means, such as heat. For the feasibility of such applications, the resulting biomedical nanonetworks need to be externally controllable. This feature will be required in a variety of applications, including targeted drug delivery systems, where the desired location and timing for releasing the drug will be determined by a physician [85].

2.1.2.3 Environmental Applications

Discoveries of plant sensing and communication capabilities have led researchers to argue that high-resolution detection of chemical compounds released by plants can provide knowledge of prevailing environmental conditions and plant interaction patterns.

Plants have been shown to intrinsically possess the ability to communicate with each other by various means [33, 34]. Through such communication techniques, they can manage to control different aspects of their biological systems. One inter-plant communication mechanism is chemical signaling, in which plants exchange a range of messages by releasing an extensive set of chemical molecules to share vital information about their surrounding environment, e.g., about insect attacks, the blooming stage or available resources in their proximity [47, 110]. As an example, in the case of detecting an insect attack, plants emit various Volatile Organic Compounds (VOCs) with different concentrations based on the insect type (Fig. 2.2). These emissions, which take place above and below the ground can activate/strengthen their defense systems. In addition, the type of emitted compounds can attract the natural predators of the attacking insects [46, 90, 94, 95].

The mentioned plant processes can be monitored at a very high precision by means of WNSNs, which can offer many advantages. For example, in the field of plant biology, the fine-grained detection of plant emissions can reveal their life cycle and any changes that may have occurred in that pattern. It can also improve the current agricultural systems in the context of quality control as well as resource management, e.g., through identifying the timing of an insect attack and also the type of the attacking insect, to determine the optimal level of pesticides and the timing of their application [17, 23, 82, 106].

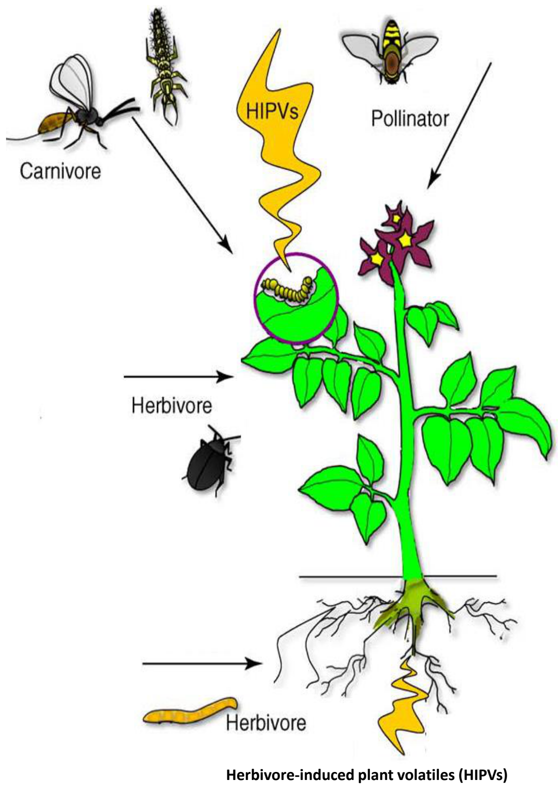

Fig. 2.2 The plant reactions on herbivore attacks by emission of volatiles, both above- and below-ground [26].

Furthermore, it has been shown that plants have sophisticated sensing capabilities. A plant can monitor chemical compounds in the soil through its roots and share such observations with other plants. Therefore, they can be utilized as bio-sensors to retrieve information on underground soil conditions [80].

2.1.3 Communication Techniques

To enable communications across a nanonetwork and among nano-machines, four techniques are proposed in the literature, namely nanomechanical, acoustic, chemical/molecular and electromagnetic [9, 13]. Nanomechanical communication defines the transmission of messages by mechanical contact between transmitter and receiver. In acoustic communication very high frequency acoustic waves can be used to encode and transmit information. Molecular communication is based on the chemical signaling mechanisms that exists in the nature. Finally, electromagnetic communication suggests the modulation and transmission of information by the means of EM waves as in traditional communication systems.

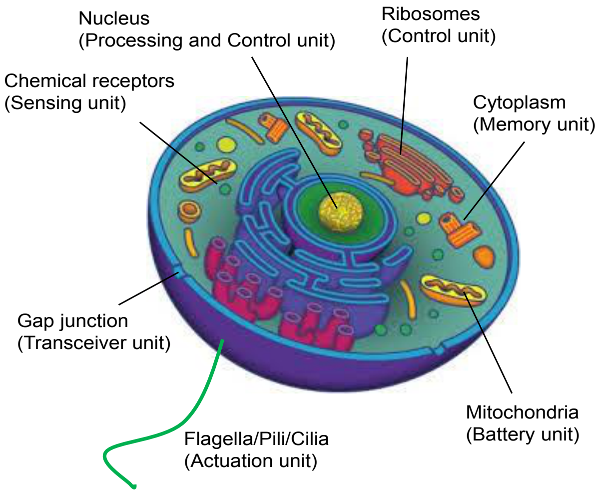

Fig. 2.3 The structure of a cell as a biological nano-machine [11].

The nanomechanical approach cannot be considered practical for nano-communications as it requires the direct contact between the communicating nano-machines. Similarly, based on the current technology, acoustic communication will not be feasible as the size and power limitations of acoustic transducers challenge their integration in the structure of a nano-machine [42]. Therefore, molecular and EM techniques can be considered as the most promising approaches for enabling communications across nanonetworks.
Next, we review the general specifications of nanonetworks based on these two communication alternatives.

2.1.3.1 Molecular Communications

Molecular communication focuses on the transmission and reception of information encoded in molecules. As stated earlier, this approach relies on natural chemical signaling. A molecular nano-communication network can be realized based on the deployment of engineered organisms or artificially fabricated devices [9, 83].

The main motivation for deploying biological organisms, e.g., a cell, bacteria, as nano-machines stems from the fact that such structures include various components which can be mapped on to the essential blocks of a generic nano-machine [11]. This mapping can be performed as follows (Fig. 2.3):

- Memory unit: In the cytoplasm of a cell, there exist a variety of molecules which are synthesized by means of DNA instructions. Such molecules can act as the nano-memory components of a biological nano-machine.

- Control and Processing units: The DNA molecules, which are comprised of genetic instructions, can be considered as the control and processing units of a nano-device. These molecules contain the required instructions for performing a variety of functions, e.g., the generation of protein molecules with different concentrations according to external stimuli.

- Communication unit: The gap junctions and hormonal receptors, located on the cell membrane, provide communication facilities for a cell.

- Sensing and Actuation units: In the structure of a cell there are different types of transient receptor potential channels and chemical receptors, which can act as the sensing block. In addition, some other components such as flagella or pili provide the actuation and movement capabilities for a cell.

- Power unit: Inside a cell there exist various molecules and structures to generate power. For example, a cell synthesizes triphosphate molecules that act as the power supplier. Furthermore, some structures such as the mitochondria or the chloroplasts can provide the required chemical fuel through energy conversion.

Molecular communications can be categorized in two main groups based on their coverage distance, namely as short-range and long-range. The former includes the inter-cell and intra-cell communications in which the transmission range falls in the range of a few nm to a few mm, and it is mostly taking place in an aqueous medium. While the latter refers to communications in the range of a few mm up to several kilometres in an aqueous or dry medium, which can be observed among communities of natural organisms such as insects.

Another classification of molecular communication can be based on their propagation technique, which falls in the following categories [6, 84]:

- Walkway-based: In this approach, which is mostly observed in intra-cell communications, the molecules are transmitted in pre-defined paths by means of carrier substances known as molecular motors. For example, Myosins and Dynein are specific protein motors, which can convert the chemical energy to mechanical energy for information transportation among cells.

- Flow-based: Flow-based molecular communication refers to the propagation of the molecules in a liquid medium, in which the flow and turbulence are guided and predicted. Hormonal communication through the blood and also pheromonal communication among colonies of ants are some examples in this category.

- Diffusion-based: The propagation in this category is based on the diffusion of the molecules throughout a liquid medium, which can be random or according to the presented turbulence in that medium. A well-known example in this category is calcium signaling among cells, in which the calcium ions with different concentrations act as the messengers.

It should be emphasized that molecular communication takes place with a very low propagation velocity, which results in very low data rates, i.e., in the order of a few bits per hour. In addition, it is argued that molecular communications can lead to interference in the natural communication system of an organ [42]. In conclusion, such specific characteristics can limit the application of molecular nanonetworks in certain areas, e.g., real-time systems.

2.1.3.2 Electromagnetic Communications

Electromagnetic communications refer to the data transfer by means of EM waves, which offers much higher propagation speeds compared to molecular communications. In the most basic form, an EM nanonetwork can be composed of the following components [15]:

- Nano-devices: nano-scale machines with energy constraints, which are capable of performing basic sensing and actuation tasks. These machines can be categorized in two major groups of basic and multimedia nano-devices, depending on their capabilities and building blocks.

- Micro-devices: micro-scale devices, which can be viewed as dedicated machines with ample power and capable of performing complex tasks compared to nano-devices. The micro-devices diffuse information collected by nano-devices and relay it to higher layers of the network. In this structure, nano-devices can be grouped as clusters with the micro-devices, as the cluster heads, for management purposes.

- Gateways: interfaces to relay the collected data from the nanonetwork to the external network, or the Internet.

In this thesis, we only focus on nano-devices as the discussion on the specifications of micro-devices or gateways are out of scope of this research.
Depending on the type of application, different topologies for an EM nanonetwork can be adopted. However, a hierarchical topology, as opposed to an ad-hoc structure, can lead to easier management and also scalability (Fig. 2.4).

The EM nano-machines, can be fabricated based on a top-down or bottom-up approach. The top-down method suggests the downscaling of the current micro-scale device components

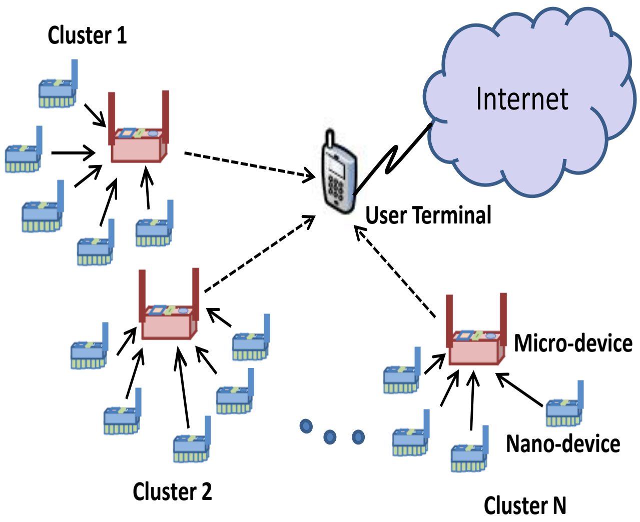

Fig. 2.4 An EM nanonetwork architecture.

into the nano-scale; while the the bottom-up method discusses the deployment of individual molecules to manufacture the building blocks of a nano-machine. Jornet and Akyildiz [7, 56], propose the first model of such a device and its relevant functional units (Fig. 2.5). In the following, each of the essential building blocks of a nano-device is discussed, with the main focus on the specifications of the power, sensing and communication units.

- Memory unit: by utilizing nanomaterials and the recent manufacturing processes, nano-scale memory units can be fabricated and integrated in a nano-machine. As an example, a Silicon-based atomic memory is proposed in [16], where the presence or the absence of an atom can indicate a binary status.

- Processing unit: graphene-based nano-structures, e.g., CNTs or GNRs, can be considered as the best candidates for the fabrication of the nano-processing unit of a nano-machine. Regarding the unique quantum properties of graphene, such a processing unit will be more compact and also much faster compared to Silicon-based processors [101].

- Communication unit: due to the limited size of a nano-device, the maximum length of an antenna in such a structure will be constrained to a few micrometres. This constraint implies that the deployment of metallic-based antennas as nano-scale communication units is not feasible, as their operational frequency will be extremely high, i.e., in the order of a few hundred THz. Hence, for the realization of EM communications across nanonetworks, Jornet and Akyildiz [59], propose the deployment of graphennas. Such

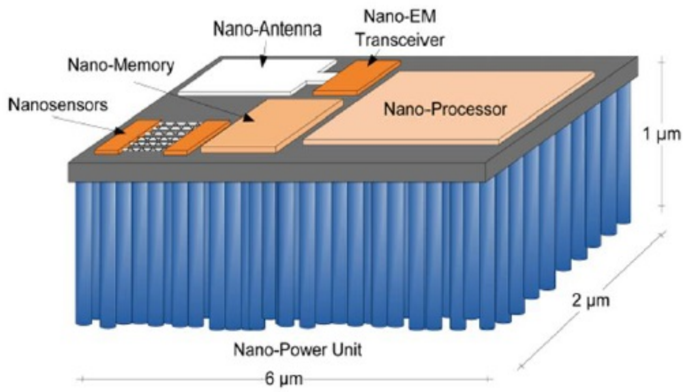

Fig. 2.5 The conceptual model of an EM nano-device [7].

nano-antenna units will operate at a much lower frequency band, and more efficiently compared to their metallic counterparts.

- Sensing and actuation unit: recently, specific types of chemical and biological nanosensors have been fabricated, which possess highly accurate sensing capabilities, i.e., detection of the presence and concentration of a given gas as well as the molecular composition of a substance. As an example, nano-scale transistors based on Silicon nano-wires can be manufactured, where the presence of different molecules changes the functional characteristics of the nano-transistor, enabling it to act as a highly accurate chemical sensor [18, 25, 86]. In addition, nano-scale actuators in different forms, e.g., nano-scissors and nano-tweezers, can be manufactured by deploying a variety of nano-structures such as CNTs [72].

- Power unit: due to the size constraints of nano-devices to accommodate a battery unit, self-powering structures are proposed as the most feasible solutions to provide their required energy. These alternatives will allow a nano-node to harvest its required energy from the environment, through the conversion of different types of energy, i.e., mechanical, vibration, thermal or hydraulic into electrical energy. Yang et al. [119] propose one of such structures, which is in the form of a pyroelectric nanogenerator and it can harvest electrical energy from the time-dependent temperature variations.

In Table 2.1, the general characteristics of EM and molecular nano-communications are compared. As can be observed in this table, both approaches have distinct advantages and also potential shortcomings. Therefore the preference of the communication method will be mainly application-specific. In this thesis, we focus on vegetation monitoring applications of nanonetworks. Due to the real-time and high-resolution requirements of such applications,

Table 2.1 Comparison between EM and molecular nano-communications [84].

Communication Type	EM-based	Molecular-based
Components	EM nano-machines	Biological nano-machines
Signal types	Optical/EM	Chemical signals
Speed	Speed of light (3×10^8 m/s)	Extremely slow (e.g., μm/s)
Range	m – Km	nm – mm (short-range) mm – Km (long-range)
Media	Air or cables	Aqueous (short-range) Aqueous/dry (long-range)
Features	Reliable, high heat dissipation	Probabilistic, bio-compatible, energy efficient

which in turn necessitate high data rate demands, EM-based approaches can be considered as the most ideal communication technique.

It should be mentioned that, despite the limitations of molecular communications in terms of transmission delay and data rate, such communication techniques can still have priority over EM-based methods in certain applications. For example, in biomedical applications the bio-compatibility of nanonetwork components is a challenge, which can be addressed by deploying molecular communications and biological nanonetworks. In order to compensate for the limitations of either of these approaches, hybrid nanonetworks can be used, which will concurrently deploy both EM and molecular communications.

Although EM nano-communications are the best fit for the mentioned applications, there are associated challenges for their feasibility, which mainly stem from their component size. We follow our discussion by focusing on those issues.

2.1.4 Communication Challenges of Electromagnetic Nanonetworks

The miniature size and also very high operational frequency of nano-devices impose severe limitations for the feasibility of EM nanonetworks. In addition, rough environmental conditions can play an important role to affect their performance, specifically in outdoor monitoring applications. In the following, we discuss such obstacles in more detail.

2.1.4.1 Limited Power Resources

As discussed before, due to the envisioned dimensions of nano-devices, integration of a power unit in their structure would be challenging. Therefore, self-powering structures with

Table 2.2 Various vibrational resources with their related frequency and acceleration magnitudes [98].

Vibration Source	Peak Frequency (Hz)	Acceleration Amplitude (m/s^2)
Refrigerator	240	0.1
Car engine compartment	200	12.0
Kitchen blender casing	121	6.4
Clothes dryer machine	121	3.5
Small microwave oven	121	2.25
Washing machine	109	0.5

energy-harvesting capabilities are proposed as their potential power units. One potential structure can be in the form of a piezoelectric nanogenerator, composed of an array of Zinc Oxide nano-wires, which is capable of generating electricity while being compressed and released; and also a nano-capacitor to store the harvested energy for later use [53, 108, 111]. The compress-release cycles can be introduced by external natural sources such as wind, or alternatively, can be artificially generated by other means such as ultrasonic waves [27]. The frequency of these vibrations determines the duty cycle of a nano-device. Some of the potential vibrational sources with their related frequency and acceleration amplitudes are listed in Table 2.2.

In order to calculate the maximum energy that can be stored on such a nanogenerator unit, first, we need to define the voltage of the charging nano-capacitor, V_{cap}. According to the provided model in [63], the latter can be calculated as a function of the compress-release cycles, n_{cyc}, as:

$$V_{cap}(n_{cyc}) = V_g \left(1 - e^{(-\frac{n_{cyc}\Delta Q}{V_g C_{cap}})}\right) \tag{2.1}$$

where V_g is the equivalent voltage of the generator, ΔQ is the harvested charge in a cycle which depends on the specification of nano-wires and also the efficiency of harvesting process, and C_{cap} is the capacitance of the nano-capacitor. Therefore, the stored energy in the nano-capacitor can be defined as:

$$E_{cap}(n_{cyc}) = \frac{1}{2} C_{cap} (V_{cap}(n_{cyc}))^2 \tag{2.2}$$

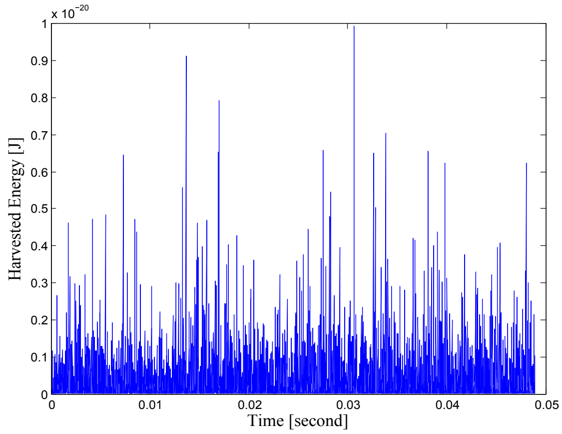

(a) Energy harvesting

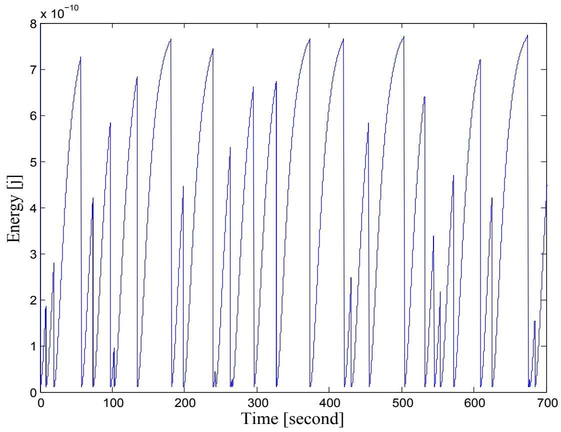

(b) Energy harvesting/consumption

Fig. 2.6 The very small magnitude of the harvested energy in each round (a), and a comparison of the relatively long energy harvesting duration versus the energy consumption periods (b) for a nano-device.

Hence, the maximum energy of the nano-capacitor can be calculated as:

$$E_{cap-max} = max\left(E_{cap}(n_{cyc})\right) = \frac{1}{2}C_{cap}{V_g}^2 \tag{2.3}$$

From the equation above, it can be concluded that the size and specifications of the nano-wire array and also the nano-capacitor are the determining factors in the maximum energy level of a nano-device.

According to the current technology and the maximum predicted size of a nano-machine, a maximum of a few hundred pJ can be harvested and stored on it. In [63], it is shown that the required number of cycles to create such an energy level will be in the order of a few thousand cycles, which, depending on the frequency of cycles, can take up to tens of seconds.

In Fig. 2.6, the magnitude of the harvested energy in each round, and also the energy harvesting duration versus the energy consumption periods can be observed. In this figure, we consider that V_g=0.42v, C_{cap} =9nF and the frequency of compress-release cycles is 50Hz, i.e., the duration of a cycle is 1/50= 0.02sec. We also assumes that 2500 cycles are required for a full charge of the nano-capacitor, which can be achieved in almost 50sec.

By considering the communication between nano-devices as the most energy consuming process, the harvested energy is only sufficient to transmit a few hundred bits in a transmission period which at most takes only a few nanoseconds. This issue shows the necessity of energy-aware communication protocols across nanonetworks.

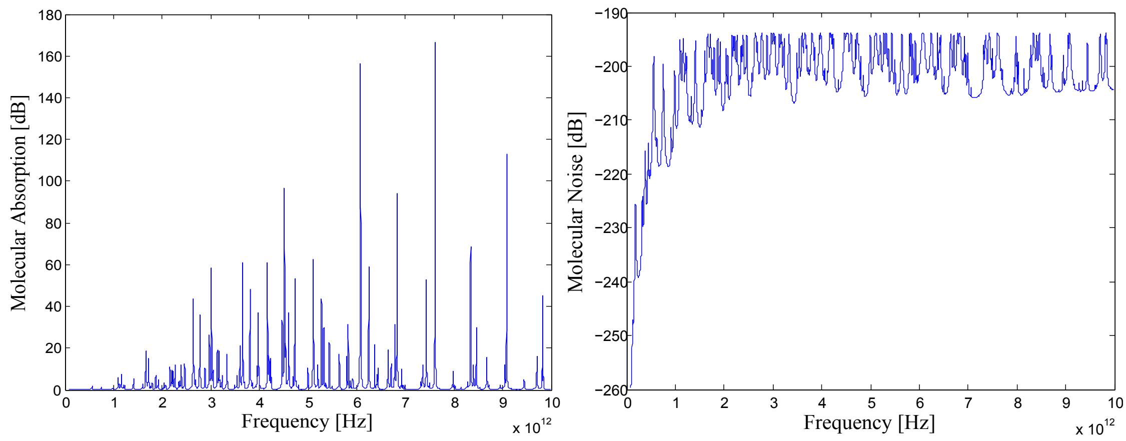

(a) (b)

Fig. 2.7 The resulting frequency-selective molecular absorption and noise for communications in a medium composed of 20% of water vapor and the transmission distance of 1cm.

2.1.4.2 High Signal Loss and Distortion

The deployment of graphennas promises the feasibility of EM communications among nano-machines, in an extremely high operational frequency in the THz range. The radiation in this part of the EM spectrum, which is commonly referred to as the sub-millimeter wave band, spans the frequency range of 0.3-10THz. However, as the vibrational frequencies of many molecule types lie in this region, the realization of THz nano-communication is not trivial [60, 93]. In this regard, one of the most challenging aspects is a very high level of signal degradation and distortion, which can be observed in the following forms:

- Molecular Absorption: As a THz wave travels through the transmission path, it collides with the constituent molecules of the medium, hence, parts of its energy is converted into kinetic energy and will be lost. This type of loss, which is referred to as molecular absorption, is frequency-selective and it strongly depends on several factors including the mixture and concentration of different molecules in the medium, transmission frequency and distance.

- Molecular Noise: The collision between a THz wave and the constituent molecules of the medium not only attenuates the signal, but it also causes those molecules to resonate. Such vibrations introduce a source of noise in the communications, known as molecular noise. This type of noise is colored and its intensity varies at different frequencies. In addition, it is only present during signal transmission, i.e., in the absence of a signal in the channel it does not exist. In general, molecular absorption can be considered as the main source of signal distortion in THz communications.

According to the provided results in [60], in free-space communications in air[1], water molecules are the main contributors of the total molecular absorption and noise. In Fig. 2.7, the total molecular absorption and noise are depicted for a 1cm long transmission path. It can be observed that these phenomena divide the THz spectrum into several transmission windows with different widths, and significantly degrade and distort the signal.

2.1.4.3 Rough Environmental Conditions

As the THz channel is a frequency-selective and moisture sensitive band, any changes in the composition and concentration of channel components can influence the magnitude of the molecular absorption and noise, and therefore, compromise the performance of communications. As a result, under certain geographical/environmental conditions the achievable data rates and the transmission range of a THz nanonetwork can be very limited.

The effects of medium characteristics and variations in performance can challenge many of the environmental applications of nanonetworks, specifically outdoor monitoring systems, where the medium composition can change frequently and rapidly. For example, Breitenstein et al. [21] and Zygielbaum et al. [122] report the variations of the moisture ratio for coffee and maize plants during dehydration and re-hydration periods. In both cases a dehydration period in the order of few days can decrease the water content of the leaves by more than 50%, while a re-hydration period in the order of a few hundred seconds can increase the water content up to 20% (Fig. 2.8). These observations suggest that the performance of a THz nano-communication in such a scenario will fluctuate as a function of the hydration cycles of the plants. In Fig. 2.9, the effect of moisture variations on reducing the transmission range and channel capacity is depicted, for transmissions at 5THz.

In addition to the previously mentioned points, other natural effects such as variations in direction and intensity of wind, temperature, pressure and so on can degrade the performance of THz nanonetworks [12]. For example, in rainy or windy climates the nano-devices are prone to be frequently blown out or washed away, which can result in a reduced accuracy of observations. All these issues necessitate the development of environmental-aware transmission protocols for nano-communications.

2.2 Literature Review

In this section the current literature in the area of EM nanonetworks, which addresses the mentioned communication challenges, is analyzed. It is important to mention that the

[1]Nitrogen, Oxygen, Argon, Carbon Dioxide and water vapor

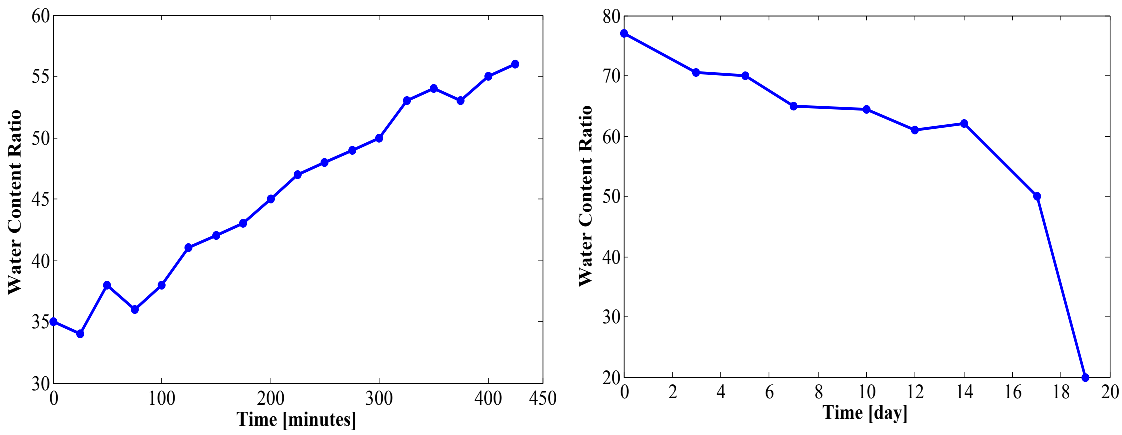

(a) Rehydration period

(b) Dehydration period

Fig. 2.8 Water content of coffee leaves following a rehydration and dehydration (replotted from [21]).

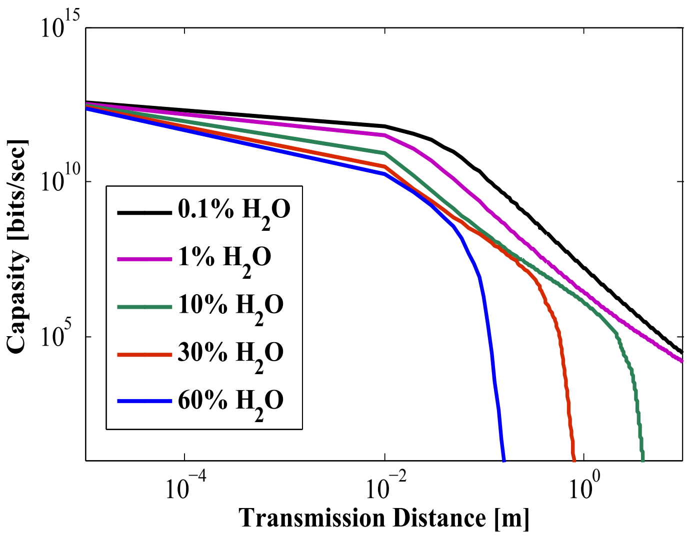

Fig. 2.9 The immense effect of the humidity level and distance on reducing the total channel capacity for communications at 5THz.

provided references are limited in number as there not many published research works on this topic. These references mainly focus on physical and data link layer specifications, and they aim to compensate those issues through the definition of efficient communication protocols with respect to power consumption and signal loss.
This discussion is followed by reviewing the proposed physical layer protocols in §2.2.1, and it is continued by summarizing the research works at the data link layer in §2.2.2.

2.2.1 Physical Layer Specifications and Protocols

The physical layer protocols provide the fundamental standards regarding the physical data transmission across a network, which include a broad range of definitions such as the communication hardware, channel models, data modulation and channel coding mechanisms, and so on. In the following, we discuss the proposed channel models and physical layer specifications for THz nano-communications.

2.2.1.1 THz Channel Models

In wireless communications, the characteristics of the transmitted signal change, as it propagates in the medium towards the receiver. These changes depend on different factors, including the transmission frequency, traveled distance, the composition of the medium, the existence of obstacles between the transmitter and receiver and so on. The behavior of a communication channel to modify the transmitted signal can be predicted by means of a model being referred to as the channel model [48]. The main components of a channel model are specifications for path-loss, scattering, multipath and noise. Given the channel model of a transmission scenario, the received signal profile can be predicted.

Path-loss mainly describes the signal power loss in LoS communications, due to the spherical expansion of the wave in the channel. In general, path-loss represents a steady degradation in the signal power as a function of distance. However, if the LoS path between the transmitter and receiver is obstructed by any objects, e.g., plants or buildings, the transmitted signal undergoes further loss due to absorption, reflection, scattering and refraction introduced by the object. The signal loss which has been introduced due to absorption, is also referred to as shadowing and it generally shows a gradual and unsteady decay in signal power, as it travels through the objects.
Furthermore, the transmitted signal can reach the receiver from indirect transmission paths due to the reflection from different objects along the path. The reflected signals and the direct path signals can reach the receiver with different phases and different experienced delays, hence, introducing a constructive or destructive effect on the received signal power. This

phenomenon in wireless channels is called multipath and it represents frequency dependant variations in the signal power at the receiver. Finally, different types of noise, e.g., thermal, ambient, can act as extra sources of power loss or distortion in wireless communications.

Jornet and Akyildiz [55, 60], proposed the first channel model for free-space and short range THz communications, which includes precise path-loss, noise and channel capacity models. The proposed models by these scientists include specifications for molecular absorption loss due to air molecules, which can be modified to accommodate various gaseous mediums with different compositions and concentrations. According to the provided results, they report that water vapor is the main contributor of signal attenuation in free-space THz communications, with greater or lesser effects at distinct frequencies. Although the introduced models and analysis are comprehensive, they lack a discussion on other common phenomena in wireless communications such as NLoS communications, scattering and multipath.

As an improvement to the mentioned model, the effect of particle scattering on LoS THz communications is studied and modeled by Kokkoniemi et al. [70]. It is shown that multiple scattering, which occurs due to the collision of the traveling signal with small aerosols such as water droplets, attenuates the signal and it also results in NLoS propagation. The latter not only degrades the signal power but it also introduces a delay in communications. In order to take such delays into account, the proposed model is provided in the time and frequency domains. In an extension to that work, the introduced multiple scattering model is modified based on a more realistic geometry and distribution of the particles in [69].
Han et al. [45] introduced a precise THz channel model based on the ray-tracing technique, which incorporates the LoS paths and also accounts for the reflection, scattering and refraction effects in communications. The proposed theoretical model is validated through comparison with measurement data that exists in the literature. Then, based on such a model, an in-depth analysis of the distance-varying and frequency-selective absorption behavior of the THz channel is carried out. The provided results suggest that distance-adaptive and multi-carrier transmissions can improve the performance of THz communications.

In many of the potential applications of nanonetworks, the signal propagation medium is not gaseous, e.g., in biomedical applications where the transmission channel is mainly blood and tissue. For an analysis on the feasibility of such applications, a discussion on THz channel behavior in solid materials is required.

In the area of biomedical applications, there are many of research works which target the body-centric wireless communications and discuss channel characterizations at microwave frequencies [2, 3, 22]. However, these works cannot be applied to THz nanonetworks due to the peculiarities of the THz channel.

To address such a need, a simple path-loss model for short-range communications through the human body is proposed by Yang et al. [114]. In that work, which focuses on blood and fat as the body components, it is concluded that blood has a more significant effect on signal degradation compared to fat, due to its higher concentration of water. It is also shown that the effect of blood and fat on attenuating THz radiation is almost steady across the entire frequency band, unlike the effect of water molecules in the air. Following that discussion, the absorption loss of the fat tissue at 1 THz is investigated by means of a simple numerical model in [115], where the authors concluded that for short transmission distances in the order of a few mm the loss is not significantly large. Then, in a more focused analysis in [116], as water is a significant composition of the human body, the THz path-loss in pure water and a NaCl solution is theoretically and numerically studied. A comparison between the provided results shows that the THz propagation loss in a medium of the NaCl solution is lower than a medium of pure water.

As an extension to the previous works and based on the proposed path-loss models, a channel capacity model is proposed in [117]. Then, by focusing on body-centric THz nanonetworks, the effect of blood, fat and skin in absorbing the THz waves is analytically studied and validated through numerical results. It is shown that the electrical properties of skin and fat are almost similar, therefore, signal loss due to reflection among such layers is not significant. Furthermore, by comparing the encountered loss through EM and molecular communications, it is concluded that molecular communication undergoes a higher degree of attenuation. Hence, the EM communication paradigm in nanonetworks will be more feasible. Finally, by studying the channel capacity as a function of different pulse shapes, it is argued that the transmission of Gaussian pulses can provide the highest data rates and transmission ranges for THz nanonetworks.

Javed and Naqvi [50], also consider the biomedical applications of WNSNs and introduce a log-distance THz path-loss model. By assuming that the network control units are located outside the body and the nanosensors are scattered within the body, it is assumed that the radiation is mainly shadowed by air and body components. Therefore, first, the absorption behavior of air molecules and the body components are studied by means of a theoretical path-loss model. In order to do so, the air is considered as mixture of different gases with the water vapor as the most dominant component to attenuate a THz signal. The human body is also considered as the composition of different components, e.g., bones, fat, blood, muscle, each with different concentrations of water. Then, by deploying the theoretical model and through extensive simulations, the components of a log-distance path-loss model are extracted. In the proposed model, the short and medium transmission distances are studied, while the transmission medium can be air, human body or a hybrid channel composed of both. The provided results indicate a very high level of attenuation in such channels due to the high ratio of water content in the body.

Guo et al. [42], propose a channel model for in-vivo applications of WNSNs, where the nanonetwork can be formed inside the human body. In order to enable communications among nanosensors, the deployment of plasmonic nano-antennas is proposed, which will operate at the optical region of the THz band, i.e., 400–750THz. As the communication medium in these applications is composed of a variety of cells, with their sizes being comparable to the THz wavelength, cell attenuation and scattering are introduced as the main source of signal loss. Therefore, first, by modeling a single cell as a multi-layer sphere, the scattering effect of such a structure is analytically modeled. Next, the proposed model is extended to account for the scattering effect of a chain of cells as well as the cells located in a 3D layered structure. The latter can be considered as a more realistic structure of the cell arrangement in the layered body tissue. Finally, based on the proposed scattering models and the resulting field intensities, a THz path-loss model is proposed. The numerical results in that work, which are validated through extensive simulations, suggest that in the frequency band under study, that cell scattering is the dominant source of signal loss compared to the cell absorption loss. These observations motivate the deployment of lower frequency bands to enable communication in WNSNs.

2.2.1.2 Nano-Antenna Unit

As discussed before, the small size of nano-machines limits the maximum size of their antenna unit to a few micro meters. At such a scale, a classical metallic-based antenna will operate in a very high frequency, in the order of a few hundred THz. According to the power limitations of nano-devices, providing the required power for communications at such a high frequency band will not be feasible. In addition, communications at the very high THz frequencies encounter a very high path-loss, which can compromise the realization of EM nanonetworks.

According to the peculiar quantum characteristics of graphene, radio scientists proposed the deployment of this material, instead of metal, to enable communication among nano-nodes. A graphene-based nano-antenna, graphenna, is capable to propagate short wavelength Surface Plasmon Polaritons (SPP) with a lower loss compared to a metallic-based antenna (Fig. 2.10). Such a structure has a very high electron mobility regardless of the temperature [29, 92]. Therefore, the wave propagation velocity in graphennas is much slower than the speed of the light in vacuum, which results in an operational frequency almost two times below the operational frequency of metallic antennas [28, 32].

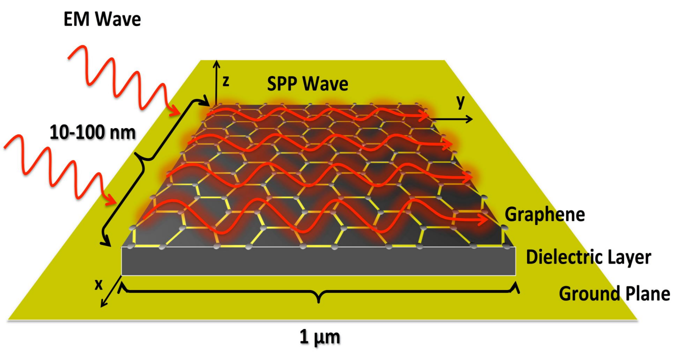

Fig. 2.10 Surface plasmon polariton (SPP) waves formation on the surface of a graphene-based nano-patch antenna [64].

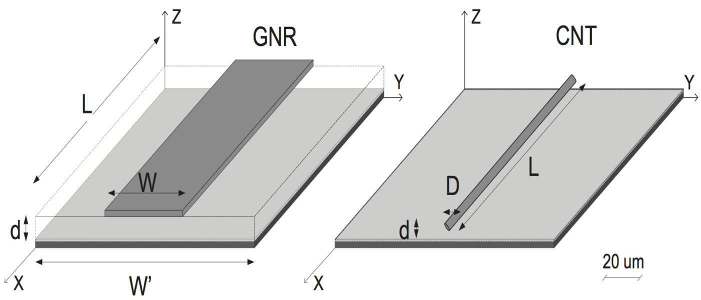

Fig. 2.11 The proposed structure of a nano-antenna based on CNTs (right) or nano-patch antennas based on GNRs (left) [59].

Jornet and Akyldiz [59], propose the antenna unit of a nanosensor node in the form of a nano-dipole antenna based on CNTs, or in the form of a nano-patch antenna based on GNRs (Fig. 2.11). These scientists show that according to the maximum size of a graphenna, it will efficiently resonate in the range of 0.1–10 THz. Although such an operational frequency is far better than the frequency range of a metallic-based antenna, the mentioned spectrum is still exposed to a very high loss level. Therefore, graphenna-based nano-communications need to be accompanied by other mechanisms to ensure a reasonable performance.
In this regard, one of the significant advantages of graphenna for nanonetwork applications is the tuning capability of its electronic properties, e.g., resonance frequency. Such a feature can enable frequency tuning of nano-nodes in order to avoid high loss frequencies.
In general, the resonance frequency of graphennas can be tuned statically or dynamically based on the following approaches:

1. Static frequency tuning: The graphenna's resonance frequency is a function of its dimensions and relaxation time, as well as the properties of the substrate which supports the nano-antenna. The relaxation time of a material is basically the time lag that it takes a perturbed system to return back into the equilibrium status.
   The relation between the resonance frequency and the dimensions of a graphenna is studied by Llatser et al. [74, 75]. It is shown that any increase in the width or any decrease in the length of the nano-antenna reduces the resonance frequency and vice versa. In these references, the relaxation time, which depends on the quality of the graphene sample, is introduced as another means to control the resonance frequency, bandwidth and the conductivity of the nano-antenna.
   Additionally in [75], the effect of the substrate's thickness and its dielectric constant on the resonance frequency of the graphenna is studied. There, the provided simulation results demonstrate that any increase in the substrate's dielectric constant as well as any decrease in the thickness of the substrate, leads to a slight decrease of the resonance frequency of the graphenna. By proposing the structure of a graphenna in the form of a nano-patch located on a dielectric substrate, Llatser et al. [76], show that the resonance frequency of the nano-antenna also depends on its position on the substrate, meaning that, locating the nano-antenna closer to the sides of the substrate will slightly increase the resonance frequency.

2. Dynamic frequency tuning: Alternatively, dynamic frequency tuning of graphennas can be accomplished through varying the temperature or the electrical conductivity of the graphenna [75]. Electrical conductivity of a graphene sample is a function of its chemical potential. The latter can be manipulated through doping or by applying an electrostatic bias voltage to the graphenna [31, 41]. Llatser et al. [74], report a slight

shift of the operational frequency to the higher frequencies through the increase of temperature. The effect of a bias voltage on the resonance frequency of a graphene-stacked dipole antenna is studied by Tamagnone et al. [104], who show that, by applying a bias voltage in the range of 0-3V to the graphene stack its chemical potential is increased in the range of 0-0.2eV, hence, its operational frequency is shifted to the upper bands of the THz range.

In order to resolve the high signal loss in THz nano-communications, Atakan and Akan [13], propose the deployment of an array of high-gain and highly directive nano-antennas. The graphennas array can greatly amplify the output signal power, which in turn results in an increased transmission rate and distance. This solution can be accompanied by NLoS communication mechanisms, in which the direct paths with a high loss level are substituted with NLoS low attenuation paths. One of such techniques is the ray-tracing based NLoS communication approach which is introduced by Piesiewicz et al. [93]. This approach is based on the installation of dielectric mirrors in the transmission environment to extend the communication reliability between nodes, where the radio system can dynamically choose between LoS or NLoS paths.

2.2.1.3 Data Modulation

Data modulation refers to a process in which some of the characteristics of a carrier signal, e.g., amplitude, phase or frequency, are varied to enable the transmission of the information over a physical link.

In classical wireless communications, a continuous wave acts as the carrier signal. However, such modulation schemes seem infeasible for EM nanonetworks due to the energy constraints of nano-devices. As such devices can only harvest and store a very limited amount of energy in a relatively long period, they cannot provide the required energy to generate continuous high-power carrier signals in the THz band.

Jornet and Akyldiz [58, 61], propose a pulse-based amplitude shift keying modulation technique, called Time Spread On-Off Keying (TS-OOK), for nano-communications. In this approach, a preamble indicates the start of a transmission, followed by a sequence of ultra-short pulses and silent periods to indicate logical “1”s and “0”s, respectively. The “1”s and “0”s are separated over time by fixed periods which are much longer than the pulse duration. Following the same idea, Peper et al. [91], suggest spike-based signaling in nanonetworks, which is inspired from the neural pulse-based communications. The proposed pulses in this mechanism are longer in duration compared to those in the TS-OOK approach.

The advantages of such modulation techniques are manifold. Firstly, the deployment of silent periods for presenting a logical status can help nano-nodes to preserve more energy.

Secondly, it can eliminate the molecular absorption and noise, as these phenomena are mainly presented upon transmission of a signal. Thirdly, in a densely populated nanonetwork such modulation techniques can reduce the probability of collisions and errors in bit detection. Finally, by presenting a logical status with an ultra-short pulse and also introducing long separation periods between symbols, the data of multiple nano-nodes can be interleaved. The latter allows the concurrent transmission of nano-devices, which consequently can increase the information capacity of the nanonetwork.

Although these modulation mechanisms promise efficient communications across nanonetworks, they can be mainly valid for very short transmission ranges, where the molecular attenuation is not drastically high. Han and Akyldiz [44] propose a distance-aware and multi-carrier-based modulation scheme for THz communications. In their proposed approach, first, the transmitter determines the available transmission frequency window based on the transmission distance, which can satisfy a desired path-loss threshold. Then, the selected window is divided into several non-overlapping sub-windows for transmission of multi-carrier signals. Finally, the carrier signal in each individual sub-window is modulated based on the MQAM modulation scheme, in which M is specified according to some constraints such as the allowed bit error rate. This approach offers the parallel transmission of data in several sub-channels, which can enhance the data rate for longer communication distances. However, the complexity of its modulation control unit can challenge the deployment of this approach for nanonetworks.

2.2.1.4 Channel Coding

In communication networks, channel coding refers to a set of mechanisms to control the errors and provide reliable transmissions via different means, e.g., transmitting extra parity bits.

In many applications of nanonetworks, a very large number of nano-machines need to be deployed to provide the required resolution and also the quality of service. Therefore, in such scenarios, collisions and interference between parallel/adjacent transmissions will be inevitable. According to the power limitation of nano-machines, this problem cannot be solved by deploying traditional solutions, e.g., transmission coordination based on a central node.

However, this issue can be addressed by means of efficient channel coding techniques for nano-communications. One of such mechanisms is introduced in [54, 62], which is based on reducing the weight of codewords in a pulse-based communication system, in order to reduce the probability of interfere in densely populated nanonetworks. Basically, the weight of a codeword refers to the number of 1's in the codeword structure, which is equivalent to the transmission of a pulse in such a system. The proposed scheme suggests the transmission of longer codewords with a smaller number of 1's and a higher number of 0's, or silent periods, instead. In addition to interference mitigation, this coding technique can preserve the energy level of nano-machines. In [4], the performance of such a mechanism is compared against traditional strategies such as Automatic Repeat reQuest (ARQ) and Forward Error Correction (FEC). It is shown that low-weight channel coding can outperform the traditional solutions in different terms, including energy consumption and latency.

An energy-efficient channel coding mechanism is proposed by Kocaoglu and Akan [65, 66], which is based on the introduction of a Hamming distance constraint. This technique tends to minimize the codeword energy in a system that uses on-off keying modulation. Such an approach can meet the energy constraints of nanonetworks, specifically in densely populated ad-hoc nanonetworks [67].

2.2.2 Data Link Layer Specification and Protocols

The data link layer is composed of two sub-layers, namely as Media Access Control (MAC) and Logical Link Control (LLC), where the former mainly includes standards for regulating the access of nodes to the shared transmission medium; while the latter mainly deals with flow and error control. In the following, we discuss the proposed MAC protocols and mechanisms for THz nano-communications.

2.2.2.1 Medium Access Control

One of the provided services by MAC protocols is the channel allocation to nodes. In wireless networks, such a process includes sharing the bandwidth among different wireless nodes in order to offer an efficient use of the bandwidth, as well as preventing collisions among concurrent transmissions of adjacent nodes.

The existing literature in the area of THz communication shows that molecular absorption and noise divide the THz band into several transmission windows of different frequency widths [20, 56, 60, 93]. These works suggest that transmission in preselected frequencies and windows based on the transmission condition, i.e., dynamic channel allocation, can enhance the robustness of communications in the THz channel.

Piesiewicz et al. [93], analyzed the free-space transmissions within the range of 0.3–1THz for distances up to 1Km. They reported several transmission windows with their corresponding attenuation level and bandwidth, and also show that communications in the introduced windows undergo a lower level of signal attenuation. In a similar approach, the frequency–selective behavior of the THz channel is studied by Boronin et al. [20]. They propose the idea of transmission in the transparency windows, where the transmittance of the medium is beyond a certain threshold. In that paper, the transparent frequencies with their corresponding bandwidths are defined for certain transmission distances – implying that communications in these windows are resilient to molecular absorption and noise. It is also shown that there exists a trade–off between the communications range, Signal to Noise Ratio (SNR) and the achievable channel capacity. It means that, if maximizing the SNR and channel capacity (in the order of a few Tbps) are of high importance, transmission in the beginning of the first defined window (0.1–0.5THz) with a bandwidth equal to 50GHz is the most efficient alternative, though, it limits the transmission distance (up to a few cm). Otherwise, if the achievable transmission distance is the main concern (over 10m), transmission in narrower windows (in the order of a few MHz) at the beginning of the first window (0.1–0.5THz) is the most efficient approach. Although this alternative decreases the channel capacity (up to a few Mbps), it still can satisfy the required bandwidth for many applications of nanonetworks.

By focusing on the biomedical applications of WNSNs, Javed and Naqvi [50], analyze THz radiation through a channel composed of air and human body components. Similar to previous works, they also reported the division of the THz channel into a set of frequency windows with variable widths, where they defined the width and the mean value of absorption in each window. Therefore, they suggest that the selection of the transmission channel can be carried out based on the transmission distance and also the windows with a lower attenuation rate.

As molecular attenuation has various effects on different frequencies in the THz channel, Zarepour et al. [120], introduce an adaptive frequency hopping mechanism for an application of nanonetworks within chemical reactors. The proposed approach tends to optimize the performance of communications in a composition variant channel, through improving the SNR. For such a purpose, the most probable composition of the reactor at any time slot is approximated to perform the frequency hopping process.

In addition to all the mentioned benefits, dynamic channel allocation mechanisms can affect the achievable transmission distance for wireless nano-nodes. In order to improve the performance of broadcast-based communications, Yalgashev et al. [113], propose the adaptive transmission range control of nano-nodes based on the density of the nanonetwork. Through simulation results, they show that such an approach can improve the connectivity of the network and also the performance of communications in different areas, including throughput and latency.

In the area of Wireless Sensor Networks (WSNs) and also Ultra Wide Band (UWB) networks, comprehensive MAC protocols have been proposed [8, 43]. However, such approaches cannot be deployed in nanonetworks, as they do not consider the unique behavior of the THz band nor the power limitations of nano-devices.

Jornet et al. [57], introduce the first MAC protocol for THz nanonetworks, referred to as PHLAME. This protocol, which deploys a novel rate division time-spread on-off keying approach as well as a low-weight channel coding scheme, is based on negotiation of the communicating nodes to select the most efficient communication parameters. The performance of this technique is analytically evaluated in terms of energy consumption, delay and achievable throughput; and it is concluded that it can support densely populated nanonetworks. In a similar approach, Wang et al. [107], proposed an energy and spectrum-aware light-weight MAC protocol for nano-communications. This mechanism attempts to improve the network throughput and offer a fair channel access among nano-machines, which are centrally controlled by a nano-controller.

The centralized structure of the previous protocol can be considered a drawback in dense nanonetworks. To resolve such a shortcoming, Mohrehkesh and Weigle [81], develop a receiver-initiated channel access protocol, called Receiver-Initiated Harvesting-Aware Medium Access Control (RIH-MAC). This protocol is scalable and it can operate in a centralized fashion, or alternatively in a distributed format to support highly populated nanonetworks. In the centralized mode, the protocol coordinates the communication between nano-machines and a central node, based on a probabilistic approach. While in a distributed scenario a distributed edge-coloring method is used to determine the channel access mechanism. RIH-MAC is an energy-aware protocol, which can adapt based on the energy harvesting rates.

2.3 Summary and Conclusion

In this chapter, we discussed the concept of nano-scale networks as the next communication paradigms. In this regard, we demonstrated how such networks can evolve the current applications to a new level as well as initiating a new generation of applications. It was discussed that more efficient agricultural monitoring systems are one of such applications, which can take advantage of the unique properties of nanonetworks, specifically through precise and real-time observations. Then, among different communication approaches, EM-based solutions were introduced as the most practical methods to accommodate the requirements of those applications.

It was argued that the operational frequency band of EM nanonetworks will be in the THz channel [59]. According to the literature, it is known that THz communications are prone to a very high degree of loss, which is medium-specific and can reduce the overall network performance. Hence, EM nanonetworks are envisioned to deal with serious obstacles at the physical layer [60]. In addition to the high loss level, other factors, including the limited power resources of nanonetwork components as well as their rough environmental conditions were introduced as issues which can challenge the realization of this type of communications [12, 63].

It was discussed that the traditional communication protocols are not suitable for EM nano-communications as they do not take the unique properties of nanonetworks and also the peculiarity of their communication channel into account. As a result, novel protocols need to be developed for the feasibility of nano-communications and their related applications. In this regard, the discussion was followed by reviewing a subset of the current research works in this area, which mainly focus on the physical and data link layers to address the mentioned issues.

It needs to be highlighted that the existing literature lacks efficient protocols/strategies, which are particularly developed for THz nano-communications in vegetation environments. The proposed approaches in this area should account for the specific communications characteristics and constraints in such conditions.

As an example, the reviewed research works in §2.2.1, included several channel models only for THz radiation in free-space or through the human body [68, 70, 115, 117]. However, those models cannot approximate the signal loss and its variations in a medium composed of plant foliage. As such estimations are required for performance analysis purposes, it can be concluded that the propagation models through vegetation are essential for the feasibility of environmental applications of nanonetworks.

To address such a shortcoming, in Chapter 3, we introduce initial THz path-loss models in the proximity of vegetation. The proposed models can estimate the encountered loss due to the absorption by air and also the absorption and surface scattering caused by plant leaves. These models can be modified based on the general properties of the communication channel, e.g., medium composition or the ratio of the traveled path through the leaves/air. As another significant aspect of the introduced models, their capability to predict the average path-loss and also its variations around the mean value can be mentioned. The calculation of the average signal loss is based on the average value of the transmission parameters and by means of our proposed primary THz path-loss model. However, the approximation of the loss variation is based on performing Monte-Carlo simulations and linear regressions.

Similarly, the reviewed literature in the area of channel allocation, in §2.2.2, were limited to free-space propagation and THz nano-communications through a body [20, 50, 120]. Furthermore, those works were centered around combating the total signal loss via locating the most clear transmission windows/frequencies, regardless of the effects of the allocated channel on other performance parameters, such as power consumption or spectrum utilization.

We account for these issues in Chapter 5, by introducing several channel assignment strategies which are combined with a basic sink node selection method, for hierarchical nanonetworks. These approaches are attenuation- and medium-aware, as they are proposed in a cross-layer fashion and based on the physical channel constraints. Therefore, they can be adjusted for nano-communications in vegetation environments. In addition to loss reduction, such approaches aim to satisfy a variety of objectives, including efficient bandwidth utilization or the efficient power consumption associated with the frequency tuning process. These mechanisms make the channel allocation decisions for individual nano-devices, given their specific transmission conditions, e.g., distance or medium composition. The latter can be considered as the main difference between the proposed strategies and the reviewed literature in this area.

Apart from the mentioned points, there is the lack of theoretical performance evaluation models for THz nano-communications in the mentioned scenarios. In this regard, we present a framework in Chapter 4, which can be used for the performance analysis of nano-communications in the vicinity of plants. By including primary models of a plant, this framework can provide a testbed for the deployment of a nanonetwork. The plant models can be defined according to the general characteristics of vegetation, e.g., leaf distribution and attributes; hence, they can take a variety of plants into account. In addition, the proposed framework is composed of performance evaluation benchmarks, for approximating the probability of success in LoS and NLoS nano-communications. The LoS probability model is centered on the simplifying assumption that THz radiation cannot propagate through the vegetation leaves due to their high moisture level. However, in order to consider more realistic scenarios, the NLoS probability model is introduced, in which the THz radiation can partially pass through leaves.

In the rest of this dissertation, the proposed models and strategies are described and analyzed in more detail.

Chapter 3

THz Channel Models

In wireless communications, the characteristics of the transmitted signal change as it propagates in the medium towards the receiver. These changes depend on different factors including the transmission frequency, travelled distance, the composition of the medium and the existence of obstacles between the transmitter and receiver. The behavior of a communication channel to modify the transmitted signal can be predicted by means of a channel model, which typically accounts for the path-loss, shadowing, scattering, multipath and noise.

As we discussed earlier, the THz channel demonstrates peculiar behavior in terms of signal distortion and degradation, which cannot be observed at the lower frequency ranges. Hence, the channel models for communications at the lower frequencies, i.e., the GHz channel, cannot be applied for communications at this range. This issue necessitates the study of precise channel models for the feasibility of communications at such a frequency spectrum and for different transmission mediums.

The current literature mainly discusses THz radiation in a gaseous medium or human tissue, which mostly benefits biomedical applications of THz nanonetworks. However, focusing on the potential environmental monitoring applications, none of the provided models discusses wave propagation within a vegetation environment.

In this chapter, first, we discuss two primary THz path-loss models which include specifications for free-space radiation as well as propagation in the proximity of vegetation. These initial models approximate the average signal degradation due to the existence of air molecules, specifically water vapor, and also the plant leaves in the transmission path. However, the introduced path-loss in practical applications of THz nanonetworks will be variable, due to the variable number and thickness of the encountered leaves, as well as the random transmission distances through air and leaves. Hence, in order to take such a randomness into account, we also propose a log-distance path-loss model. This model, which

is based on fixed transmission frequencies, incorporates a random shadow fading variable and approximates the variation of the path-loss from its mean value. In the absence of THz nano-devices, we extract the parameters of the log-distance path-loss model and the attributes of the shadow fading variable by means of Monte-Carlo simulations. In addition, we define a THz channel capacity model for communication in the mentioned environments based on the proposed path-loss models. Finally we evaluate the proposed models through simulation and numerical results.
This chapter is structured as follows: §3.1, discusses the primary THz path-loss models and in §3.2 the log-distance based model is described. §3.3 presents the THz channel capacity model. In §3.4 and §3.5, we present the numerical and simulation results based on the proposed models. Finally §3.6 summarizes this chapter.

3.1 Primary THz Path-Loss Models

The primary path-loss models for THz radiation can be categorized into the following groups:

1. Free-space path-loss: A basic model that only considers the free-space wave propagation, in which the main sources of loss are the wave expansion along the path and also the absorption effect of the air molecules.
2. Path-loss in the vicinity of vegetation: A more advanced path-loss model, an extension to the basic model, which considers the presence of objects, i.e., plant leaves, along the transmission path. In such a model, extra sources of signal loss will be introduced due wave absorption or scattering by the objects.

In the following, first, we introduce the components of the basic path-loss model to predict the free-space propagation loss. Then, by considering communications in a vegetation environment, we extend the basic model and add extra terms to account for absorption and surface scattering loss of leaves.

3.1.1 Free-Space Path-Loss Model

A basic path-loss model for free-space THz communications can be defined as:

$$PL_{P1}(f,d) = \frac{P_{Tx}(f)}{P_{Rx}(f,d)} = S(f,d)\zeta(f,d) \tag{3.1}$$

where f is the frequency, d is the transmission distance, $P_{Tx}(.)$ and $P_{Rx}(.)$ are the power spectral density (psd) of the transmitted and the received signals, respectively; $S(.)$ defines

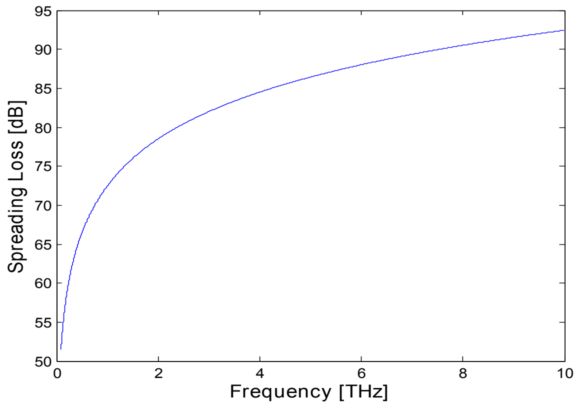

Fig. 3.1 The THz free-space spreading loss for a transmission distance of 0.01m.

the spreading loss and $\zeta(.)$ accounts for the absorption loss. In free-space transmissions, the absorption loss is mainly introduced by air molecules.
Next, we describe each of these terms in more details.

3.1.1.1 Spreading Loss

The spreading loss, also known as free-space path-loss, indicates the attenuation of the signal power due to its spherical spread around the transmitting antenna, for an omnidirectional antenna. This loss can be defined based on the well-know Friis equation as:

$$S(f,d) = \left(\frac{4\pi f d}{c}\right)^2 \tag{3.2}$$

where f is the transmission frequency, d represents the path length and c is the speed of light in a vacuum.
As it can be observed, this type of loss only depends on the transmission frequency and distance. Furthermore, this equation suggests that increasing the transmission frequency at a certain distance results in a very high and quadratic decay of the signal power. The spreading loss frequency dependence for a fixed length transmission path of 0.01m is plotted in Fig.3.1).

3.1.1.2 Absorption Loss

Once a traveling EM wave collides with the constituent molecules of a transmission medium, part of its energy is converted into kinetic energy and will be lost to the traveling wave. This type of loss, which is referred to as the molecular absorption, can be defined based on the transmittance of a medium, $\tau(.)$, as:

$$\zeta(f,d) = \frac{1}{\tau(f,d)} \tag{3.3}$$

where f is the transmission frequency and d is the path length. In fact, the transmittance of a medium represents the fraction of the signal power that can pass through that medium. By employing the Beer-Lambert law, this parameter can be quantified based on the absorption coefficient of the medium, $\alpha(.)$, as well as the length of the traveled path through that medium, as:

$$\tau(f,d) = e^{-\alpha(f)d} \tag{3.4}$$

The absorption coefficient of a medium represents the intensity of the signal loss in that medium, per unit of distance, and it depends on several factors including the electrical properties of the substances in the medium. As is shown in the equations above, the absorption coefficient and the molecular absorption loss of a medium are directly related, i.e., a larger absorption coefficient implies higher loss and vice versa.

For free-space transmissions, we can consider that the absorption coefficient of the medium is the same as the absorption coefficient of air, $\alpha_a(f)$, i.e.,

$$\alpha(f) = \alpha_a(f) \tag{3.5}$$

In the following, we discuss the calculation of $\alpha_a(f)$ based on the specific composition of the air.

- **Absorption Coefficient of Air Molecules**: Air is composed of different gas molecules, each with different concentrations and various effects on attenuating the traveling THz wave. The absorption coefficient of air is a frequency-dependent parameter which represents the overall absorption of air molecules per unit of distance. Jornet and Akyildiz [55, 60], defined such a parameter for THz radiation by deploying the radiative transfer theory. This theory discusses the interaction, or specifically the absorption, of an EM wave with matter as it passes through a medium. In order to define the air absorption behavior, they used the provided data in the High Resolution Transmission (HITRAN) database [97], which specifies the transmission characteristics of a variety of molecular types at different frequency bands.
  According to their observations, the magnitude of the air absorption coefficient depends on the particular mixture and concentration of different gas molecules found in the air.

Therefore, this parameter can be defined based on the weighted sum of the absorption coefficients of individual gases, $\alpha_t^a(.)$, as:

$$\alpha_a(f) = \sum_{t=1}^{G} C_t \alpha_t^a(f) \tag{3.6}$$

where G is the total number of various gases in the medium and C_t represents the volumetric fraction of each gas. It should be highlighted that several factors contribute to the overall absorption of an individual gas including temperature, pressure and the resonance frequency of the gas. The proposed model can be deployed to predict the absorption coefficient of any gaseous medium, given the medium composition and the volumetric fraction of each substance.

Through the provided numerical results, Jornet and Akyildiz concluded that among all constituents of normal air, water vapor has the highest impact on attenuating THz radiation. Further details for calculating the overall absorption coefficient of air based on its constituents can be found in [60].

3.1.2 Path-Loss Model in the Vicinity of Plants

If the transmission path is obstructed by random objects, e.g., vegetation foliage, some additional elements need to be added to the proposed path-loss model in equation (3.1) for a more precise approximation of signal loss. Such an extended model can be presented as:

$$PL_{P2}(f,d) = \frac{P_{Tx}(f)}{P_{Rx}(f,d)} = S(f,d)\zeta(f,d)\Psi(f,d) \tag{3.7}$$

where f is the frequency, d is the transmission distance, $P_{Tx}(.)$ and $P_{Rx}(.)$ are the psd of the transmitted and the received signal, respectively; $S(.)$ is the spreading loss defined in equation (3.2), $\zeta(.)$ represents the total absorption coefficient of the channel defined in equation (3.3), and $\Psi(.)$ is the encountered scattering loss. In this extended model, $\zeta(.)$ accounts for the total absorption created by different objects along the path. For communications through vegetation, the latter can be obtained by calculating the total absorption coefficient of a hybrid channel. It means that $\alpha(.)$ in equation (3.4) should be modified for a medium composed of air and the plant components, e.g., leaves, fruits, stalks and so on.
Next, we discuss the formulation of $\alpha(.)$ in such a scenario.

3.1.2.1 Absorption Coefficient of a Hybrid Channel

In the most basic scenario, we can assume that transmissions through vegetation are obstructed and attenuated by air molecules and leaves. This assumption can simplify the development of an initial THz path-loss model for communications in the vicinity of plants. In future work, this model can be extended to take the encountered loss due to other components of a plant, and consequently the overall loss of a plant, into account.

Therefore, we define the total absorption coefficient for such a hybrid channel as a function of the absorption coefficients of air and leaves, $\alpha_a(f)$ and $\alpha_l(f)$, as:

$$\alpha(f) = A\alpha_a(f) + B\alpha_l(f) \tag{3.8}$$

In this definition, A and B are weighting factors which represent the proportion of the total path traveled by the wave through the air and leaves, respectively (Fig. 3.2). These weighting coefficients are defined as:

$$\begin{aligned} &A = \frac{1}{d}\sum_{i=1}^{n+1} d_i^a, \quad B = \frac{1}{d}\sum_{j=1}^{n} d_j^l \approx \frac{nT}{d} \\ &s.t. \quad \sum_{i=1}^{n+1} d_i^a + \sum_{j=1}^{n} d_j^l = d \end{aligned} \tag{3.9}$$

where d is the total path length, n is the number of the encountered leaves between transmitter and receiver, $\sum_i d_i^a$ and $\sum_j d_j^l$ are the total path length through air and leaves, respectively, and T is the average thickness of leaves. It should be noted that n and T are random in practice and depend on the characteristics and the statistical distribution of leaves in a specific plant type.

The absorption coefficient of the air can be calculated by deploying equation (3.6), based on the transmission frequency and the particular mixture of air. However, the absorption coefficient of a leaf can be defined differently and based on the electrical properties of the leaf at specific frequencies. In the following, we discuss an analytical approach for modeling and calculation of $\alpha_l(.)$.

Absorption Coefficient of Plant Leaves:

The absorption coefficient of leaves at THz frequencies defines the signal loss as it passes through the leaf tissue. Such a parameter for a leaf, as a solid transmission medium, can be

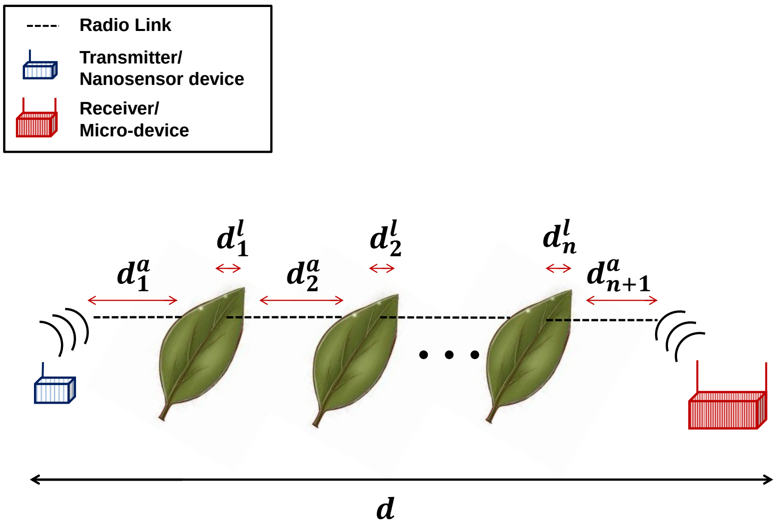

Fig. 3.2 A single radio link, where the traveling signal undergoes attenuation due to air molecules and the encountered leaves.

extracted from its extinction coefficient, $\kappa_l(.)$. The latter, which also represents the magnitude of signal loss, can be related to the absorption coefficient by the following expression [114]:

$$\alpha_l(f) = \frac{4\pi\kappa_l(f)f}{c} \tag{3.10}$$

where f is the transmission frequency and c is the speed of light in a vacuum.

The extinction coefficient depends on the complex relative permittivity of a material, $\varepsilon_r(.)$. In general, permittivity is a frequency-dependent value which depends on the polar moments of the material molecules and decides both the amount of energy temporarily stored in the substance and the permanent energy transfer to the substance. The relative permittivity, also referred to as the dielectric constant, represents the ratio of the permittivity of the material to that of vacuum, i.e.,

$$\varepsilon_r(f) = \frac{\varepsilon(f)}{\varepsilon_0(f)} \tag{3.11}$$

where $\varepsilon_0(.)$ is the vacuum permittivity.
The relative permittivity is commonly represented in a complex format as:

$$\varepsilon_r(f) = \varepsilon_R(f) + j\varepsilon_I(f) \tag{3.12}$$

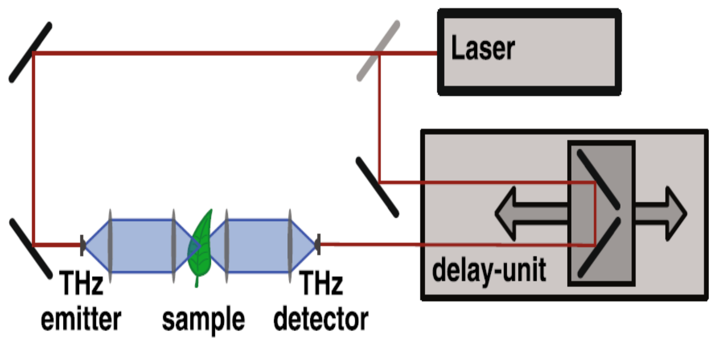

Fig. 3.3 Schematic of a THz-TDS system for detecting the electrical properties of a leaf [37].

In this definition, the real part, $\varepsilon_R(.)$, defines the proportion of wave energy stored within the material, whereas the imaginary part, $\varepsilon_I(.)$, represents the proportion of energy transferred from the wave to the material.

Therefore, the extinction coefficient of a substance can be calculated as a function of the real and imaginary parts of its complex relative permittivity as [114]:

$$\kappa_l(f) = \sqrt{\frac{\sqrt{\varepsilon_R^2(f) + \varepsilon_I^2(f)} - \varepsilon_R(f)}{2}} \tag{3.13}$$

In order to approximate the absorption coefficient of leaves at THz frequencies, their complex relative permittivity should be accurately measured and modeled.

Among different approaches to measure such a parameter, THz-TDS can be considered as a well-known technique. In this measurement approach, a broadband pulse, which is a narrow time domain impulse, referred to as a THz pulse, is transmitted through air and its magnitude and phase is compared with the same pulse being passed through the intended material to infer the permittivity of the sample [109]. An example of such a system to detect the permitivity of a leaf is illustrated in Fig 3.3.

It should be emphasized that a leaf does not have a homogeneous structure, but rather it is a complex composition of different components, including air cavities, water, sugars and proteins. As a result, providing a precise permittivity model of a leaf can be complex, as different components in its structure have different permittivity values [38].

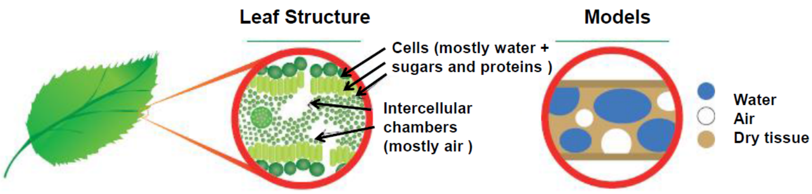

Fig. 3.4 Model of a leaf as a complex structure which is composed of air, water and dry tissue [19].

As an alternative to address this problem, Ulaby and Jedlicka [105], considered that such a heterogeneous structure can be modeled as a mixture of water, air and bulk/dried plant material as the most effective components on EM radiation (Fig. 3.4). Then, based on the proposed model of a leaf they demonstrated the accuracy of several permittivity models against the actual measured values at GHz frequencies.

One of the well-known models to approximate the complex permittivity of a non-uniform multi-compound material is the Landau, Lifshitz, Looyenga (LLL). This model is derived from the Effective Medium Theory (EMT), and it is developed based on the proportion of constituent components of a substance [78]. As a result, it is well-suited to characterize the permittivity of a material such as a leaf. However, it mainly describes the effective permittivity of a substance composed of two components.

This constraint is resolved in [52, 99], by adding an extra term to the existing LLL model, which takes all the significant elements of a leaf into account.

In the proposed model, the permittivity of a leaf can be calculated as a function of the volumetric fraction, V , and the relative complex permittivity, ε, of the leaf constituent elements as:

$$\sqrt[3]{\varepsilon_l(f)} = V_s\sqrt[3]{\varepsilon_s(f)} + V_w\sqrt[3]{\varepsilon_w(f)} + V_a\sqrt[3]{\varepsilon_a(f)} \tag{3.14}$$

where indices l, s, w and a stand for leaf, solid plant material, water and air, respectively.

The relative complex permittivity of water in THz frequencies is widely studied in the literature, as a function of frequency and also of temperature [51, 73]. Therefore, the proposed model in equation (3.14) can approximate the permittivity of any type of leaf given the permittivity of the solid leaf material and also the volumetric fraction of each component of a leaf. This equation in turn can be deployed to calculate the extinction coefficient in equation (3.13), and consequently the absorption coefficient of leaves in equation (3.10).

3.1.2.2 Surface Roughness Scattering Loss

Due to the short wavelength of the THz radiation, which is in the sub-millimeter range, THz transmissions are exposed to a very high degree of various types of scattering loss, e.g., scattering made by very small particles or from the rough surfaces [49, 70]. In the case of nano-communications in vegetation environments, as the THz wavelength is comparable with the surface roughness profile of plant leaves, part of the radiation can be lost due to surface roughness scattering. In general, we can define the signal loss due to the scattering effect as:

$$\Psi(f,d) = e^{\alpha_s(f)d} \tag{3.15}$$

where $\alpha_s(.)$ is the scattering coefficient. As we are only concerned with the scattering due to the surface roughness of leaves, the latter can be presented as:

$$\alpha_s(f) = \alpha_{s,l}(f)B \tag{3.16}$$

where B is the fraction of the path traveled through leaves defined in equation (3.9), and $\alpha_{s,l}(.)$ represents the scattering coefficient of leaves. For THz radiation, this coefficient can be described by a Rayleigh roughness factor as follows [52]:

$$\begin{aligned} \alpha_{s,l}(f) &= \frac{1}{T}\left(\Delta\varepsilon(f)\frac{4\pi\sigma_l f\cos(\phi)}{c}\right)^2 \\ \Delta\varepsilon(f) &= \sqrt{\varepsilon_l(f)} - 1 \end{aligned} \tag{3.17}$$

where $\Delta\varepsilon(f)$ is the contrast in the permittivity of leaves and it can be calculated by deploying equation (3.14), σ_l stands for the standard deviation of the leaves height profile, ϕ and f are the angle and frequency of the incident wave and T is the average thickness of a leaf.

3.1.2.3 Total Attenuation Coefficient of a Hybrid Channel

Jördens et al. [52], observed that for THz communications in the proximity of leaves, the total signal loss can be more accurately approximated if the absorption and surface scattering loss are concurrently taken into account. In this regard, they suggest the addition of the scattering coefficient to the absorption coefficient, to formulate the total attenuation coefficient of leaves.

In a similar approach and by assuming that the transmission medium is mainly composed of leaves and air molecules, we define the total attenuation coefficient as:

$$\alpha_{tot}(f) = A\alpha_a(f) + B(\alpha_l(f) + \alpha_{s,l}(f)) \tag{3.18}$$

where $\alpha_a(.)$ is the absorption coefficient of air, $\alpha_l(.)$ and $\alpha_{s,l}(.)$ are the absorption and scattering coefficients of leaves, respectively; while A and B represent the ratio of the total transmission path through the air and leaves.

3.2 A Log-Distance Path-Loss Model

In addition to the discussed primary models, the total path-loss in a medium can be approximated by means of a log-distance model, for a fixed frequency and as a function of distance [39, 50]. In such a model, a random variable can be incorporated to represent the shadow fading effect. In fact, shadowing is the variation of the path-loss from its mean value, as the signal travels through random and possibly different objects that exist in the transmission path. This type of path-loss model can be defined as:

$$PL_E(d)[dB] = PL_0 + 10\gamma \log_{10}(d) + X_\sigma \tag{3.19}$$

where d is the path length, PL_0 shows the path-loss at a reference point, γ is the path-loss exponent and X_σ defines a random variable which represents the shadow fading characteristics of the transmission medium.

In general, the parameters of a log-distance path-loss model, i.e., PL_0, γ and attributes of X_σ, can be extracted based on empirical measurements, or alternatively, by Monte-Carlo simulations and fitting a curve to the measured/simulated data.

3.2.1 Log-Normal Shadow Fading

In a vegetation monitoring application, we can assume a random and large number of air molecules and leaves exist between the communicating endpoints, which cause the shadowing phenomenon. Therefore, according to the central limit theorem, the shadow fading variable in such an environment, X_σ, can be considered as a Gaussian/Normal random variable [103]. As X_σ is in logarithmic scale, it is commonly referred to as log-normal shadowing with the following distribution:

$$p(X_\sigma) = \frac{1}{\sqrt{2\pi}\sigma_s} \exp\left[-\frac{(X_\sigma - \mu_s)^2}{2\sigma_s^2}\right] \tag{3.20}$$

where σ_s and μ_s stand for the standard deviation and the mean value of the shadowing variable.

3.3 THz Channel Capacity

In a wireless channel, the theoretical upper limit of the total channel capacity can be calculated based on the Shannon theorem as [40]:

$$C(d) = B_w \log_2 \left(1 + \frac{S_p}{N_p}\right) \tag{3.21}$$

where d is the distance, B_w is the transmission bandwidth, S_p is the psd of the transmitted signal and N_p is the encountered noise power. However, as the THz channel is frequency-selective, the noise power cannot be considered flat, so the mentioned channel capacity model will not be valid.

To address this constraint, Jornet and Akyildiz [60], proposed to divide the transmission bandwidth into very narrow sub-bands, within which the psd of the colored noise can be considered flat. Then, the total capacity can be calculated by summing up the capacity of narrow frequency windows over the desired THz spectrum. Therefore, the introduced model in equation (3.21) can be redefined as:

$$C(d) = \sum_z \Delta f \log_2 \left[1 + \frac{S_p(f_z)}{PL(f_z,d)N_p(f_z,d)}\right] \quad \text{for } z = 1, 2, \ldots \tag{3.22}$$

where f_z stands for the central transmission frequency in the zth window with a width equal to $\Delta f = f_z - f_{z-1}$, $PL(.)$ is the total path-loss and the rest of parameters are the same as defined above.

It is worth noting that, if we tend to study the total channel capacity in free-space communications, $PL(.)$ will be defined based on the primary model in equation (3.1). Otherwise, if transmissions are taking place in the proximity of plant leaves, $PL(.)$ will be defined according to the primary model in equation (3.7), or via the log-distance model in equation (3.19).

Next, we discuss the relevant noise and signal models.

3.3.1 Molecular Absorption Noise

The frequency-selective nature of the THz channel causes a non-steady absorption behavior across this spectrum, which in its turn introduces a colored noise in communications. In fact, the origin of this noise is the collision of the traveling signal with the channel molecules, in which part of the signal energy causes the molecules to oscillate and create noise. This type of noise, known as molecular noise, can be considered as the main source of signal distortion in the THz transmissions, and it can be modeled as:

$$N_p(f,d) = k_B B_w T_m(f,d) \tag{3.23}$$

where f, d and B_w define the transmission frequency, distance and bandwidth, respectively; k_B is the Boltzmann constant and $T_m(.)$ represents the molecular noise temperature with the following definition:

$$T_m(f,d) = T_0 e(f,d) \tag{3.24}$$

where T_0 is the reference temperature and $e(.)$ stands for the emissivity of the channel. The latter represents the effectiveness of a channel to emit the thermal energy, and it can be defined based on the channel transmittance, $\tau(.)$ in equation (3.4), as follows;

$$e(f,d) = 1 - \tau(f,d) \tag{3.25}$$

We emphasize that for free-space communications, $\tau(.)$ is calculated based on the absorption coefficient of the air as in equation (3.5); whereas, in communications in the vicinity of vegetation the absorption coefficient of the hybrid channel is employed, i.e., equation (3.8).

3.3.2 Signal Model

Jornet and Akyildiz [60], carried out a comprehensive analysis to show the effect of the transmitted signal characteristics on the achievable THz channel capacity. According to the presented results, transmission of a signal with flat psd is the most efficient approach for maximizing the total channel capacity. However, due to the power constraints of a nano-device, transmission of continuous carrier-based signals is not a feasible communication approach. Hence, pulse-based transmissions can be considered as an alternative, which can preserve the limited energy of the nano-devices. In this regard, the exchange of ultra-short pulses are proposed as the enabling technique for the data transmission in nanonetworks, where the duration of the pulse is in the order of a few picoseconds and its power is consequently mainly contained in the THz frequency range.

In the most basic form, such a pulse can be considered as Gaussian-shaped with the following format:

$$p(t) = \frac{a_0}{\sqrt{2\pi}\sigma_p} \exp\left[-\frac{(t-\mu_p)^2}{2\sigma_p^2}\right] \tag{3.26}$$

where a_0 is a constant value for adjusting the pulse energy, σ_p defines the standard deviation of the pulse in seconds, and μ_p represent the pulse centre in seconds. Accordingly, the psd of the transmitted pulse can be defined as:

$$S_p(f) = {a_0}^2 \exp\left[-(2\pi\sigma_p f)^2\right] \tag{3.27}$$

3.4 Evaluation of the Primary Models

In this section, we deploy the proposed primary models to approximate the average signal loss and channel capacity for free-space THz communications as well as communications in the proximity of plants. For such a purpose, first, we define the environmental conditions for the numerical study of the primary path-loss models. Such specifications include the relative humidity of the transmission medium as well as the ratio of the traveled path by the signal through air/leaves. Then, we study the effect of the variation of these parameters on the total attenuation coefficient, path-loss and achievable channel capacity for both models.

3.4.1 Numerical Study Setting

In the following, we review the environmental conditions, which are the basis for the numerical analysis of the proposed models. In this analysis, we consider the encountered loss for communications across a single radio link.

3.4.1.1 Transmission Conditions

As the host environment, a coffee plant is considered, where the THz radiation can be obstructed by a random number of coffee leaves (in this study we ignore any types of obstruction causes by other parts of the plant such as fruits, stalks and so on). As the total attenuation coefficient of a fresh coffee leaf, i.e., $\alpha_l(.) + \alpha_{s,l}(.)$ in equation (3.18), we use the measured data in [52].

For an analysis on the total attenuation coefficient and path-loss, we assume that the ratio of the traveled path through leaves, i.e., B in equation (3.9), varies from 0 to 0.005. It should be noted that a value of $B = 0$ corresponds to free-space transmissions, and the variation in

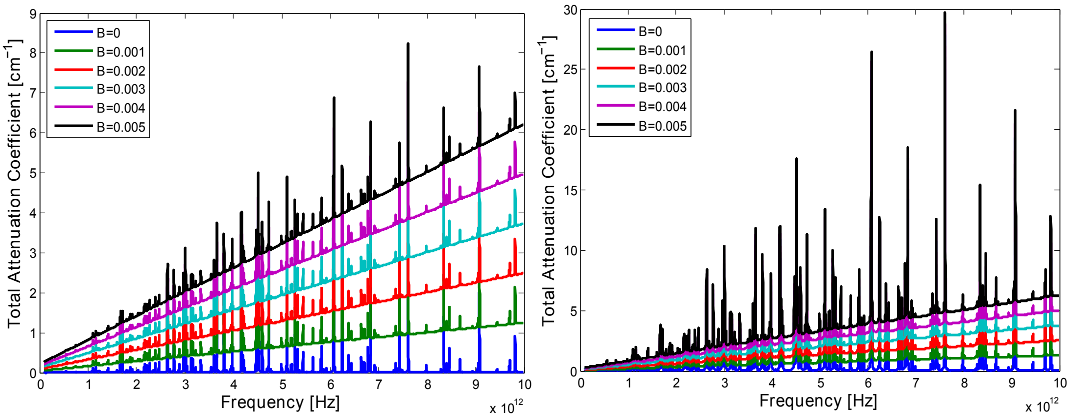

(a) Relative humidity= 1% (b) Relative humidity = 10%

Fig. 3.5 The total attenuation coefficient for THz communications in free-space, $B = 0$, and in the vicinity of fresh coffee leaves, $B \neq 0$.

the range of 0.001 to 0.005 accounts for a sparse and a dense plant structure, respectively. The relative humidity is set as 1% and 10%; and three different transmission distances as 0.01m, 0.1m and 0.2m are considered. It is worth noting that the selected moisture levels only tend to show the lower range and also the pattern of signal loss, as the actual humidity level in a typical vegetation environment will be much higher.

To study variations of channel capacity as a function of leaf attributes, we consider a uniform distribution of leaves with the mean value in the range of 0–20 [leaves/m] with the relevant leaf thickness of 100μm or 200μm as addressed in [99]. The provided results are based on considering 80% of humidity, and the transmission of 100fs long Gaussian pulses with a sub-channel width of 50GHz at 0.3THz.

3.4.2 Total Attenuation Coefficient

To calculate the attenuation coefficient for free-space transmissions and also for communications in a channel of air and leaves, we used equations (3.5) and (3.18), respectively. In Fig. 3.5, the total attenuation coefficients for the specified channel condition is shown. Firstly, we can see in free-space communications, i.e., $B = 0$, the air molecules are the only attenuating components of the medium and the THz band is divided into transmission windows with different widths. This observation is in good agreement with the results reported in [60]. Secondly, for propagation through air and leaves , i.e., $B \neq 0$, we see that just the magnitude and slope of the attenuation coefficient varies, while the size of the transmission windows are intact. We therefore conclude that the effect of leaves on the attenuation coefficient is linear for all the frequencies, while that of the air molecules is random and frequency-selective.

3.4.3 Total Path-Loss for the Entire THz Spectrum

Next, we calculate the total path-loss as a function of frequency and humidity for three transmission distances. In Fig. 3.6a–3.6b, the free-space path-loss is shown by deploying equation (3.1), where the great effect of moisture level on the total loss can be observed. Then, by deploying equation (3.7) the total path-loss in a hybrid channel is plotted in Fig. 3.6c– 3.6f. For a fixed humidity level, it can be seen that increasing B by five times causes a significant increase in the total loss. This observation shows the high impact of leaves on attenuating the THz radiation. In all the plots, we can see a very high level of path-loss for transmission distances exceeding a few cm, which challenges the feasibility of plant monitoring applications of nanonetworks, specially for high ratios of leaf density and humidity. From the provided results it can be concluded that THz communications in such environments will be limited to extremely short transmission distances by means of specific communication protocols, e.g., transmission in pre-defined absorption resilient frequencies or multi-hop communications approaches. In addition, it can be observed that lower THz frequencies, sub-1THz, seem to be a more practical frequency spectrum for the realization of such applications.
We emphasize that the main goal of this study is to demonstrate the magnitude of signal loss across THz band. However, it is known that the reception of a signal with loss levels more than 90dB is practically infeasible.

3.4.4 The Effect of Leaf Attributes on Channel Capacity

The total channel capacity for the described environment is plotted in Fig. 3.7, based on equation (3.22). In this scenario, we study the variation of channel capacity as a function of distance and also the number of encountered leaves, n. Therefore, we deploy the path-loss models defined in equations (3.1) and (3.7), which correspond to free-space transmissions and transmissions through leaves, respectively. The noise model is the one defined in equation (3.23). It can be observed that transmission through leaves, i.e., $n \neq 0$, has a drastic effect in degrading the channel capacity compared to free-space transmissions, i.e., $n = 0$. In addition, the great effect of leaves thickness and the number of encountered leaves on reducing the effective transmission range is shown.

3.5 Evaluation of the Log-Distance based Model

In this section, we deploy the proposed primary models to perform Monte-Carlo simulations in order to define the variations of the path-loss. Therefore, we consider a plant monitoring

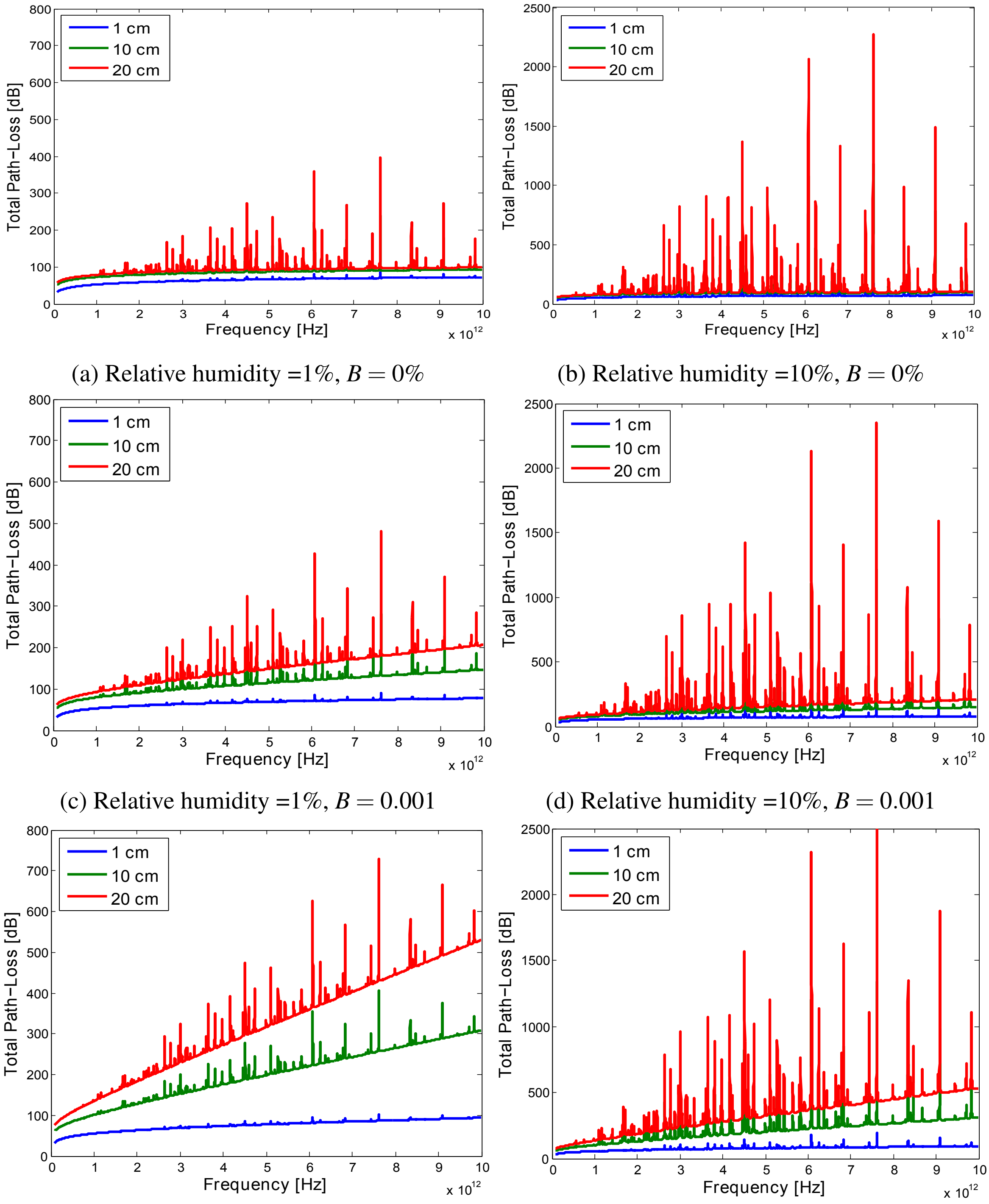

(a) Relative humidity =1%, $B = 0\%$

(b) Relative humidity =10%, $B = 0\%$

(c) Relative humidity =1%, $B = 0.001$

(d) Relative humidity =10%, $B = 0.001$

(e) Relative humidity =1%, $B = 0.005$

(f) Relative humidity = 10%, $B = 0.005$

Fig. 3.6 The total path-loss in vicinity of coffee leaves with different humidity levels and ratios of the travelled path through leaves, B. Plots (a) and (b) represent the path-loss in free-space, plots (c) and (d) are the path-loss in a sparse plant environment; while plots (e) and (f) show that of a denser plant.

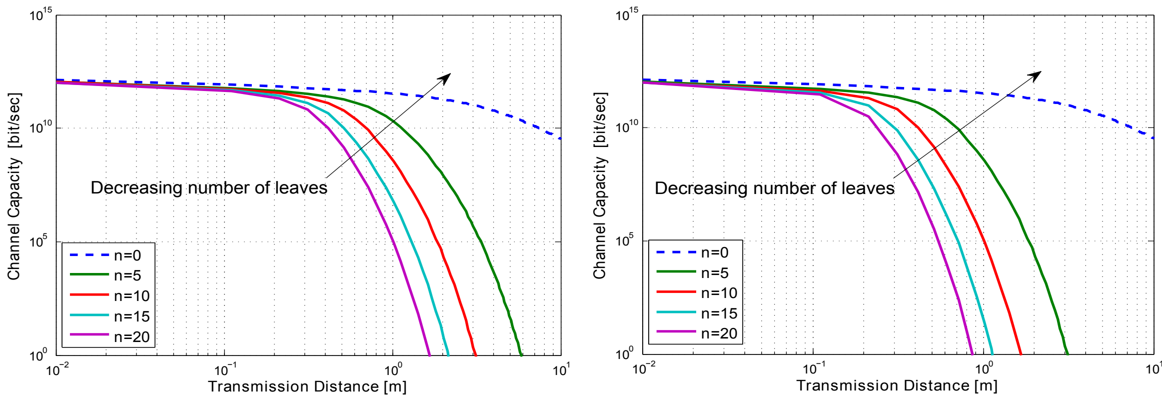

(a) Leaf thickness= 100μm (b) Leaf thickness= 200μm

Fig. 3.7 Channel capacity comparison for free-space communications, $n = 0$, and communications in a plant environment, $n \neq 0$, while communicating at 0.3THz.

nanonetwork composed of a large number of nano-nodes. In such a scenario, we describe specific simulation assumptions for extracting the parameters of the proposed log-distance path-loss model. These assumptions range from the attributes of the plant such as the distribution and thickness of leaves, to the number of nano-nodes. Finally, we discuss the effect of the variation of each parameter on the magnitude of the path-loss, through simulation results.

3.5.1 Simulation Setting

In the absence of fabricated THz nano-devices, we use simulation results to define parameters of the proposed log-distance based model in equation (3.19).
Next, we discuss our assumptions for the implementation of Monte-Carlo simulations. These assumptions include specifications of the environmental condition and also the deployed nanonetwork.

3.5.1.1 Plant Structure

As the host environment, we consider the same coffee plant structure as the previous experiments. We assume that the thickness of coffee leaves is a random value in the range of 100 – 220 μm and the distribution of leaves for any random radio link (or between any pair of nano- and micro-device) is either Poisson point or Uniform with a mean value of 10 or 15 [leaves/m]. Furthermore, we assume that the relative humidity varies in the range of 10% - 80%.

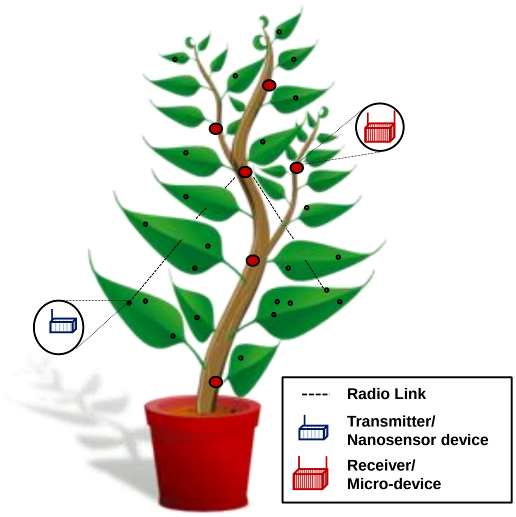

Fig. 3.8 The nanonetwork structure for Monte-Carlo simulations.

3.5.1.2 Nanonetwork Specifications

We assume that the intended monitoring nanonetwork is composed of a large number of nano-devices/transmitters and several micro-scale receivers as the sink nodes. In the following simulations, the number of nano-devices varies between 10^4, 10^5 and 10^6 which transmit their data in 50GHz wide transmission windows at fixed frequencies in the range of 0.3 – 1 THz. The transmission distance for any communicating pair is a random value in the range of 0.01 – 1m, which varies based on the position of nodes. It is worth noting that in each scenario the transmission frequency of all nodes is identical, though, their experienced transmission conditions are different.

3.5.1.3 Monte-Carlo Simulations

The main idea of Monte-Carlo simulations for nanonetwork communications is having a very large number of nodes randomly scattered in the area under inspection. Hence, the communication condition for each node is influenced based on its random position in the simulation environment (Fig. 3.8). The random positioning of nodes let the simulation parameters adopt a variety of values in predefined ranges. Hence, the variations of some parameters of interest can be studied as a function of the random variations of simulation parameters. In our specific monitoring application, we are interested to study the effect of the features of a random physical link, e.g., the number and thickness of the encountered leaves or the transmission distance, on the variations of the path-loss.

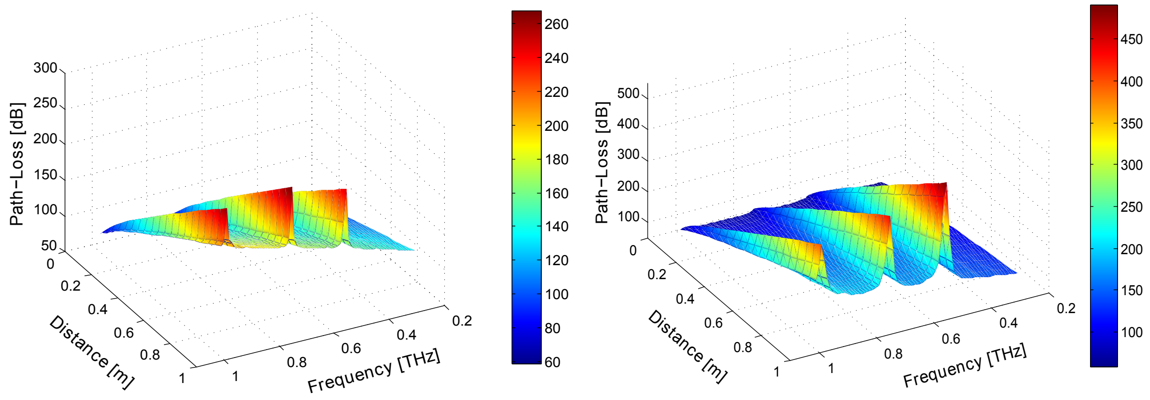

(a) Relative humidity = 10% (b) Relative humidity = 80%

Fig. 3.9 The total path-loss in the vicinity of a plant, with variable moisture ratios.

To simulate a 3D model of a plant, we can consider a cylindrical shape as the stem and oval shapes to represent leaves, which are attached to the stem at random coordinates. We can assume that the attributes of the stem and leaves, i.e., radius, thickness and so on, are random values and there can be a variable number of leaves on the plant. Then, by scattering nano-nodes at random locations on leaves, and positioning receivers on specific points on the stem, the actual length of each individual link and also the number of the shadowing leaves in that link can be calculated.

However, creating such a model is complex and computationally intensive. In addition, our main concern in such simulations is to infer the attributes of each physical link in order to determine the variation of path-loss. Concluding, rather than using such a complex model to retrieve the link attributes, in the most basic form, we can create several sets of random values in specific ranges to account for the properties of a link.

Then, regardless of the implementation type, the total path-loss can be approximated based on the obtained link attributes and by means of the proposed primary path-loss model in equation (3.7). Next, the resulting path-loss can be demonstrated by a scatter plot. Finally, the parameters of the log-distance path-loss model can be extracted by fitting a curve to the scatter path-loss plot. We use the MATLAB bisquare robust fitting tool to find the best fit values for PL_0, γ as well as the mean and standard deviation of the shadowing variable, X_σ. In the following, the simulation results are presented based on the mentioned settings.

3.5.2 The Path-Loss for Lower THz Band based on the Primary Model

Firstly, the path-loss based on equation (3.7) is plotted in Fig. 3.9, for a single radio link and different humidity ratios. We assume that the average number of leaves per unit of distance is

10 [leaves/m], and the average thickness of leaves is 160μm. This plot can provide a higher resolution insight on the loss behaviour for short distance communications at the lower THz band, as practical condition for plant monitoring nanonetworks. Once again the immense effect of leaves and humidity in the total path-loss can be seen. In addition, it can be observed that the magnitude of the path-loss has local peaks, specifically in the range 0.5–0.6THz, 0.7–0.8THz and 0.9–1THz.
We use this plot as a reference to compare against the resulting path-loss based on Monte-Carlo simulations.

3.5.3 Determination of the Type of Shadow Fading

As the first step to infer the parameters of the log-distance path-loss model, we need to determine the type of shadowing occurred by a random number of leaves and also the random proportion of the path through the air.

In order to do so, we consider the scenario where there are 10^4 nano-devices randomly scattered on the coffee plant, with a random distance in the range of 0.01–1m to their sink nodes. In addition, we assume that there exists a random number of leaves between any communicating pair, which follows the spatial Poisson point distribution with a mean equal to 10 [leaves/m]; and a random thickness in the predefined range. The transmission frequency of nano-devices is set as 0.3THz.

The resulting path-loss as a function of distance is plotted in Fig. 3.10a. In this figure the great effect of the transmission distance on the magnitude of the path-loss can be observed. To remove the effect of shadow fading from our numerical results, we averaged the path-loss values over the distance (Fig. 3.10b), which in turn simplifies the proposed model in equation (3.19) as:

$$PL_E(d)[dB] = PL_0 + 10\gamma\log_{10}(d) \tag{3.28}$$

The resulting averaged path-loss can be approximated by a regression curve as in Fig. 3.10b, whose intercept and slope define PL_0 and γ, respectively. In this figure, the reference path-loss and the path-loss exponent can be approximated as PL_0 = 128.25dB and γ = 6.93.
Subtracting the mean path-loss in equation (3.28) from the total path-loss in equation (3.19) results in data which represents the shadow fading of the transmission medium, X_σ, as shown in Fig. 3.11.

In order to determine the distribution of shadowing variable, the probability distribution function (pdf) and the cumulative distribution function (cdf) of the obtained data is presented in Fig. 3.12; and the results are compared with those of a normal distributed variable. Due

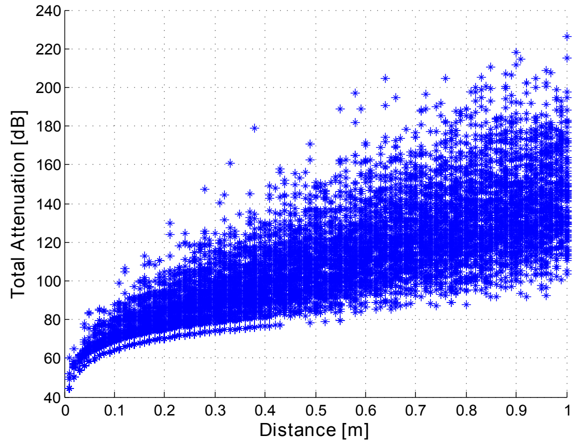

(a) Total path-loss

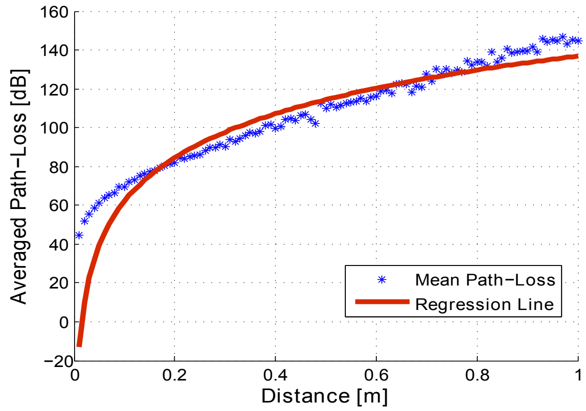

(b) Averaged path-loss and related regression curve

Fig. 3.10 The path-loss as a result of the spreading and shadow fading effects.

to the similarity with pdf and cdf of a normal distribution, the resulting shadowing in a plant environment can be considered as a log-normal random variable, defined in equation (3.20), with mean μ_s and standard deviation σ_s. In the presented results in Fig 3.10, the standard deviation and mean of the shadowing variable are equal to σ_s = 16.34 and μ_s =1.85, respectively.

3.5.4 Path-Loss based on Monte-Carlo Simulations

After determination of the shadowing type, in the next set of experiments we extract parameters of the proposed path-loss model in equation (3.19) for different transmission conditions.

Following the same assumptions as the previous experiment, we consider a nanonetwork of 10^4 nano-nodes randomly scattered on the coffee plant. This time we consider a broader

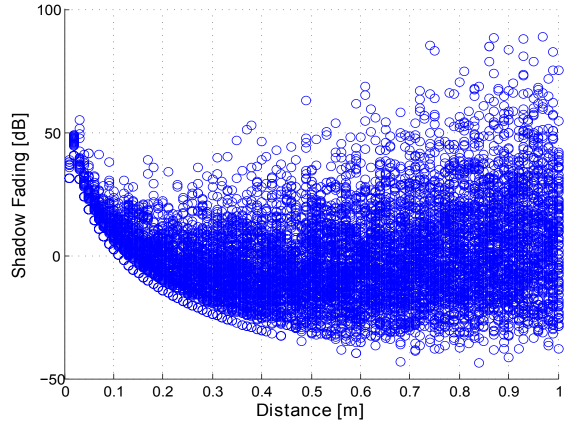

Fig. 3.11 Shadow fading effect of a medium composed of air molecules and plant leaves.

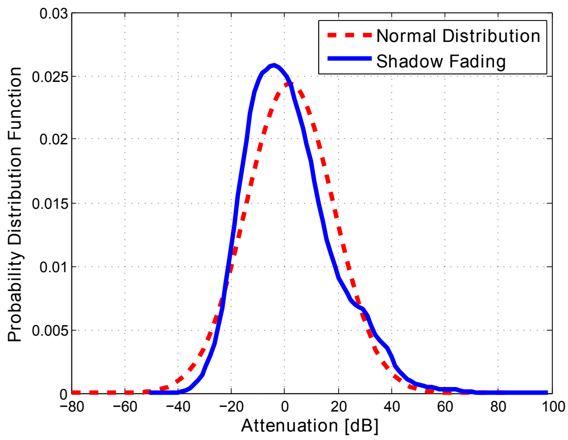

(a)

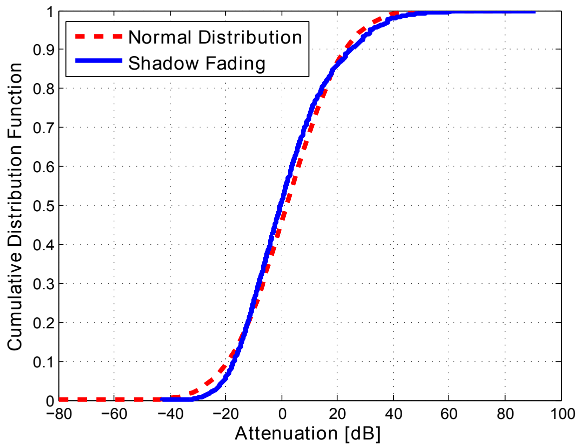

(b)

Fig. 3.12 Probability and cumulative distribution function of the shadow fading.

Table 3.1 Parameters of a log-distance path-loss model for transmission distances up to 1m.

Frequency [THz]	PL_0	γ	σ_s	μ_s
0.30	128.10	6.65	16.36	1.39
0.35	133.69	7.09	17.56	1.46
0.40	139.27	7.51	18.75	1.48
0.45	147.94	8.22	20.08	1.55
0.50	157.11	9.17	21.65	1.83
0.55	**423**.09	**35**.92	**48**.32	−**4**.37
0.60	182.59	11.53	24.57	1.79
0.65	170.73	10.48	25.09	2.11
0.70	177.77	11.18	26.45	2.28
0.75	**374**.16	**30**.57	**43**.47	−**2**.10
0.80	189.27	11.92	28.67	1.76
0.85	185.07	11.50	29.29	1.86
0.90	193.22	12.44	30.81	2.16
0.95	209.95	14.16	32.72	2.18
1.00	**289**.91	**21**.83	**38**.87	**1**.18

range of frequencies in the 0.3–1THz spectrum, and in each round of simulation we increase the frequency by 50GHz.

In Table 3.1, the extracted parameters based on the simulated path-loss values are presented for each frequency. As is shown, there are some rapid increases in the values of PL_0 at 0.55THz, 0.75THz and 1THz. These observations are in good agreement with the local peaks observed based on the primary path-loss model in Fig. 3.9.

Next, the total path-loss based on the proposed log-distance model in equation (3.19) and also the relevant parameters from Table 3.1 is presented in Fig. 3.13. The provided results suggest a higher level of path-loss at the mentioned frequencies compared to the rest of the spectrum under study, for all the transmission distances.

Finally, we compare the path-loss based on Monte-Carlo simulations and the primary model in Fig. 3.14, for a transmission distance of 1m and the same channel settings as before. It is worth noting that, in simulations we consider the variation of the input parameters in the predefined range; while, the averaged values of these parameters are used for the path-loss approximation based on the primary model. The data presented in this figure are extracted from Fig.3.9 and Fig.3.13. The results show that the proposed log-distance/Monte-Carlo based model approximates the primary model, where the former defines the path-loss variations while the latter represents the mean path-loss.

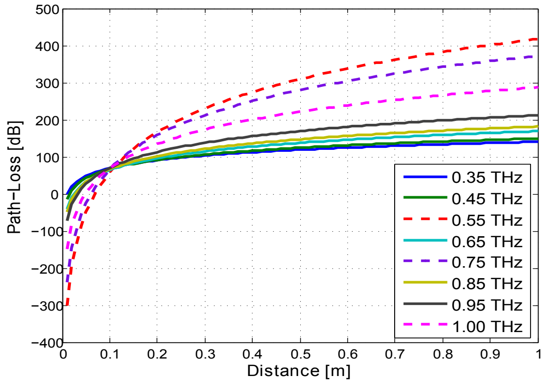

Fig. 3.13 The path-loss curves based on a log-distance model and the extracted data from Monte-Carlo simulations.

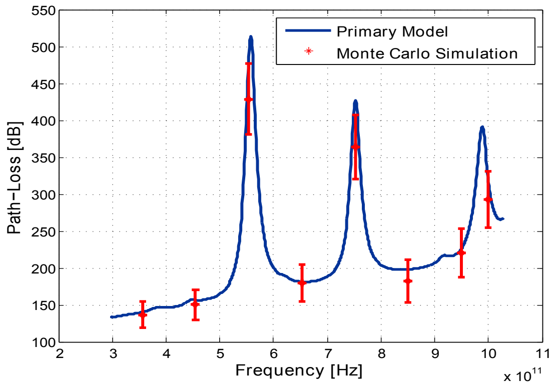

Fig. 3.14 A comparison between the path-loss curves based on the Monte-Carlo simulations and the primary model, for a transmission distance of 1m.

3.5.5 Number of Nano-Devices and the Log-Distance Path-Loss

In order to study the effect of the number of nano-nodes on the path-loss parameters, we extend the number of nano-nodes. For this purpose, we carried out the Monte-Carlo simulations by deploying 10^4, 10^5 and 10^6 nano-devices/or individual radio links. The environmental and channel settings are the same as before, in which the transmission distances vary in the range of 0.01–1m and the frequency spectrum of 0.3–1THz is covered. The resulting path-loss parameters can be observed in Table 3.2. It can be concluded that repeating the simulations for different numbers of nano-devices results almost in the same data.

Table 3.2 A comparison between the extracted path-loss parameters with different number of nano-devices/radio links.

Frequency [THz]	10^4 nano-devices				10^5 nano-devices				10^6 nano-devices			
	PL_0	γ	σ_s	μ_s	PL_0	γ	σ_s	μ_s	PL_0	γ	σ_s	μ_s
0.30	128.68	6.82	16.19	1.56	128.00	6.60	16.30	1.40	128.18	6.67	16.40	1.43
0.35	133.77	7.13	17.38	1.40	134.00	7.20	17.60	1.60	133.89	7.16	17.58	1.56
0.40	139.81	7.65	19.17	1.70	139.90	7.70	19.00	1.90	139.44	7.60	18.81	1.63
0.45	148.31	8.44	20.10	1.84	147.70	8.10	20.10	1.40	148.44	8.46	20.23	1.82
0.50	156.57	9.00	21.33	1.61	156.90	9.10	21.50	1.60	157.49	9.28	21.70	1.94
0.55	424.84	36.70	48.63	-3.81	424.20	36.40	48.60	-4.30	424.63	36.50	48.77	-4.16
0.60	183.16	11.73	24.77	2.08	183.10	11.80	24.70	2.00	182.86	11.64	24.66	1.86
0.65	170.70	10.43	24.86	1.99	170.60	10.40	25.20	2.10	170.10	10.23	25.02	1.86
0.70	176.96	10.99	26.08	1.95	176.60	10.80	26.20	1.80	176.88	10.87	26.24	1.93
0.75	374.44	30.71	43.45	-1.52	375.50	31.20	43.80	-2.00	375.91	31.27	43.96	-2.14
0.80	189.36	12.09	28.78	2.02	189.50	12.10	28.70	2.00	190.16	12.23	28.77	2.12
0.85	185.22	11.76	29.24	2.23	184.80	11.30	29.50	1.80	185.57	11.65	29.46	2.02
0.90	194.89	12.88	31.01	2.60	193.30	12.40	30.90	2.00	192.92	12.31	30.73	2.01
0.95	209.59	13.96	32.43	2.13	209.20	13.90	32.30	1.90	209.53	13.99	32.55	1.99
1.00	291.23	22.49	38.63	0.67	291.10	22.10	38.70	0.50	291.22	22.30	38.61	0.56

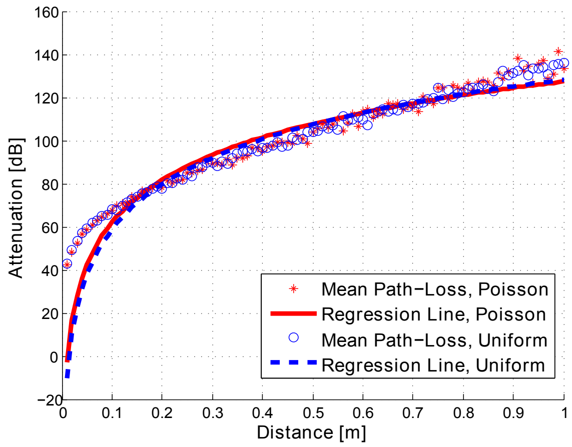

Fig. 3.15 Path-loss comparison for different distributions of leaves.

3.5.6 Leaf Distributions and the Log-Distance Path-Loss

Next, we are interested to study the path-loss parameters based on different distributions of leaves. Due to the fact that the spatial distribution of coffee leaves, or similar plant species, is not addressed in the literature, we consider spatial Poisson point and Uniform distributions for such a parameter. These distributions are generic and can simplify our analysis, whilst they can be replaced by other distribution functions. As the number of nano-nodes does not have a significant effect on the results, in this scenario we deploy 10^4 nano-devices which operate at 0.6THz. We consider the mean value of 10 [leaves/m] for both distributions. The resulting averaged path-loss is plotted in Fig. 3.15. As expected, both distributions lead to the same attenuation behavior and consequently similar values for PL_0 and γ. However, they result in different mean and standard deviation values of the shadowing variable, i.e., μ_P = 1.9 and σ_P = 24.79 for Poisson distribution versus μ_U = -4.2 and σ_U = 32.45 for the Uniform distribution.

3.5.7 Monte-Carlo based Path-Loss for Various Moisture Contents and Density of Leaves

Finally, we discuss the effect of the humidity ratio and the density of leaves on the path-loss parameters. In this case, we deploy 10^4 nano-devices in the nanonetwork, where the transmission distance vary up to 1m and the distribution of leaves is Uniform. The resulting data is presented in Table 3.3. It can be observed that for lower frequencies and a certain value of leaf density, an increase in the humidity results in a minor increase in PL_0. Whereas, for higher frequencies, PL_0 increases greatly with an increase in the humidity ratio, independent

Table 3.3 Path-loss parameters for different density of leaves and humidity ratio of air.

Leaf density [leaves/m]	Water content [%]	Frequency [THz]	PL_0	γ	σ_s	μ_s
10	10	0.30	127.05	6.47	16.40	1.42
		0.40	137.96	7.50	18.73	1.62
		0.50	146.28	8.11	21.48	1.90
		0.60	155.40	8.89	23.25	1.98
		0.70	163.40	9.60	26.00	2.08
		0.80	170.98	10.22	27.72	2.16
		0.90	179.25	10.96	30.30	2.38
		1.00	193.81	12.21	32.66	1.74
	80	0.30	128.68	6.82	16.19	1.56
		0.40	139.81	7.65	19.17	1.70
		0.50	156.57	9.00	21.33	1.61
		0.60	183.16	11.73	24.77	2.08
		0.70	176.96	10.99	26.08	1.95
		0.80	189.36	12.09	28.78	2.02
		0.90	194.89	12.88	31.01	2.60
		1.00	252.69	18.03	35.99	1.16
15	10	0.30	150.82	9.05	21.00	1.72
		0.40	163.99	10.30	23.67	2.08
		0.50	175.89	11.00	27.81	1.74
		0.60	188.31	12.18	30.43	2.19
		0.70	200.86	13.61	32.93	2.05
		0.80	209.84	13.92	36.15	1.62
		0.90	224.92	16.14	39.73	2.15
		1.00	241.13	17.23	42.47	1.56
	80	0.30	150.42	8.83	21.33	1.58
		0.40	164.93	10.13	24.50	2.03
		0.50	187.41	12.33	27.82	1.77
		0.60	215.65	15.11	31.58	1.94
		0.70	213.38	14.62	33.71	1.63
		0.80	229.24	16.11	36.97	1.55
		0.90	237.09	17.03	40.01	1.75
		1.00	340.18	27.79	49.22	−0.98

of density. It also can be concluded that for a given ratio of moisture content, increasing the average density of leaves results in a great increase in PL_0.

3.6 Summary and Conclusions

In this chapter, we introduced initial path-loss models for THz nano-communications in the proximity of plants, which can be modified based on the transmission medium characteristics, e.g., attributes of vegetation and channel composition. The proposed models mainly take the attenuative effect of air and leaves into account by incorporating spreading, absorption and leaf surface scattering loss phenomenons.

The first model, introduced as the primary model, provides an approximation of the mean path-loss based on the average values of transmission parameters, e.g., average number or thickness of the encountered leaves. The second model is log-distance based, which was introduced for an estimation of the path-loss variations around its average value. It should be highlighted that although the latter can provide more realistic approximations of the encountered loss, it is less suitable for real-time applications as it relies on simulations. Furthermore, we reviewed a THz channel capacity model, which can deploy the proposed path-loss models to estimate the theoretical data rates in such communication scenarios.

In the later discussions, we analyzed the total loss and channel capacity under different transmission assumptions, e.g., various physical attributes of leaves. Through the numerical and simulation results, we demonstrated that leaves attenuate the THz radiation to a much higher degree, compared to air. It was also shown that the attenuation cause by leaves is linear for all frequencies. However, air has a non-linear attenuation behavior across the THz spectrum, e.g., for transmission frequencies below 1THz it has local peaks in the range of 0.5–0.6THz, 0.7–0.8THz and 0.9–1THz. Such a frequency-selective behavior, which mainly depends on the moisture content of the air, splits the frequency band into several transmission windows with various widths. Transmissions in those windows will be more resilient to the air absorption effects. We also discussed the great effect of leaf attributes on signal loss, which can consequently cause a drastic reduction of the channel capacity and also the effective transmission distance in nano-communications.

The proposed models in this chapter can provide a better understanding of signal attenuation patterns in vegetation environments. Therefore, they can be deployed for an analysis of THz nano-communications in those scenarios, which will be useful in different aspects. For example, by locating transmission windows and their related bandwidths, higher level communication protocols can be used for allocating such clear frequency channels to nodes.

Chapter 4

Performance Evaluation Models

In the previous chapter, we discussed how the performance of THz communications can be affected based on frequency, variations of the medium composition - specifically the moisture content, and also the existence and the distribution of objects in the LoS communications, i.e., plant leaves. In this regard, we provided models to approximate the signal attenuation and the total channel capacity under a variety of channel assumptions.

Our proposed models can be used for an analysis on THz nanonetworks communications and describe the challenges of such networks at the physical layer. These challenges can influence the performance of communications in different terms, including the packet loss ratio, delay and so on. Hence, for the feasibility of nanonetworks applications, these effects on performance need to be studied.

However, as the research and development of THz nanonetworks are still in the early stages, the deployment of actual nano-devices in a real vegetation environment is not yet possible. As a result, the performance analysis for these networks is mainly limited to modeling. This issue, necessitates the development of precise models for the deployment environment of nano-devices as well as accurate models for performance evaluation purposes.

Therefore, in this chapter, we provide a framework which can be utilized for the analysis of THz communications in a plant monitoring nanonetwork. This framework includes models of a plant as the hosting environment, which can be modified based on the plant characteristics. Then, by using the proposed plant models, two benchmarks are defined to approximate the probability of successful transmissions across a nanonetwork. The proposed models define such a probability by taking the LoS and NLoS communications into account. The structure of this chapter is as follows: In §4.1 and §4.2, the relevant models of a plant and the probability of successful transmissions are described. In §4.3, the proposed models are evaluated and, finally, §4.4 summarizes this chapter.

4.1 Plant Models

In this section, we introduce our plant structures, as the hosting environment for a monitoring nanonetwork. In order to do so, first, we propose a simplified plant model by taking the physical attributes of a plant into account. Then, we refine the proposed model to consider more realistic communication scenarios.

4.1.1 Basic Plant Model

We assume that in specific types of plants, leaves, which are attached to the stem with certain angles, can be categorized based on their average length. According to the literature, the height of a plant can be divided into various moisture regions, depending on the ratio of water content [122], where typically those parts closer to the ground contain higher moisture levels.

Based on these assumptions, in the most basic form a plant can be modeled as I concentric cylinders, C_i, with related radius, r_i, which are centered on a stem with a given height, h, for $i = 1...I$. In this model, which is illustrated in Fig. 4.1 and Fig. 4.2, the average leaf length, L_i, the average leaf density/distribution, λ_i (average number of leaves per unit of distance), and also the leaf angle, θ_i, can be considered as constant values within individual cylinders. The classes of leaf lengths specify the total number of cylinders, I, and the radius of each cylinder can be calculated as a function of the related average leaf length and angle, e.g., $r_i = L_i.Sin(\theta_i)$.

The proposed cylindrical model can be divided into four quadrants, $Q_1 - Q_4$, on a top view. Due to the high volume of leaves, we assume that only nodes located in the same quadrant can communicate. Additionally, the plant structure can be horizontally divided into J moisture regions with relevant humidity ratios, w_j, for $j = 1...J$. All of the described parameters in this model can be extracted through measurements of specimens of a particular plant species/variety.

4.1.2 Refined Plant Model

In the previous subsection, we introduced a basic model of a plant by considering certain assumptions in the plant structure. Here, we slightly refine those assumptions to enhance the proposed model and provide more realistic scenarios for nanonetwork communications.
As stated before, in a cylindrical model, we assumed that the average leaf density/distribution, λ_i, is a constant value within individual cylinders.

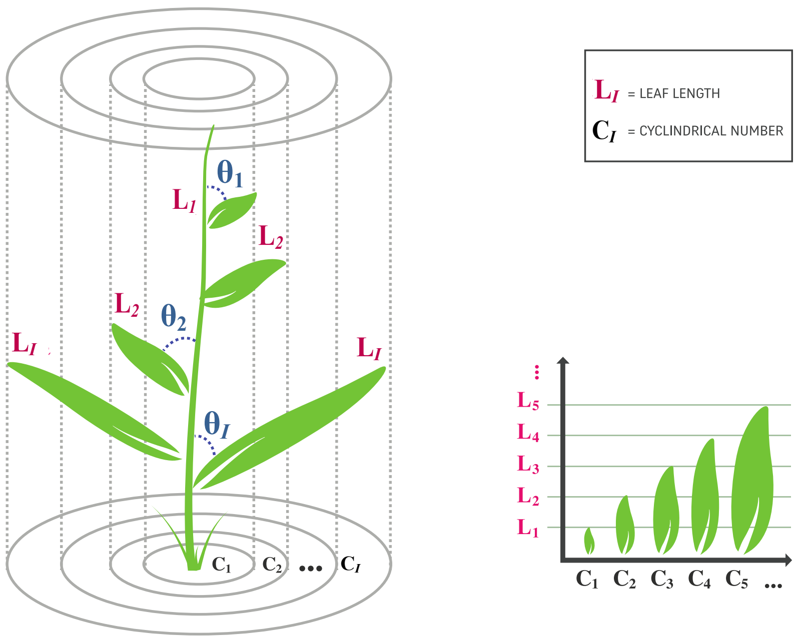

Fig. 4.1 Concentric cylindrical model of a plant.

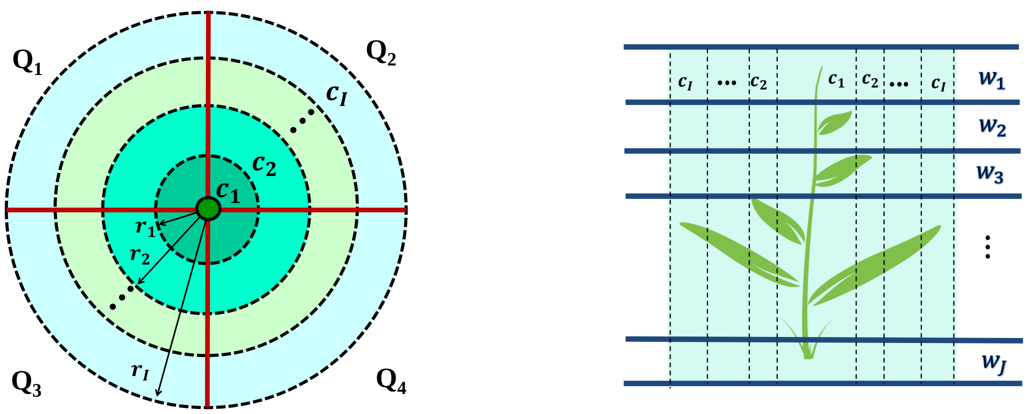

(a) Top view

(b) Side view

Fig. 4.2 Sub-division of a plant into vertical quadrants and horizontal moisture regions.

Firstly, we refine such an assumption by considering $\lambda_1 \leq \lambda_2 \leq ...\lambda_{i-1} \leq \lambda_i$, for $i = 1...I$. It means that further cylinders have a higher density of leaves compared to those closer to the stem. In other words, it is assumed that as we move from the stem towards the circumference of a plant the number of the encountered leaves increases.

In addition, previously we considered the division of the cylindrical model into four quadrants, and we assumed that if nodes are in different quadrants around the stem, they cannot communicate. However, such an assumption is not realistic as there might be cases in which the communicating nodes are in very close proximity, though located in different quadrants. Therefore, the proposed quadrant regions suggest that such nodes cannot communicate. As a result, we redefine our model by assuming that in a hierarchical topology nano-nodes can communicate if they are located in the field of view of their designated sink nodes. In other words, the quadrant-based approach would not be used anymore, but rather the field of view approach instead.

4.2 Successful Transmission Probability Models

In this section, we propose two models to measure the probability of successful transmissions across a nanonetwork. These models are introduced based on the defined plant structures and they can be categorized as follows:

1. Line of Sight Communications: The proposed model in this category requires a variety of conditions for successful transmissions; one of which is the existence of obstruction-clear radio links between communicating nodes.

   Such a condition necessitates LoS paths for successful communications, which implies that if there exists any obstacle, e.g., leaves or branches, between nodes the THz radiation cannot reach the receiver. For performance analysis of THz nano-communications, this model will be used along with the basic plant model, defined in §4.1.1.

2. Non-Line of Sight Communications: The second model can be considered as a refinement of the previous model, and it will be used together with the plant structure defined in §4.1.2. Here, we assume that NLoS communications among nodes are feasible. This statement is based on the fact that THz radiation can partially pass through obstacles such as leaves, depending on their physical and chemical properties.

Once again, it should be highlighted that these models were developed at different stages of this research work.
Next, we discuss each of the mentioned models in more detail.

4.2.1 Line of Sight Communications

The successful transmission probability across a nanonetwork depends on the following criteria [63]:

1. The energy level of the receiver;
2. The collisions between packets transmitted by interfering nano-devices;
3. The transmissivity characteristics of the THz channel;
4. The existence of obstructions in LoS communications.

By considering synchronized single-hop communications in a nanonetwork, based on handshaking and receiver initiated transmissions [81], packet loss due to lack of the energy at the receiver can be ignored.

We can also make the simplifying assumption that collisions can be ignored in the scenarios studied here. To justify this assumption, we calculate the maximum transmission duration of a fully charged nano-device, based on the following conditions:

- A pulse-based on-off keying modulation technique is deployed, where the pulse duration, T_p, and the separation periods between symbols, T_s, are 100 femtoseconds and 100 picoseconds, respectively.
- With the maximum stored energy on a nano-device, the maximum transmittable traffic, M_{bits}, is 1600 bits (considering equal probability of transmitting "1"s and "0"s, p_1 and p_0). After depleting energy, it takes almost 50 seconds for a nano-device to be fully recharged [7, 63].

Therefore, the maximum transmission duration for a nano-device, T_{tr}, can be approximated as:

$$\begin{aligned} T_{tr} &= M_{bits}\,[p_1(T_p + T_s) + p_0(T_s)] \\ &= 1600[0.5(100 \times 10^{-15} + 100 \times 10^{-12}) + 0.5(100 \times 10^{-12})] \\ &\approxeq 160 \times 10^{-9} = 160 \quad \text{nanoseconds} \\ s.t. \quad & p_1 = p_0 = 0.5 \end{aligned} \tag{4.1}$$

In order to avoid collisions, the number of required time slots, N_{slot}, can be calculated as:

$$N_{slot} = \frac{1}{T_{tr}} = \frac{1}{(160 \times 10^{-9})} = 625 \times 10^4 \quad \text{slots/sec} \tag{4.2}$$

This value can also be interpreted as the maximum number of nano-devices that can transmit concurrently at the same frequency within a second. Considering our specific application, where a limited number of nano-devices are deployed, having more than one node communicating at the same time slot and frequency band is justifiably improbable.

However, if the nanonetwork consists of a very large number of nano-devices and also if nano-devices require to transmit a huge volume of traffic, i.e., multimedia traffic, collisions can occur with a high probability. In such scenarios, a Multi Frequency Time Division Multiple Access (MF-TDMA) mechanism such as the one proposed in [118] can be deployed to provide collision avoidance as well as the efficient use of bandwidth.

Therefore, the successful transmission probability at time t can be formulated as:

$$P_{success}(t) = (1 - P_{prop-loss}(t)) \times (1 - P_{obst-loss}(t)) \tag{4.3}$$

In this definition $P_{prop-loss}(.)$ is the packet loss probability due to the attenuative characteristics of the THz channel, which depends on the intensity of the path-loss; while $P_{obst-loss}(.)$ is the packet loss probability due to the existence of an obstacle between the nodes in a LoS communication fashion.
In the following, the calculations of these probabilities are discussed.

4.2.1.1 Loss Probability due to THz Path-Loss

In order to model the probability of loss due to signal degradation, first, we define the required ratio of the channel capacity for a nano-node as:

$$R_i = \frac{Cap_i(f_i, d_i)}{A_{bits}} \tag{4.4}$$

where f_i and d_i are the transmission frequency and distance for the ith nano-node, $Cap_i(.)$ is the channel capacity at the given point and defined in equation (3.22), and A_{bits} represents the average number of bits that a fully charged nano-device can transmit in a second.

According to our previous assumptions, a nano-device can transmit a maximum of 1600 bits in a few nanoseconds and it takes almost 50 seconds to be fully recharged. Therefore, on average it can transmit 1600/50 = 32 bits/sec. Hence, R_i resembles the proportion of the

required channel capacity for the successful transmission of a nano-device.
Then, we define the ratio of the traffic that a nano-device can pass through the channel as:

$$\eta_i(t) = \begin{cases} 1, & \text{if } R_i \geq 1. \\ R_i, & \text{otherwise.} \end{cases} \tag{4.5}$$

This equation means that if $R_i \geq 1$, the available capacity is greater than the need of the nano-device, so, all its traffic can pass. Otherwise, a portion of the traffic will be lost due to the path-loss.

Finally, the the probability of loss due the path-loss can be defined based on the ratio of the aggregated traffic that cannot pass through the channel as:

$$P_{prop-loss}(t) = \frac{\sum_{i=1}^{N} (1 - \eta_i(t)).tr_i(t)}{\sum_{i=1}^{N} tr_i(t)} \tag{4.6}$$

where N is the number of active nano-devices at a given time, $tr_i(.)$ is the traffic transmitted by a nano-device.

4.2.1.2 Loss Probability due to Obstruction

Here we assume that the THz radiation cannot pass through objects, so, the existence and distribution of the plants components can greatly affect the total loss probability.
The magnitude of the encountered loss due to obstruction, $P_{obst-loss}(.)$, mainly depends on the plant structure and characteristics. Hence, we employ the introduced plant model in §4.1.1 to define this probability.

By considering a plant as concentric cylinders, which is divided into equal quadrants and also assuming a constant leaf density/distribution within a cylinder, the obstruction probability can be formulated as:

$$P_{obst-loss}(t) = \prod_{i=1}^{N} P_i^{\text{obs}-\text{loss}}(t) \tag{4.7}$$

where N defines the number of active nano-devices at a given time and $P_i^{\text{obs}-\text{loss}}(.)$ defines the obstruction probability for individual nano-devices, based on their position and distance regarding sink nodes. By assuming that sink nodes are located at fixed spots on the stem and nano-devices are randomly scattered on leaves, this probability is defined as follows:

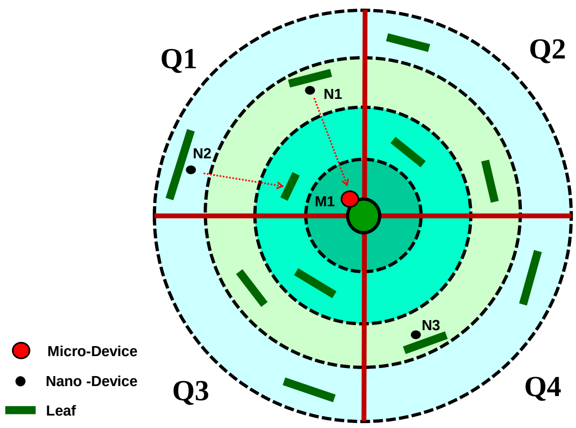

Fig. 4.3 Line of sight communications based on the proposed plant model.

- If a nano-device and its designated sink node are located in different quadrants around the stem, we assume that there exists no direct path between them. In this case, the obstruction probability is:

$$P_i^{\text{obs}-\text{loss}}(t) = 1 \tag{4.8}$$

- Otherwise, if a nano-device and its designated sink node are located in the same quadrant around the stem, the obstruction probability depends on the distance and the leaf distribution between them.

  Here, we assume the distribution of leaves follows a spatial Poisson point process. Therefore, the probability of finding k leaves between a nano-device in the mth cylinder and its sink node, which are d m apart, can be calculated as:

$$P(k \text{ in } d) = \frac{(\lambda_m d)^k}{k!} e^{-\lambda_m d} \tag{4.9}$$

  where λ_m is the average number of leaves in [leaves/m], and according to the plant model it can be interpreted as the leaf density in the mth cylinder. Finally, the probability of obstruction can be defined by having at least one leaf between the communicating nodes, i.e.

$$P_i^{\text{obs}-\text{loss}}(t) = 1 - P(k=0) = 1 - e^{-\lambda_m d} \tag{4.10}$$

As an example, the obstructed and non-obstructed communications are illustrated in Fig. 4.3. In this figure, N_1 can communicate with M_1, whereas the LoS between N_2 and M_1 is blocked. Also, N_3 cannot communicate with M_1 as it is located in a different quadrant.

4.2.2 Non-Line of Sight Communications

The proposed successful transmission probability can be further refined by considering the following conditions:

1. The energy level of the receiver;
2. The collisions between packets transmitted by interfering nano-machines;
3. The ability of the THz radiation to adequately propagate through a hybrid channel composed of obstacles and air.

According to this definition, we assume that the THz radiation can partially pass through some obstacles, e.g., plant leaves. Hence, the ratio of the propagated signal affects the probability of successful transmissions. This assumption is based on the possibility of NLoS THz communications and it is in contrast with our assumption in the previous subsection, e.g., the full blockage of THz radiation by any type of objects.

Based on our previous discussion, packet loss due to lack of energy at the receiver can be avoided by employing synchronized MAC layer protocols. We also showed that collisions are unlikely to happen in certain network scenarios, where there are only few nano-nodes in the network and the transmission rate is low due to the energy constraints.

Therefore, the probability of successful transmissions can be mainly determined based on the ratio of the THz radiation which can pass through the channel. Hence, by focusing on single-hop communications, we can redefine such a probability as:

$$P_{success}(t) = \prod_{i=1}^{N}(1 - P_i^{\mathrm{l}} l_i(t)) \tag{4.11}$$

where N is the number of nano-devices, P_i^{l} is a time independent value which determines the loss probability for individual nano-nodes, and $l_i(.)$ indicates whether a node is active at a given time. The latter depends on the active periods of a nano-nodes, T_i^{a}, and it is defined as:

$$l_i(t) = \begin{cases} 1, & \text{if } t \in T_i^{\mathrm{a}} : \{t_1, t_2, ..., t_z\} \\ & \quad where \quad t_1 = unif(T_1, T_2) \quad and \\ & \quad t_z = t_{z-1} + unif(T_1, T_2) \\ 0, & \text{otherwise.} \end{cases} \tag{4.12}$$

where $unif(T_1, T_2)$ is a uniform random value in seconds, which accounts for the full charging duration of a nano-node.

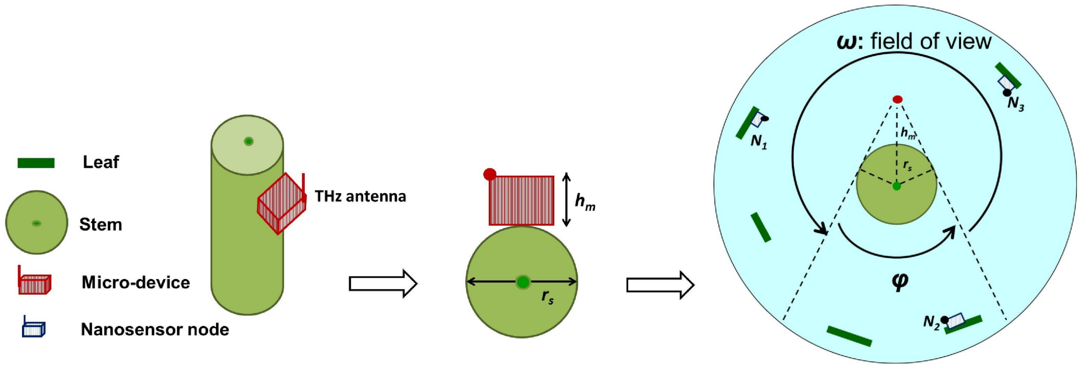

Fig. 4.4 The top view of the cylindrical plant model, demonstrating the field of view of a micro-device.

It is worth noting that equation (4.11) is proposed for a network scenario in which nano-devices are deployed at random locations on a plant for real-time monitoring of various chemical emissions. Therefore, there will be a failure in network communications if any of the nano-nodes fails to transmit its sensed data.

The loss probability for a nano-node, i.e., P_i^{l} in equation (4.11), can be defined based on the existence of an obstruction in the line of sight and also the attenuative characteristics of the THz channel. In addition, the limited field of the view of sink nodes/micro-devices can affect such a probability.

We assume that in the network structure under study, i.e., micro-devices installed on the stem, the field of the view for a micro-device is limited to a certain angle as ω. Such an angle can be approximated based on the illustrations in Fig. 4.4 as:

$$\begin{aligned} &\omega = 2\pi - \varphi \\ &\quad \textit{where} \\ &\tan(\varphi) = \frac{2\tan(\frac{\varphi}{2})}{1-\tan^2(\frac{\varphi}{2})} \longrightarrow \quad \varphi = \arctan\left(\frac{2\tan(\frac{\varphi}{2})}{1-\tan^2(\frac{\varphi}{2})}\right) \end{aligned} \tag{4.13}$$

where $\tan(\frac{\varphi}{2})$ can be calculated according to the depth of a micro-device, h_m, and the radius of stem, r_s, as:

$$\tan(\frac{\varphi}{2}) = \frac{r_s}{\sqrt{(h_m+r_s)^2 - r_s^2}} \tag{4.14}$$

Next, we propose a loss probability model for individual nano-devices, which takes their positions into account.

4.2.2.1 Nano-Device Outside the Field of View of Micro-Device

We assume, if a nano-device is outside the field of view of its designated micro-device, its radiated signals cannot reach the destination. This statement is based on the assumption that the stem does not pass the THz radiation due to its high volume of water content. Therefore, the loss probability for an individual nano-device is:

$$P_i^{\mathrm{l}} = 1 \tag{4.15}$$

For example, in the scenario depicted in Fig. 4.4, N_1 and N_3 can communicate with the micro-device, while all the communications of N_2 is obstructed by the stem.

4.2.2.2 Nano-Device within the Field of View of Micro-Device

If a nano-device is within the field of view of its sink node, the loss probability depends on the magnitude of the path-loss, which is introduced by air and possibly several layers of leaves.

In order to discuss the calculation of this probability, first, we need to review our proposed primary THz path-loss model in §3.1.2. According to that model, the path-loss in the vicinity of vegetation can be approximated as:

$$PL_{P2}(f,d) = S(f,d)\zeta(f,d)\Psi(f,d) \tag{4.16}$$

where f and d are the transmission frequency and distance, $S(.)$ stands for the spreading loss, $\zeta(.)$ is the absorption loss and $\Psi(.)$ defines the scattering loss due to surface roughness. By replacing the spreading, absorption and scattering loss in equation (4.16) with their relevant models from §3.1.2, it can be defined as:

$$PL_{P2}(f,d) = \left(\frac{4\pi f d}{c}\right)^2 e^{\alpha(f)d} e^{\alpha_s(f)d} \tag{4.17}$$

In this definition c is the speed of light in vacuum, $\alpha(.)$ is the total absorption coefficient of the hybrid transmission medium and $\alpha_s(.)$ is the total scattering coefficient. If we consider that air and leaves are the main sources of absorption and the uneven surface of the leaves is the main source of scattering, the equation above can be redefined as:

$$PL_{P2}(f,d) = \left(\frac{4\pi f d}{c}\right)^2 e^{(A\alpha_a(f)+B(\alpha_l(f)+\alpha_{s,l}(f)))d} \tag{4.18}$$

which in dB is equal to:

$$PL_{P2}(f,d)[dB] = 20\log\left(\frac{4\pi f d}{c}\right) + \\ +10d\big(A\alpha_a(f) + B(\alpha_l(f) + \alpha_{s,l}(f))\big)\log_{10} e \tag{4.19}$$

where $\alpha_a(.)$ and $\alpha_l(.)$ are the absorption coefficients of the air and leaves, respectively, and $\alpha_{s,l}(.)$ is the scattering coefficient due to the surface roughness of leaves. In this equation A and B are weighting factors, which represent the ratio of the total path traveled by the wave through the air and leaves. These factors are defined as:

$$\begin{aligned} &A = \frac{1}{d}\sum_{i=1}^{n+1} d_i^a, \quad B = \frac{1}{d}\sum_{j=1}^{n} d_j^l \approx \frac{nT}{d} \\ &s.t. \quad \sum_{i=1}^{n+1} d_i^a + \sum_{j=1}^{n} d_j^l = d \end{aligned} \tag{4.20}$$

where d is the total path length, n is the number of encountered leaves between the transmitter and receiver, $\sum_i d_i^a$ and $\sum_j d_j^l$ are the total path length through air and leaves, respectively, and T is the average thickness of leaves.

To calculate the probability of loss for a nano-node, we need to know what is the maximum number of leaves between a communicating pair that allows the correct reception of the signal at the receiver. This in turn depends on the specific distribution and physical attributes of the leaves.

We assume the path-loss threshold for THz communications is L_{th} dB, i.e., the maximum permitted path-loss for a correct signal demodulation process at the receiver. So, by replacing the desired value of the path-loss threshold in equation (4.19), and also replacing the A with its equivalent from equation (4.20), the maximum proportion of the path that can be traversed through leaves, B_{max}, can be calculated as:

$$B_{max} = \frac{\frac{L_{th} - 20\log\left(\frac{4\pi f d}{c}\right)}{10d\log_{10} e} - \alpha_a(f)}{\alpha_l(f) + \alpha_{s,l}(f) - \alpha_a(f)} \tag{4.21}$$

where f and d are the transmission frequency and distance, c is the speed of light, $\alpha_a(.)$ and $\alpha_l(.)$ are the absorption coefficients of air and leaves, and $\alpha_{s,l}(.)$ is the scattering coefficient due to surface roughness of leaves.

According to equation (4.20), we can define B_{max} based on the average thickness of leaves,

T, and also the maximum number of encountered leaves, N_{max}. Therefore, equation (4.21) can be redefined as:

$$N_{max} = \frac{\left(\frac{L_{th} - 20\log\left(\frac{4\pi f d}{c}\right)}{10 d \log_{10} e} - \alpha_a(f) \right) d}{\left(\alpha_l(f) + \alpha_{s,l}(f) - \alpha_a(f)\right) T} \tag{4.22}$$

This equation can be interpreted as if the number of leaves between any communicating pair is less than N_{max}, the total path-loss will be less than the predefined threshold, hence the signal can be demodulated at the receiver; and conversely, if the number of leaves is greater than N_{max}, the signal cannot be properly demodulated.

It should be highlighted that if the spreading loss is greater than the predefined path-loss threshold, the numerator in equation (4.22) and consequently N_{max} will be negative values. In such a case, the signal will be considered as lost and the loss probability is:

$$P_i^{\mathrm{l}} = 1 \tag{4.23}$$

In order to calculate the probability of loss for a nano-node, given positive values of N_{max}, we need to calculate the likelihood of having more than N_{max} leaves in a distance equal to d m between communicating nodes, i.e.

$$P_i^{\mathrm{l}} = P(k \text{ in } d \geq N_{max}) = 1 - P(k \text{ in } d \leq N_{max}) \tag{4.24}$$

where k is the number of encountered leaves in the LoS communication.

The precise analysis of equation (4.24) requires an accurate model of the spatial distribution of leaves in a specific type of plant. In our research, we mainly focus on the coffee plant. However, we have not found any studies on the spatial distribution of coffee leaves in the literature. As a result, we consider the latter as spatial Poisson point. Hence, according to the provided plant model, the probability of finding exactly k leaves in a distance equal to dm between a nano-device, located in the mth cylinder, and its sink node is:

$$P(k \text{ in } d) = \frac{(\lambda_m d)^k}{k!} e^{-\lambda_m d} \tag{4.25}$$

where λ_m is the average number of leaves in [leaves/m], and it represents the leaf density in the mth cylinder. To approximate the probability of having exactly or less than N_{max} leaves between two nodes, we can use the cdf of the spatial Poisson point distribution as:

$$P(k \text{ in } d \leq N_{max}) = e^{-\lambda_m d} \sum_{s=1}^{\lfloor N_{max} \rfloor} \frac{(\lambda_m d)^s}{s!} \tag{4.26}$$

Finally, by replacing the equation above in equation (4.24), the loss probability of a nano-device can be obtained as:

$$P_i^{\mathrm{l}} = 1 - e^{-\lambda_m d} \sum_{i=1}^{\lfloor N_{max} \rfloor} \frac{(\lambda_m d)^i}{i!} \tag{4.27}$$

4.3 Evaluation of the Proposed Framework

In this section, we analyze the performance of THz communications for a single radio link, based on the provided models. The intended scenario considers a nano-device which is located in the field of view of its sink node, where its radiation is shadowed by air and a random number of leaves.

Firstly, we review the environmental assumptions which are deployed in our numerical analysis. These assumptions include the characteristics of the leaves and also the transmission medium. Then, the total path-loss for free-space transmissions as well as communications in the proximity of a plant are discussed. In this case, we consider the entire THz frequency spectrum, i.e., 0.3–10THz, and also transmission distances up to 1m. Next, by focusing on a more practically realizable case, i.e., a frequency range of 0.3–0.8THz [100] and distances up to 0.5m, the path-loss threshold range is defined and the maximum allowed ratio of leaves in the transmission path is studied. In our numerical study, we vary a combination of parameters such as the humidity ratio of the medium and the attributes of leaves to study their effect on the link performance.

Finally, through varying environmental conditions and the path-loss threshold limits, the loss probability based on the proposed models is discussed.

4.3.1 Numerical Study Setting

In this subsection, the general transmission conditions are reviewed. The numerical analysis of the proposed models is performed based on these specifications.

4.3.1.1 Transmission Conditions

We study THz communications in the vicinity of a coffee plant, where plant leaves are considered as the main source of signal obstruction. Therefore, the THz waves propagate in free-space or alternatively through a hybrid channel composed of air and leaves.

In our numerical study, we assume the transmission of Gaussian pulses with a sub-channel width of 50GHz, and in a medium that can contain 10% or 80% of moisture. The average number of leaves between the communicating nodes varies in the range of 5 – 20 [leaves/m] and the average leaf thickness is considered as 100μm.

The total attenuation due to absorption and scattering of a fresh leaf, i.e., $\alpha_l(.) + \alpha_{s,l}(.)$ in equation (4.19), are set based on the measured data in [52]. As the ratio of the travelled path through leaves, i.e., B in equation (4.20), we consider values of 0.001 and 0.01.

4.3.2 The Total Path-Loss for Distances Up to 1m

As the first experiment, the total path-loss is presented in Fig. 4.5, based on equation (4.18). In this figure, the signal loss for transmission distances up to 1m and the entire THz band is presented. The moisture level of the air is considered as 10% and 80% to convey two extreme conditions. In addition, we account for communications in free-space as well as a sparse and a dense plant by considering $B = 0$, $B = 0.001$ and $B = 0.01$, respectively. It is worth noting that, earlier, the path-loss was studied in §3.4.3 for only a subset of transmission distances. Therefore, the provided results in this section can be considered more comprehensive.

Firstly, it can be observed that for a fixed humidity ratio, an increase in B and consequently the number of encountered leaves causes a considerable increase in the path-loss. Therefore, the effective transmission distance is decreased greatly. Secondly, for a fixed value of B an increase in the moisture content results in an increase of the path-loss at certain discrete frequencies. Finally, a comparison between all plots shows that leaves have a higher impact on attenuating the THz radiation compared to the moisture content of the air.

4.3.3 Path-Loss Threshold Definition

To analyze the loss probability across a radio link with a random number of leaves, a value for the path-loss threshold, L_{th}, should be defined and justified. As previously demonstrated, the path-loss varies along with several parameters, such as the moisture level of the medium, transmission distance and frequency, leaves attributes and so on.

In order to take the variations of the path-loss into account, we calculate the upper and lower bounds of this parameter by considering the best and the worst transmission conditions.

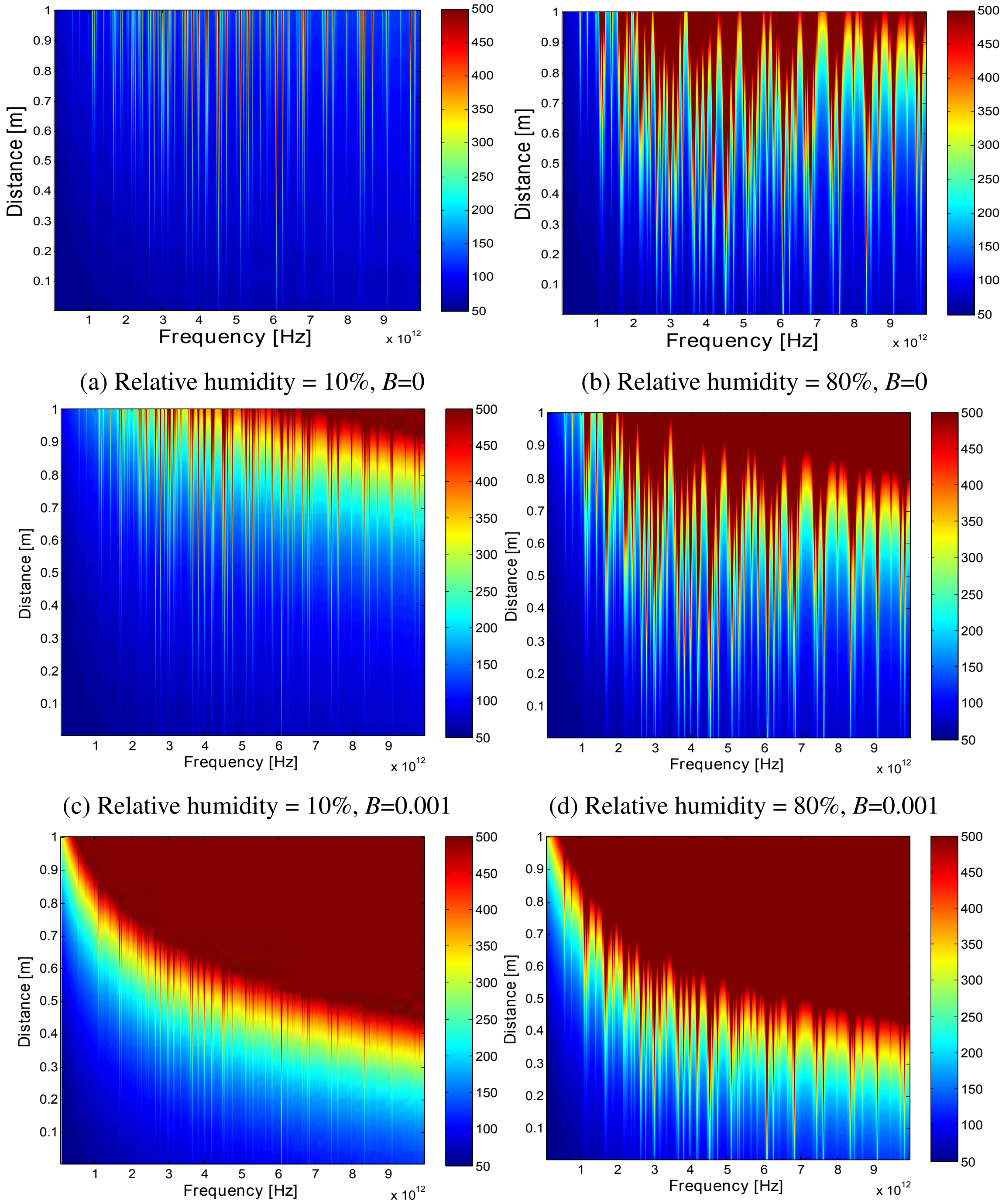

(a) Relative humidity = 10%, *B*=0

(b) Relative humidity = 80%, *B*=0

(c) Relative humidity = 10%, *B*=0.001

(d) Relative humidity = 80%, *B*=0.001

(e) Relative humidity = 10%, *B*=0.01

(f) Relative humidity = 80%, *B*=0.01

Fig. 4.5 The total path-loss as a function of distance and frequency, for different humidity levels in the air and the proportion of path through leaves, *B* (the presented results are truncated at 500 dB). Plots (a) and (b) represent the path-loss in free-space, plots (c) and (d) are the path-loss in a sparse plant environment, and plots (e) and (f) show that of a denser plant.

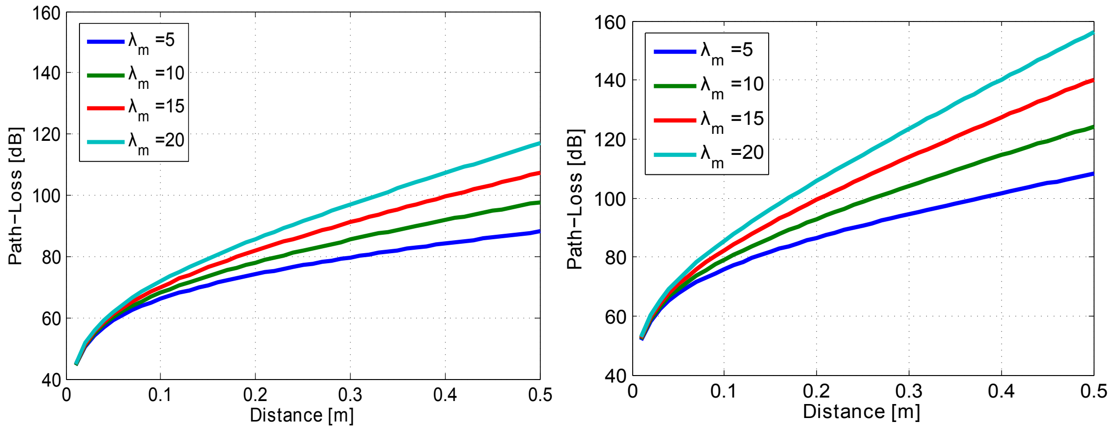

(a) Relative humidity= 10% , Frequency = 0.3THz

(b) Relative humidity= 80% , Frequency = 0.8THz

Fig. 4.6 The total path-loss [dB] for a variety of leaf ratios in [leaves/m]; where (a) represent the best and (b) shows the worst transmission conditions.

Hence, we can assume that the total path-loss for the rest of the scenarios will fall into the defined boundaries. To account for a more practical condition, we limit the previous scenario by considering the maximum transmission distance as 0.5m and a frequency range of 0.3–0.8THz; while having the same moisture levels. Therefore, the transmission frequency and a moisture level of 0.3THz and 10% can be considered as the best communication scenario; whereas these parameters for the worst case transmission can be considered as 0.8THz and 80%.

In Fig. 4.6, the total path-loss versus distance is plotted for a variety of the average number of leaves, i.e., $\lambda_m = 5,...,20$ [leaves/m], and the average leaf thickness of 100μm. Therefore, the required path-loss threshold in a specific plant type can be inferred, given its statistical leaves distribution. For example, by assuming the average number of leaves per unit of distance in a typical coffee plant as 15 [leaves/m], the path-loss threshold can be considered in the range of 110–140dB. Similarly, if an average of 5 [leaves/m] is assumed, then the path-loss threshold need to be defined in the range of 90–110dB.

4.3.4 Analysis of the Maximum Number of Leaves

After defining the threshold values for path-loss, we want to discuss the maximum allowed number of leaves, N_{max}, based on such values. The latter affects the signal degradation level and consequently the probability of loss for individual radio links.

In this regard, the variation of N_{max} is studied based on equation (4.22) and by varying different parameters such as distance, frequency and the path-loss threshold. Here, we consider the transmission distances up to 0.5m, the frequency range of 0.3–0.8THz and moisture levels of 10% and 80%. Following the assumption of previous experiment, average number of leaves is considered as 15 [leaves/m], which results in a path-loss threshold of 110–140dB.

In Fig. 4.7, it can be observed that for 10% of moisture content, an increase in the frequency or distance results in an almost steady decrease of the number of leaves for both values of threshold. Whereas, for a high moisture content equal to 80%, an increase in the frequency can result in a rapid decrease **or** increase in the maximum leaf number. This peculiar behavior, specifically for distances over 0.2m is due to the variable magnitude of molecular absorption and noise which affects random THz frequencies.

To justify this claim, the total path-loss for the same frequencies and moisture levels and also a subset of transmission distances, i.e., 0.2, 0.3, 0.4 and 0.5 m, is presented in Fig. 4.8. As it is shown, the magnitude of the path-loss for a higher moisture content has local peaks, specifically in the range 0.5–0.6THz and 0.7–0.8THz. It can be concluded, when these peaks occur, there is less link budget left for attenuation by leaves and the maximum number of leaves drops accordingly (in Fig. 4.7), before rising again as we move away from the peak.

4.3.5 Loss Probability for a Single Radio Link

Finally, we want to analyze the loss probability for a single radio link scenario. As stated before, the aggregated loss probabilities of the individual nano-devices determine the total probability of the loss/success of nano-network communications.

In our study, we deploy equation (4.27), while covering transmission distances up to 0.5m and two frequency bands of 0.3THz and 0.8THz. In addition, by assuming the average number of leaves in the plant as 15 [leaves/m], we consider a subset of path-loss thresholds, i.e., 110, 120, 130 and 140 dB.

As the loss probability is defined based on the maximum number of leaves in a link (according to equation (4.27)), first, we plot N_{max} for the aforementioned transmission conditions in Fig. 4.9a and Fig. 4.9b. In these plots, an increase in the distance shows a step-shaped and gradual decrease in the maximum allowed number of leaves. The observed step behavior in these figures are due to rounding up the calculated values of N_{max}, based on equation (4.22).

Then, by employing the extracted N_{max} values, the resulting loss probability for the same channel conditions are presented in Fig. 4.9c and Fig. 4.9d. It can be observed that whenever the number of leaves stays constant over distance, it results in a steady increase in the related loss probability. Whereas, whenever the number of leaves changes at a given distance, it causes a step behavior in the loss probability value as well. In addition, a comparison between

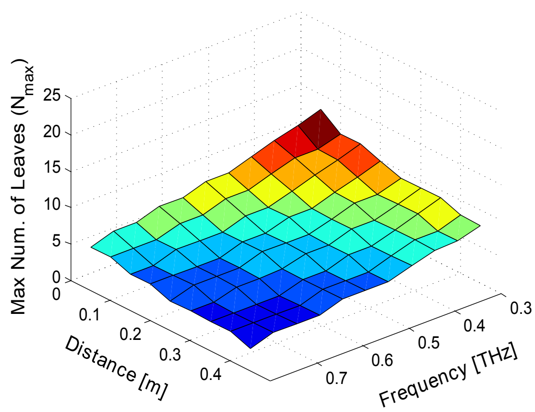

(a) Relative humidity= 10%,
Path-loss threshold = 110dB

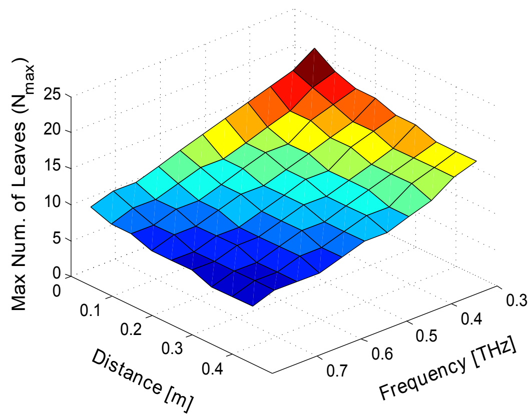

(b) Relative humidity= 10%,
Path-loss threshold = 140dB

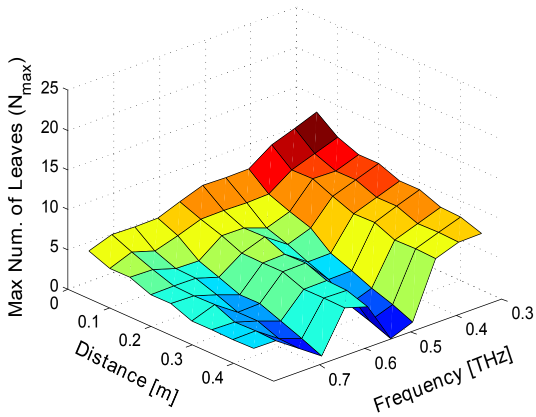

(c) Relative humidity= 80%,
Path-loss threshold = 110dB

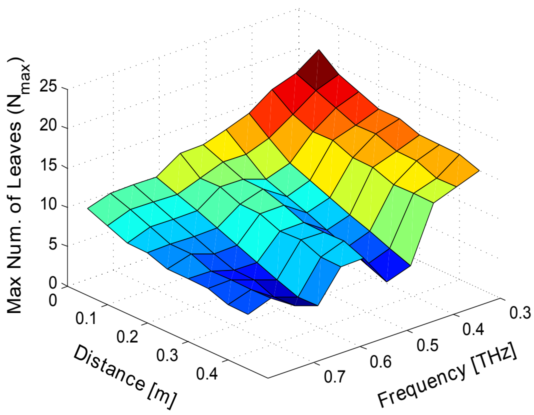

(d) Relative humidity= 80%,
Path-loss threshold = 140dB

Fig. 4.7 Maximum number of leaves for a given channel condition and predefined path-loss thresholds.

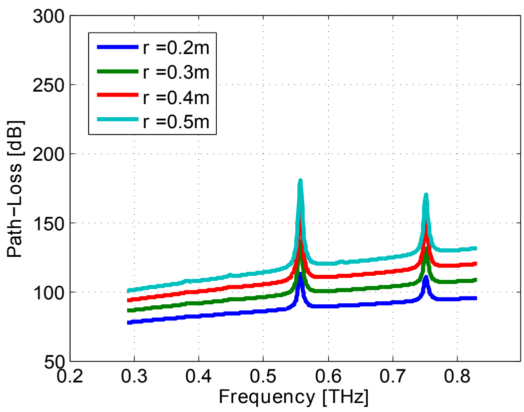

(a) Relative humidity= 10%

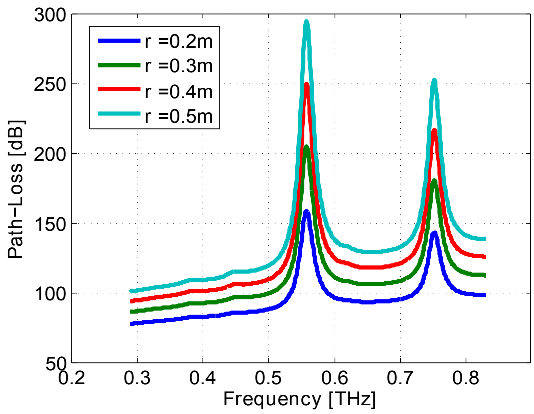

(b) Relative humidity= 80%

Fig. 4.8 The total path-loss for specific transmission distances.

the loss probability plots shows the high impact of the moisture content, frequency and also the path-loss threshold on the effective transmission distance.

4.4 Summary and Conclusions

In this chapter, we proposed a framework to evaluate the performance of THz communications across a plant monitoring nanonetwork. This framework includes abstract models of a plant, which can be modified based on the physical characteristics of a plant. In addition, it can accommodate different plant types. For the performance analysis purposes, this framework also includes models to approximate the probability of successful transmissions for LoS and NLoS communications.

Through numerical study, we approximated the total path-loss for transmission distances up to 1m, and based on the obtained results, we defined a boundary for the path-loss threshold. The proposed boundary, which depends on the structure of the plant and the communication scenario, can be utilized for defining the demodulation threshold at the receiver. The latter can be considered as an initial guideline for receiver design purposes.
Then, we analyzed the effects of the channel conditions and also the boundaries of the path-loss threshold on the maximum number of leaves that can be encountered along the transmission path, and consequently the performance of single radio links in terms of loss.

Our analysis suggests that the plant characteristics, e.g., the thickness and density of leaves, the moisture content of the medium, transmission frequency and also the path-loss threshold have a great impact on the performance of THz nano-communications. Therefore, for network design purposes, all such parameters should be taken into account to provide the desired performance level. The provided models and analysis can form the foundation of vegetation monitoring applications of WNSNs.

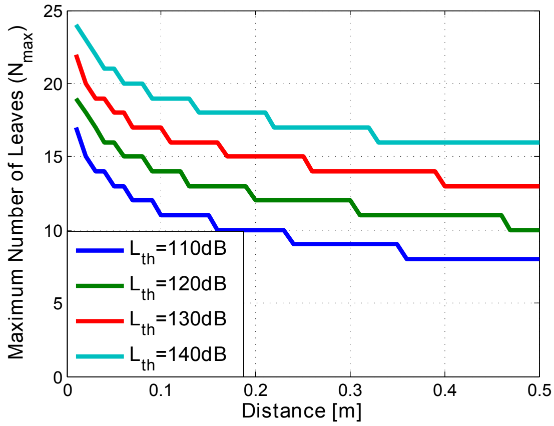

(a) Relative humidity= 10%,
Frequency = 0.3THz

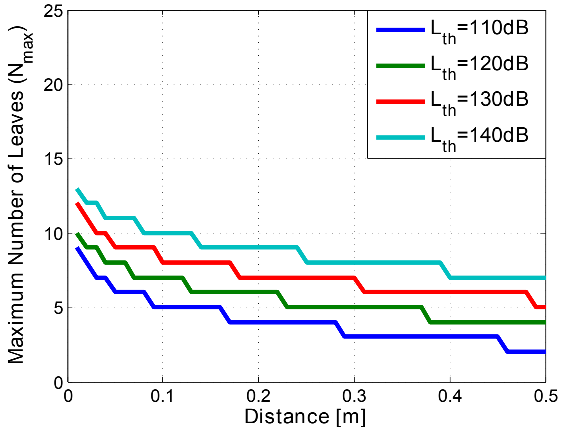

(b) Relative humidity= 80%,
Frequency = 0.8THz

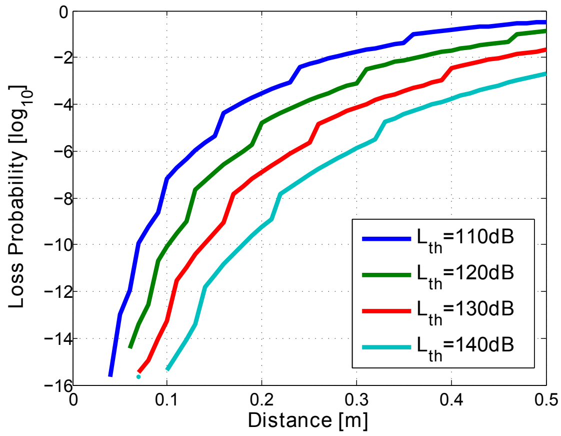

(c) Relative humidity= 10%,
Frequency = 0.3THz

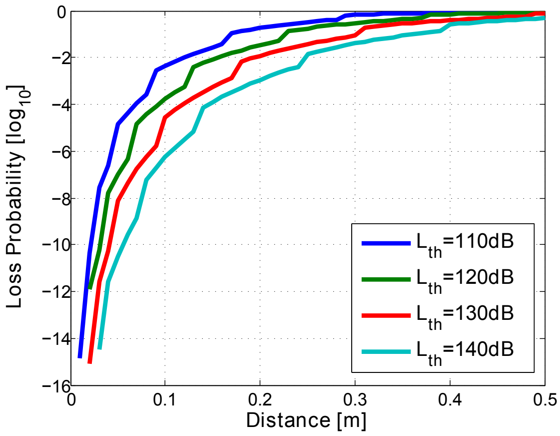

(d) Relative humidity= 80%,
Frequency = 0.8THz

Fig. 4.9 The maximum number of leaves for a certain transmission condition and predefined path-loss thresholds in (a) and (b). The resulting loss probability for a single radio link in (c) and (d).

Chapter 5

Dynamic Channel Allocation in Plant Monitoring Nanonetworks

One of the main goals of channel allocation techniques in traditional wireless networks is to share the bandwidth among nodes in order to offer an efficient use of the spectrum, as well as preventing collisions among concurrent transmissions of adjacent nodes. Such mechanisms can be implemented in a static or a dynamic fashion, depending on the network condition and mobility of nodes.

According to our discussion in the previous chapters, there exists a high level of signal loss and distortion at specific frequencies in the THz channel. It was shown that such a loss has a great influence on the performance of communications across single radio links, and consequently the overall performance of nanonetworks. However, as this phenomenon has various effects on different frequencies, it can be controlled/decreased by efficient channel assignment to nano-nodes.

Therefore, in addition to all the mentioned benefits, channel allocation mechanisms can be considered as a means to decrease the signal loss, and hence to improve the performance of THz nanonetworks. Focusing on monitoring applications of nanonetworks, the deployed frequency assignment techniques need to take the variations of the environmental conditions into account. As a result, dynamic channel allocation seems to be well aligned with the requirements of such applications.

In this chapter, we propose several bio-inspired strategies for dynamic channel assignment to nano-devices. The proposed approaches, which are based on the capability of graphennas to be tuned to the desired frequency, aim to optimize several performance metrics in a vegetation monitoring nanonetwork, i.e., optimizing the achievable channel capacity, power consumption, spectrum utilization and so on. Then, by deploying our proposed framework from the previous chapter, we analyze the performance of the introduced strategies under various plant and network configurations.

We emphasize that the introduced approaches are developed based on a prior knowledge of the nanonetwork environmental condition and also the position of nano-nodes. Hence, their direct application in a real world scenario can be challenging, due to the resource constraints of nano-nodes. As a result, the proposed approaches should be considered as a guideline, defining the ideal communications setting for nanonetworks, which need to be approximated by real world implementations.
The structure of this chapter is as follows: In §5.1, the frequency tuning capabilities of graphennas are discussed and several strategies for such a purpose are introduced. We propose our performance optimization algorithms in §5.2. Then, we evaluate the proposed strategies in §5.3 and summarize this chapter in §5.4.

5.1 Dynamic Frequency Tuning of Nano-devices

As the molecular absorption and noise in the THz spectrum are frequency-selective, dynamic channel assignment to nodes can make nano-communications resilient to high power loss. In this regard, first, we discuss the frequency tunability of graphennas and the required energy in this process. Then, based on such a capability at the physical layer, we discuss several frequency selection strategies, which can be implemented in the data link layer.

5.1.1 Frequency Tuning of Graphennas

The resonance frequency of graphennas can be tuned statically or dynamically [75]. In this thesis, we focus on dynamic frequency tuning approaches, which enable the dynamic channel assignment to nano-nodes according to the medium conditions and also the transmission distance. The dynamic frequency selection can be performed by varying the electrical conductivity of the graphenna. The latter is a function of the chemical potential of the graphene sample, which can be manipulated through applying an electrostatic bias voltage to the nano-antenna. The required energy to shift the resonance frequency, f, of a graphenna patch can be approximated based on curve fitting of data provided in [75], as:

$$\begin{aligned} E(f) =& 0.048\times f^2 - 0.005\times f - 0.033 \\ & \forall f > \ 0.918 \text{ THz} \end{aligned} \tag{5.1}$$

This equation suggests a quadratic relation between the frequency and the required energy consumption to tune the antenna into the desired channel.

5.1.2 Frequency Selection Strategies

In general, we assume that the monitoring nanonetwork under investigation follows a hierarchical and cluster-based structure, composed of nano-devices and micro-nodes/sink nodes, i.e., the discussed topology in §2.1.3.2. In such a structure, nano-devices will be triggered by detecting certain chemical substances in the environment, and consequently they transmit their sensed data to a designated micro-device.

In addition to the proper channel assignment to nano-nodes, an efficient sink node/cluster selection approach can improve the overall performance of nanonetwork communications. Such an approach needs to take the proximity of nano-nodes to their sink nodes and also the balanced distribution of nano-nodes among sink nodes into account. The former promises a higher channel capacity for each nano-device, while the latter ensures a fair energy consumption at the micro-device level.

In the following, we investigate several frequency selection strategies for nano-devices, which are accompanied by an initial approach for the micro-node assignment. We measure the performance of these strategies in different terms, including balancing the number of nano-devices among micro-devices, minimizing the associated energy consumption through the frequency tuning process and also maximizing the aggregated channel capacity.
Next, we formally define our target objectives, which should be satisfied while finding a solution.

5.1.2.1 Distribution of Nano-Nodes Among Micro-Devices

We define the first objective as balancing the number of nano-nodes among micro-devices/clusters, which can be formulated as:

$$Obj_1 = max \left(\frac{1}{\sum_{q=1}^{Q} \frac{1}{ND_q}} \right) \tag{5.2}$$

where Q is the total number of micro-devices/clusters in the nanonetwork and ND_q represents the total number of nano-devices assigned to the qth micro-device. Through this objective, we aim to ensure a fair distribution of nano-devices among micro-devices.

5.1.2.2 Energy Consumption

As stated earlier, the frequency tuning of graphennas is a energy consuming process. Therefore, we introduce the second objective as minimizing the energy consumption associated with the frequency tuning process of nano-devices. This objective can be defined as:

$$Obj_2 = min\left(\sum_{k=1}^{ND} E(f_k)\right) \tag{5.3}$$

where ND is the total number of nano-devices, f_k is the selected transmission frequency for the kth nano-device and $E(.)$ is the required energy for tuning a nano-antenna at f_k, which can be calculated from equation (5.1).

5.1.2.3 Channel Capacity

According to the channel capacity model discussed in §3.3, we define the last objective which tries to tune the frequency of nano-devices based on transmission conditions. This objective aims to maximize the aggregated channel capacity of the nanonetwork according to different strategies; namely as Basic, Off-line, Constraint-based, Swarm-based and Two-phase.
In the following, these strategies are discussed and formulated.

1. *Basic*: This strategy aims to optimize the total channel capacity through maximizing the capacity for each individual nano-device. This goal can be achieved through dynamically tuning the operational frequency of nano-devices to the most noise and absorption resilient frequency, regarding the channel conditions. Here, frequency overlapping is allowed, therefore among the selected frequencies, duplication or even convergence to the best frequencies can be observed. To avoid the probable collisions in this case, a time division mechanism can be employed, which prevents the transmission of the nano-nodes with the same frequency at the same time. This objective can be formulated as:

$$Obj_3 = max\left(\sum_{i=1}^{ND} Cap(f_i, d_i)\right) \tag{5.4}$$

where ND represents the total number of nano-devices, f_i defines the allocated frequency to the ith nano-device, d_i is the distance between the ith nano-device and its designated micro-node and $Cap(.)$ is the channel capacity function based on equation (3.22);

2. *Off-line*: This strategy maximizes the channel capacity of the nanonetwork based on the precalculated data, in an off-line fashion. Here, we assume that the best transmission frequencies in the desired THz band are calculated for a variety of destinations and also medium conditions; and the obtained data is stored in a database. Therefore the frequency assignment process is performed by retrieving the data from the database, given the transmission conditions of individual nano-devices.

   Similar to the Basic approach, this strategy can result in frequency duplication and it needs to be accompanied by a time division multiple access algorithm to avoid potential collisions. This approach can be formulated the same as in equation (5.4) and depending on the nanonetwork size and the computational resources, it might be costly under certain network scenarios;

3. *Constraint-based*: While trying to maximize the aggregated channel capacity, this approach prevents any overlapping of frequencies through defining hard constraints. This strategy is well suited to a frequency division multiple access algorithm to mange transmissions within the nanonetwork. This objective can be formulated with the same parameters as:

$$\begin{aligned} &Obj_3 = max\left(\sum_{i=1}^{ND} Cap(f_i, d_i)\right) \\ &s.t. \\ &f_i \neq f_j, \quad \forall j = 1, 2, \cdots ND, \quad i \neq j \end{aligned} \tag{5.5}$$

4. *Swarm-based*: Providing the same general goal as previous strategies, this approach ensures that no frequency overlapping exists between interfering nano-devices. It also ensures that there is an efficient use of the THz spectrum. To satisfy such goals, this approach utilizes a biological swarming mechanism proposed by Gazi and Passino [35, 36], through the introduction of frequency attraction/repulsion functions. Equation (5.6) formulates this objective, where the first term tries to maximize the capacity and the second term tries to avoid frequency overlapping among nano-devices, while controlling the spread of frequencies across the desired band:

$$Obj_3 = max\left(\sum_{i=1}^{ND} Cap(f_i, d_i) - \frac{1}{2}\sum_{i=1}^{ND}\sum_{j=1, j\neq i}^{ND} a_{ij}.g(f_j - f_i)\right) \tag{5.6}$$

   where all the parameters are the same as described above and a_{ij} is an element taken from the adjacency matrix of the network. Such a matrix represents the connectivity

of the nano-nodes in the nanonetwork, i.e., if nano-devices i and j are interfering the related element is “1” otherwise it is “0”. In the equation above, $g(.)$ is a function which represents the attraction and repulsion between selected frequencies.
This function has the following format:

$$g(f_j - f_i) = \big(g_a(f_j - f_i) - g_r(f_j - f_i)\big)\,|f_j - f_i| \tag{5.7}$$

where $g_a(.)$ and $g_r(.)$ represent attraction and repulsion functions, respectively.

In this thesis, we consider a constant attraction and a bounded repulsion, which can be defined as following:

$$\begin{aligned} g_a(f_j - f_i) = C_A, \quad g_r(f_j - f_i) = \frac{C_R}{(f_j - f_i)^2} \\ s.t. \\ C_A, \quad C_R > \quad 0 \end{aligned} \tag{5.8}$$

where C_A and C_R are the attraction and repulsion constants.
The deployment of the aforementioned swarming mechanism can be beneficial in different aspects, including:

- Frequency reuse among non-interfering nano-devices;
- Swarming the nanonetwork around a central frequency, i.e., $\frac{1}{N}\sum_{i=1}^{N} f_i$, which controls the spread of frequencies across the band and enables efficient use of the spectrum;
- Shorter frequency hops for micro-devices, hence reducing energy consumption at the micro-device level.

It is worth noting that the degree of attraction/repulsion between selected frequencies depends on the deployed swarming functions and also the constants, i.e., C_A and C_R;

5. *Two-phase*: This approach seeks to maximize the aggregated capacity in a two-phased fashion. In the first phase, the best transmission frequencies are located by deploying the introduced Off-line strategy. Then in the second phase, the output of the first phase is fed to the Swarm-based strategy, i.e., equation (5.6), to avoid any frequency duplication between interfering nano-nodes and to control the spread of frequencies.

We emphasize that the introduced objectives can be in contrast. For example, the energy consumption function in equation (5.1) shows a quadratic relation between the transmission

frequency and the consumed energy during the frequency tuning, which implies that the energy consumption is minimized by tuning the graphennas into lower frequencies, while the channel capacity maximization objective will not be necessarily satisfied by transmitting at lower frequencies, due to the random molecular absorption and noise in the THz band.
Similarly, the first objective of fair distribution of nano-nodes among micro-devices and the third objective of the maximization of the channel capacity cannot be simultaneously satisfied. Meaning that, while the former tries to assign an equal number of nano-devices to each micro-node, the latter tries to assign the closest sink node to each nano-device in order to maximize the channel capacity.

5.2 Performance Optimization by Genetic Algorithms

In the previous section, we introduced several frequency assignment algorithms in order to optimize several objectives. Since this optimization problem is multi-objective in nature, we need to employ heuristic solutions such as Genetic Algorithms (GAs) to define the most efficient communication setting for a nano-device. Therefore, we use a weighted sum multi-objective GA approach, which is defined in Appendix A. The proposed method suggests the definition of separate objective functions, Obj_s, according to the number of intended objectives, S, and assignment of weights, W_s, to each of the them, for $s = 1, 2, ..., S$. Hence, by summing up the weighted normalized objective functions, the problem can be converted into the optimization of a single objective problem as:

$$Obj_f = W_1.Obj_1 + W_2.Obj_2 + \ldots + W_S.Obj_S \tag{5.9}$$

In such an approach, the objective functions can have equal weights if they have the same level of importance; otherwise, they can have various weighting factors.
It is worth noting, the proper selection of GA parameters, e.g., the population size, mutation and elitism rates and so on, can guarantee the efficiency of the found solutions as well as the convergence time of the algorithm.

Our proposed GA-based frequency and sink node selection algorithm is presented in Alg. 5.1. Upon running, this algorithm randomly divides the nano-devices into clusters by assigning a random micro-device to each of them. Then, it assigns a random operational sub-frequency in a predefined boundary to each of the nano-devices. Following this step, the efficiency of the frequency and micro-device assignments is evaluated against the intended objectives.

In the next phase, the algorithm tries to improve the objective values by assigning different frequency and micro-device to each nano-device, through crossover and random mutation

Algorithm 5.1 The frequency and sink node selection approach, based on Genetic Algorithms.

Inputs:

F_{range}: Intended frequency range, Ch_{comp}: Channel composition,
Q :Number of micro-devices, ND: Number of nano-devices,
N_{ind}: Population size, G_{gap}: Generation gap,
P_{mut}: Mutation probability, δ: Number of iterations,

Outputs:

$N_{ind} \times ND$ solutions in (M_i,f_i) format, where
M_i: Designated micro-device id for the ith nano-device,
f_i: Selected frequency for the ith nano-device

Main algorithm:

Generate N_{ind} rows of ND random pair of solutions, (M_i,f_i);
Save them in population Pop;
for $r = 1$ to δ **do**
    Evaluate Pop based on objectives;
    Select $N_{ind} \times G_{gap}$ of the best solutions in Pop;
    Save them in population Pop_1;
    Crossover population of Pop_1;
    Mutate population of Pop_1 with probability of P_{mut};
    Evaluate Pop_1 based on objectives;
    Update Pop with best solutions in Pop_1;
end for
Return the Pop as the best solutions

operands. Then, it evaluates the efficiency of new assignments and replaces the old solutions with a proportion of the new improved solutions. This loop continues for a certain number of generations, or alternatively, the convergence of the solutions to assure that the best solutions have been found. The final output of this algorithm defines the best pair of micro-node and frequency for each of the nano-devices, in order to satisfy a subset of objectives.

Here, we assume that micro-devices are interfaces between nano-devices and external networks. Hence, for the sake of the computational complexity of the GA-based mechanism, we assume that the proposed algorithms are being run on an external computationally efficient resource, e.g., a cloud service. Therefore, the micro-devices retrieve the optimized settings and dictate them to the nano-nodes to dynamically tune their antennae. Then, the micro-devices in each cluster start a frequency hopping process to probe and collect the data from nano-devices based on the dictated frequencies.

5.3 Evaluation of the Dynamic Channel Allocation Algorithms

We now analyze the performance of our proposed strategies, based on the associated nanonetwork and channel models defined in chapter 3 and also the introduced framework in chapter 4.
In this regard, we consider two different configurations:

- Scenario 1: This configuration is based on the LoS communications and by deploying the basic quadrant-based model of a plant. In this case, we chose a maize plant and we assume that the THz radiation cannot pass through the plant leaves. As a result, any such radiation will be fully absorbed by leaves. In addition, we consider the free-space THz propagation model.
- Scenario 2: This configuration is based on the NLoS communications and according to the refined plant model. Here, we assume that the THz radiation is not fully blocked by leaves, but rather a ratio of it can pass through, as shown in [99]. In this case, we select coffee as the plant type, and we consider the hybrid channel model for THz radiation through air and leaves.

We highlight that the selection of these plants species are based on the limited literature in this area. In the following, we discuss the general simulation setting used for our experiments. Then, we specify our assumptions for each of the plant types and communication scenarios. For each of the mentioned scenarios, we vary a combination of parameters including the number of nano- and micro-devices, the moisture ratios and also the leaf density to measure the performance of the resulting nanonetwork. We evaluate the performance of communications in different contexts, including the aggregated channel capacity, efficient spectrum utilization, fair distribution of nano-nodes among micro-devices, probability of successful transmissions and so on.

5.3.1 General Simulation Setting

In this section, we review our general simulation settings for the components of the nanonetwork and also the specifications of the deployed GA. These settings are in common for simulations based on scenario 1 and scenario 2.

5.3.1.1 Nanonetwork Specifications

The nanonetwork under study is composed of micro-devices, nano-devices and data relaying gateways. However, we are only concerned about the details of nano-devices. Here, we assume the deployment of chemical nano-nodes with the size of 1000 μm^3 [10, 63], which comprise power and communication blocks along with the relevant chemical sensor, processing and storage units. In our simulation setting, we only define the power and the antenna unit specifications as their properties will directly affect the performance of communications.

The nano-nodes are supposed to be self-powering. So, the piezoelectric nano-generator discussed in §2.1.4.1 is considered as their power unit, which includes a Zinc Oxide nano-wires array and a nano-capacitor for energy storage. In our simulations, we consider a nano-wire array of 1000 μm^2, along with a nano-capacitor with the capacitance and charging voltage of 9nF and 0.42V, respectively. According to such attributes, the nano-device can store a maximum of 800pJ with a full charge.

We assume the bending/releasing cycles of nano-wires, which determines the duration of the energy harvesting process in a nano-device, are provided by the means of ultrasonic waves at a frequency equal to 50Hz. By considering the harvested electric charge in each cycle to be 6pC and also the required cycles for the full charge to be 2500 rounds, it takes a nano-device around 50 seconds to be fully charged [63]. We also adopt the pulse-based modulation mechanism proposed in [58], based on the transmission of 100 femtosecond long Gaussian pulses which are separated by 100 picoseconds periods. By assuming that the required energy to transmit a pulse is equal to 1pJ, and also an equal probability of transmitting "1"s and "0"s, the total harvested energy will be enough to transmit 1600 bits in each event detection round.

In our specific plant monitoring application, we assume that nano-devices are randomly scattered on the plant leaves (e.g., applied via suspension in a spray) and based on their location regarding the micro-devices, they form clusters; While micro-devices or cluster heads are located at predefined points on the stem to manage clusters of nano-devices.

5.3.1.2 Genetic Algorithm Settings

As stated earlier, the proposed GA-based strategies try to find the best configuration setting for each nano-node, i.e., a pair of transmission frequency and the micro-device id, in order to address certain objectives. We use the introduced MATLAB GA toolbox in [24], to implement our proposed algorithms. This toolbox contains implementations of GA functions and operands, which can be modified for our specific optimization problem. It is clear that the proper initialization of GA parameters can affect the performance of the algorithm, e.g., an efficient convergence time. However, such discussion is out of the scope of our research. Therefore, the adopted values for various GA parameters in our simulations are based on the provided data in the mentioned reference.

In the following, we review the structure and settings of the deployed GA, while more details in this regard can be found in Appendix A.

1. **Chromosomes and Genes**: In GA implementations, a chromosome or an individual is composed of several genes. Each individual can be considered as a potential solution of a given problem, in which the value of each gene corresponds to a value in the search space.
   In our proposed solution, we consider that each chromosome contains ND integer values as genes, which corresponds to the total number of nano-devices deployed in each simulation scenario. Each single gene contains a pair of micro-device id and frequency values, i.e., (M_i,f_i), as the communication setting for the ith nano-node. Such a pair of values can be encoded as a single integer value into a gene as follow:

$$g_i = M_i Pr_n + f_i, \quad for \quad i = 1,2,\cdots ND \tag{5.10}$$

   where ND is the total number of nano-devices and Pr_n is a large prime number. The primary values of the micro-device id and the frequency can be retrieved by decoding genes, i.e., dividing the value of an encoded gene over the given prime number and storing quotient and remainder. According to such a presentation of genes, an individual can be defined as:

$$Chr = \begin{bmatrix} g_1 & \dots & g_i \end{bmatrix} \tag{5.11}$$

2. **Population**: Several chromosomes or potential solutions of a problem create the initial population of the GA. The population size, N_{ind}, indicates the number of chromosomes in that population. In our simulations, we consider that the size of a population is twice the number of genes/nano-nodes, i.e., $N_{ind} = 2ND$, and its structure can be defined as:

$$Pop = \begin{pmatrix} Chr_1 \\ \vdots \\ Chr_j \end{pmatrix}, \quad for \quad j = 1,2,\cdots N_{ind} \tag{5.12}$$

   where Chr_j is the chromosome structure defined in equation (5.11).

3. **Objective Function**: The performance of each individual of a population in the problem domain is evaluated based on the objective functions. We introduced several functions in §5.1.2 to optimize the overall performance of nanonetworks in terms of the distribution of nano-nodes among micro-nodes, the consumed power for frequency tuning of graphennas and also the aggregated channel capacity.

   As there exist more than one function to be optimized, we use the introduced weighted sum multi-objective GA to convert this problem into a single objective optimization problem. In our simulations, we seek to address only two of the aforementioned objectives at each scenario. We also consider that objectives are equally important, hence, the final objective function is defined as:

$$Obj_f = 0.5Obj_a + 0.5Obj_b \tag{5.13}$$

   where Obj_a and Obj_b correspond to the introduced functions in §5.1.2.

4. **Fitness Function**: The relative effectiveness of each individual to solve the problem, compared to the rest of the population, is determined by a fitness function. For such a purpose, a non-negative scalar value in the range of [0, F_{val}] can be assigned to individuals, where F_{val} is an arbitrary number showing the upper bound of the fitness value. In this work, we set the value of this parameter as F_{val} =2. Therefore, the most efficient solutions have a fitness value closer to 2, while the fitness value of the worst alternatives is closer to 0.

5. **Selection**: At each iteration of a GA, a subset of the created population will be chosen based on a selection operand for the crossover or the reinsertion processes. In our proposed algorithms, we use stochastic universal sampling as the selection operand. The ratio of the selected individuals from the initial population, S_{ind}, is determined by a term referred to as the generation gap, G_{gap}, where $S_{ind} = G_{gap}.N_{ind}$. In our simulations we set $G_{gap} = 0.7$.

6. **Crossover (Recombination)**: Along the crossover operation, the selected individuals are mated to create a subset of offspring. The crossover function deployed in this thesis is based on the definition of an internal mask, which specifies the contribution of each of the parent chromosomes to their offspring structure. In such an implementation, after parents selection, the adjacent individuals swap genes based on the created crossover mask to breed an offspring.

7. **Mutation**: To avoid the convergence of the population into a local optimum value, a mutation operand is used to guarantee that a diverse range of variables from the search space are selected. This process alters the genes of a chromosome within an specified range, and based on a very low probability defined by P_{mut}. As the individual genes in our implementation are encoded values, i.e., composed of the frequency and micro-device id, we need to retrieve their primary components before the mutating process. As a result, we decode each gene to its initial parameters and store the results in separate data structures. Then, the mutation operand is applied to the decoded data structures separately. Finally, the mutated data structures are encoded again to form an integer single value gene. In our simulations, we set the mutation probability as $P_{mut} = 0.07$.

8. **Reinsertion**: A fraction of the generated and mutated offspring should be inserted into the old parents population by means of a reinsertion operand. We deploy a fitness-based reinsertion, where the best-fitted offspring replace their least-fitted parents. To ensure the propagation of the most fit individuals through several generations an elitism value, E_{rate}, will be deployed. We set this value as $E_{rate} = 0.3$, meaning that through the reinsertion process only 70% of generated offspring will be reinserted into the old population.

9. **Termination**: We set the termination of the algorithm based on the convergence of individuals as well as the number of generations, which varies according to the size of the nanonetwork.

For the frequency tuning process, we set a minimum frequency distance between frequencies of 1GHz, while transmitting 50GHz wide pulses. We also set our swarming constants as $C_R = 2$ and $C_A = 1$, however, these values are chosen arbitrarily and can be changed to maximize the performance of the algorithm.

5.3.2 Plant Structure for Line of Sight Communications

For simulations based on scenario 1, i.e., free-space communications in a basic plant model, we choose a maize plant. We assume that such a plant is 2m tall with two classes of leaf lengths equal to 0.85m and 1.25m, and a leaf angle equal to 60° [96, 102]. The height of the plant can be divided into three equal regions with different moisture levels. According to the provided basic model in §4.1.1, this plant can be modeled as two concentric cylinders with the following related parameters: h =2m, I =2, J =3, L_1 =0.85m, L_2 =1.25m and $\theta_1 = \theta_2$ =60°. Following these assumptions, next, we present the simulation results.

Table 5.1 Comparison of relative error between exhaustive search and GA-based channel allocation approaches.

Number of nano-devices	Relative Error	Iterations of Algorithm
20	0.0041	500
50	0.0459	1200
100	0.0753	1800
200	0.1333	3000

5.3.2.1 Comparison of GA-Based and Exhaustive Search Results

As the first experiment, we study the efficiency of our proposed strategies to locate the global optimal solutions for frequency assignment to nano-nodes. Therefore, we compare the results of the GA-based channel allocations with those of the exhaustive search of the desired band in the range of 1–2THz. In this scenario, we deploy the Basic strategy, while setting the main objectives as optimizing the channel capacity and the power consumption in the frequency tuning process. The simulations are carried out up to a convergence point of the algorithm, i.e., the results provide a standard deviation equal to 20GHz. We configure our plant model with three moisture regions with 10%, 40% and 80% water content from top to the bottom, respectively. The simulated nanonetwork is composed of 5 micro-devices and 20, 50, 100 and 200 nano-devices.

For the comparison purpose, the relative error between the provided results by two approaches is used, which can be defined as:

$$R_{error} = \frac{1}{ND}\sum_{z=1}^{ND}\frac{|f_z^{\mathrm{GA}} - f_z^{\mathrm{exh}}|}{f_z^{\mathrm{exh}}} \tag{5.14}$$

where ND is the total number of nano-nodes, f_z^{GA} is the selected frequency for the zth nano-node based on our proposed algorithm, and f_z^{exh} is the located frequency according to the exhaustive search of the defined band.

The resulting relative errors are presented in Table 5.1. According to the provided values, it can be concluded that the GA-based channel allocation approach can approximate the exhaustive search results.

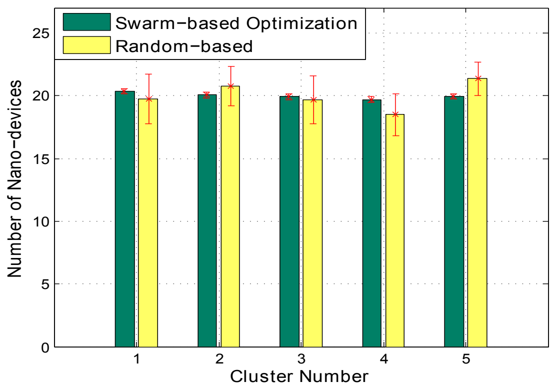

(a) 5 micro-devices

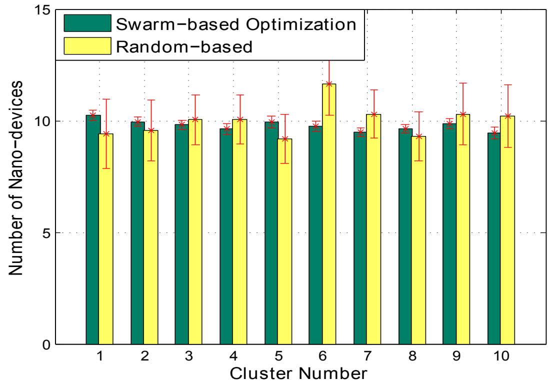

(b) 10 micro-devices

Fig. 5.1 Comparison of the distribution of 100 nano-devices between various number of micro-devices with 95% confidence, and based on a random and the Swarm-based approach.

5.3.2.2 Distribution of Nano-Nodes Among Sink Nodes

In order to discuss the distribution of nano-devices between micro-nodes/clusters, we consider a nanonetwork of 100 nano-nodes and 5/10 micro-nodes. Such a nanonetwork is deployed in the mentioned plant structure which contains 10%, 40% and 80% water content in its moisture regions. We deploy the Swarm-based approach and compare its output with a random frequency and sink node selection strategy, while optimizing the aggregated channel capacity and also a balanced distribution of nano-devices among clusters are our main objectives. Here, we only consider the Swarm-based approach as the rest of the proposed strategies share the same objective in terms of distribution of nano-devices across clusters.

The simulation results are shown in Fig. 5.1, for both number of micro-devices. We can observe the efficiency of the Swarm-based approach to balance the distribution of nano-devices between clusters in both scenarios.

5.3.2.3 Channel Capacity Comparison Among Different Approaches

Next, we want to compare the achievable channel capacity based on the proposed approaches against random frequency assignment to nano-nodes. In this scenario, the nanonetwork is composed of 50 nano-devices, 5 micro-devices and the same moisture levels as in the previous experiment. The main objective functions deployed in this case are channel capacity maximization and also minimization of power consumption in the frequency tuning process.

According to the simulation results in Fig. 5.2, it can be concluded that the random channel allocation is the worst strategy as it does not consider the specific medium conditions. A comparison between the proposed strategies shows that the Two-phase and Off-line

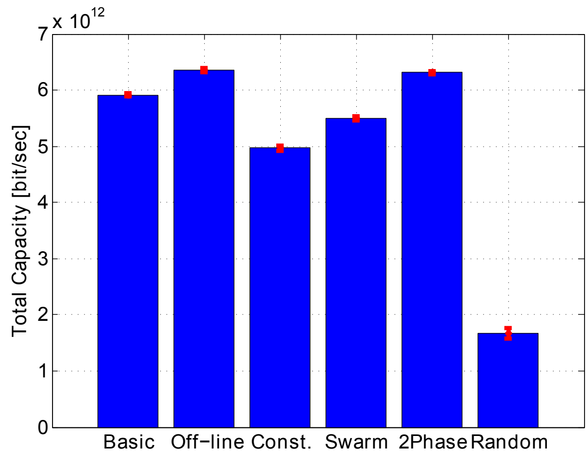

Fig. 5.2 Aggregated channel capacity comparison among strategies with 95% confidence, in a nanonetwork of 5 micro-devices and 50 nano-devices.

approaches are the best solutions as they are based on precalculated optimal frequencies. Then, the Basic and Swarm-based approaches can be considered as next best solutions as they permit frequency overlapping. The performance of the Constraint-based approach is the worst among our proposed solutions, as it avoids any frequency duplication even among non-interfering nano-devices.

It is worth noting that although the Two-phase and Off-line approaches are the best solutions, they need prior knowledge of the best transmission frequencies for individual nano-devices under a wide range of conditions. Such a requirement can be costly in certain conditions, hence, limit their application.

5.3.2.4 Frequency Distributions and Energy Consumption

We refer to the energy consumption as the required energy for tuning the graphennas at the desired frequency. Therefore, we define the total energy consumption across a nanonetwork as:

$$E_{tot} = \sum_{m=1}^{ND} E(f_m) \tag{5.15}$$

where ND is the number of nano-devices and $E(.)$ is based on equation (5.1), which defines the consumed energy in tuning a nano-antenna at f_m. According to that equation, the distribution of frequencies can affect the magnitude of the consumed energy, i.e., tuning the graphennas in higher frequencies consumes more energy and vice versa.

In order to study the frequency distribution and the resulting energy consumption among different approaches, the same nanonetwork scenario and the objectives as the previous

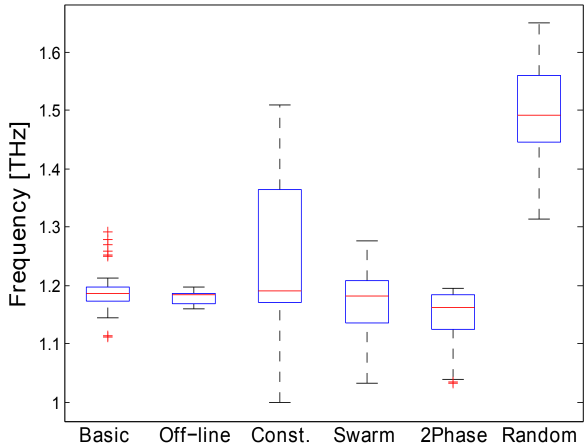

Fig. 5.3 Comparison of the proposed approaches regarding the distribution of frequencies assigned to nano-devices.

experiment are considered. Fig. 5.3 represents the distribution of frequencies across the 1–2THz range. It is shown that the Off-line and Basic approaches have the least frequency spreads as they try to converge the network to the most clear channels. Then, Two-phase and Swarm-based are the next efficient approaches to control dispersion of frequencies as they allow duplication among non-interfering nano-devices. Finally, the Constraint-based algorithm has the widest spread frequencies as it does not have any mechanism to control such an issue.

A comparison between all the proposed approaches against random channel assignment shows that the former have smaller frequency median values, which implies a more efficient energy consumption behavior. In order to validate such a statement, we calculate the total consumed energy of the nanonetwork in Table 5.2, according to the mentioned frequency distributions. It can be observed that the Two-phase and Random approaches have the lowest and highest energy consumption values, respectively, based on their median frequency values.

5.3.2.5 Probability of Successful Transmission in Line of Sight Communications

We now study the probability of successful LoS transmissions based on equation 4.3, which was defined in chapter 4. Therefore, we consider the deployment of 100 nano-devices and 10 micro-devices in the nanonetwork. As the Two-phase strategy demonstrated a good performance in the previous simulations, it is adopted as the channel allocation mechanism for this scenario. We also assume that the plant moisture regions contain 10%, 20% and 30% water and the nano-devices are evenly distributed among horizontal and vertical regions.

According to the defined cylindrical plant model, we assume different leaf densities for the internal and external cylinders, which are shown by λ_1 and λ_2, respectively. We consider

Table 5.2 Comparison of the proposed approaches regarding the required energy for frequency tuning of nano-devices.

Approach	Median Frequency (THz)	Energy Consumption (eV)
Basic	1.18	1.48
Off-line	1.18	1.38
Constraint-based	1.19	1.74
Swarm-based	1.18	1.34
Two-phase	1.16	1.18
Random	1.5	3.34

the case that these parameters are set as $\lambda_1 = 2$ and $\lambda_2 = 4$ [leaves/m]; and then we vary these values as $\lambda_1 = 4$ and $\lambda_2 = 8$ [leaves/m].

First, we compare the successful transmission probability for the nano-nodes located in the internal cylinder, i.e., closer to the stem and the sink nodes, against those nano-nodes in the external cylinders. The resulting performance, which is averaged over 10 second periods, is shown in Fig. 5.4a and Fig. 5.4b. In both plots, it can be observed that the successful transmission probability in the external cylinder is considerably lower than that of the internal cylinder. By comparing these plots, it can also be concluded that increasing the leaf densities by 2 times in either of the cylinders, decreases the successful transmission probability by more than 1.5 times.

Following the same configuration, next, we study the probability of successful transmissions for nano-nodes located in each of the moisture regions on the plant. The results are demonstrated in Fig. 5.5a-5.5c, for two sets of leaf densities in the cylindrical regions. According to these plots, it can be concluded that an increase in the moisture content in different regions slightly reduces the probability of successful transmissions, for all values of leaf densities. In addition, a comparison of the successful transmission probability at each region shows that an increase in the ratio of leaves degrades the mentioned probability. In the simulations carried out, it can be observed that an increase in the leaf density by a factor of 2, leads to the decrease of successful transmissions probability almost by 1.3 times at each moisture region.

We repeated the same simulations for different combinations of water content in these 3 regions, ranging from 1% to 80%, and observed that results were not significantly different.

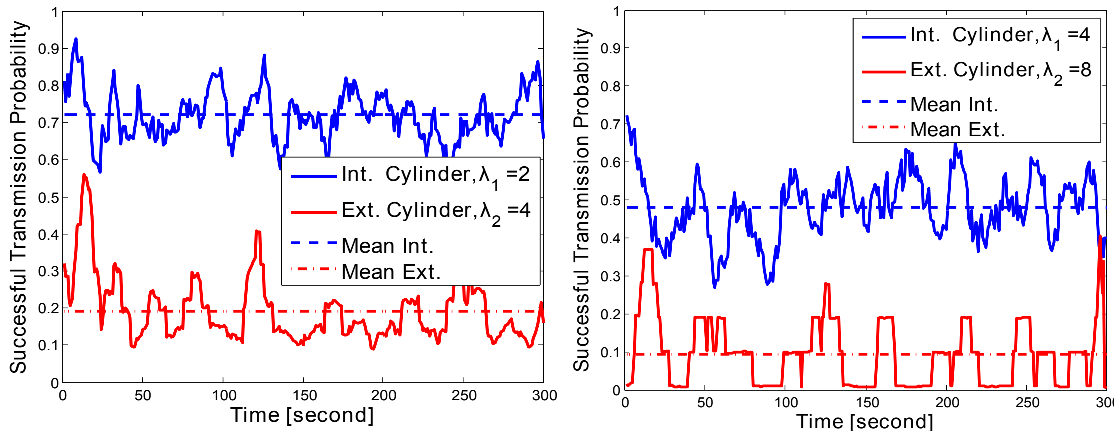

(a) $\lambda_1 = 2$, $\lambda_2 = 4$ [leaves/m] (b) $\lambda_1 = 4$, $\lambda_2 = 8$ [leaves/m]

Fig. 5.4 Successful transmission probability in LoS communications, for nano-nodes located in different cylindrical regions of a plant.

Concluding, the successful transmission probability is majorly affected by the leaf density rather that the moisture content.

5.3.2.6 Instantaneous Throughput for Line of Sight Communications

We define the instantaneous throughput as the successfully transmitted data across the nanonetwork per unit of time. This term can be defined as:

$$Throughput(t) = tr(t).P_{success}(t)/t \tag{5.16}$$

where t is the transmissions duration in second, $tr(.)$ is the aggregated transmitted traffic by nano-devices, and $P_{success}(.)$ is the successful transmission probability as defined in equation (4.3).

For throughput calculation, we consider the communications at the internal cylinder and at the topmost part of the plant. The total transmission duration is set as 300 seconds. First, we analyze the effect of the number of nano-devices on the achievable throughput. In this scenario, we assume the moisture level in the area under study varies in the range of 1%-80% and a leaf density in the range of 0–9[leaves/m]; while there are 5 micro-devices, and 20/100 nano-devices deployed. By implementing the Two-phase strategy, the achievable throughput is shown in Fig. 5.6.

A comparison between two plots shows that increasing the number of nano-devices increases the throughput. Such an observation can be due to the increased volume of the traffic which is transmitted by a larger number of nodes. Alternatively, it can be the result of an improved probability of success in transmissions, due to the deployment of more nodes.

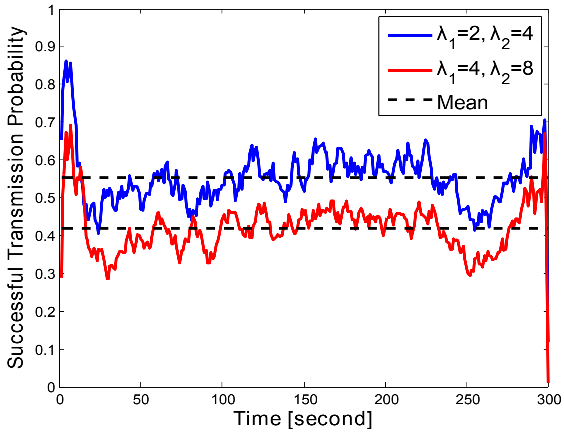

(a) Region 1 with 10% moisture content

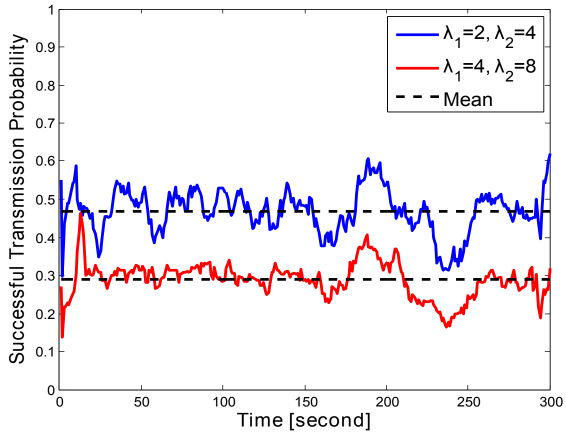

(b) Region 2 with 20% moisture content

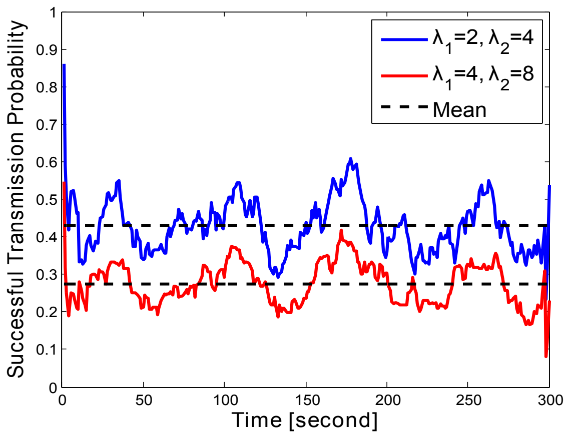

(c) Region 3 with 30% moisture content

Fig. 5.5 Successful transmission probability in LoS communications, for nano-nodes located in different moisture regions of a plant.

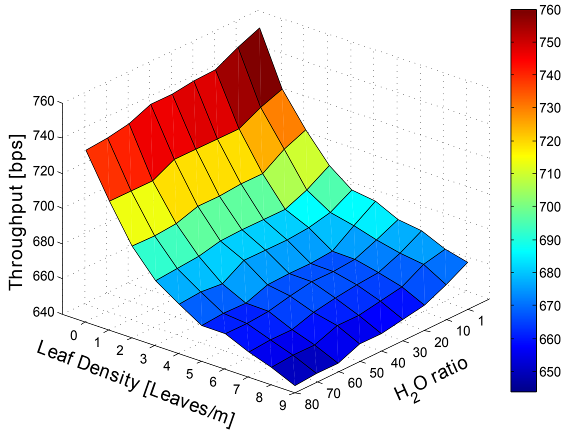

(a) 20 nano-devices.

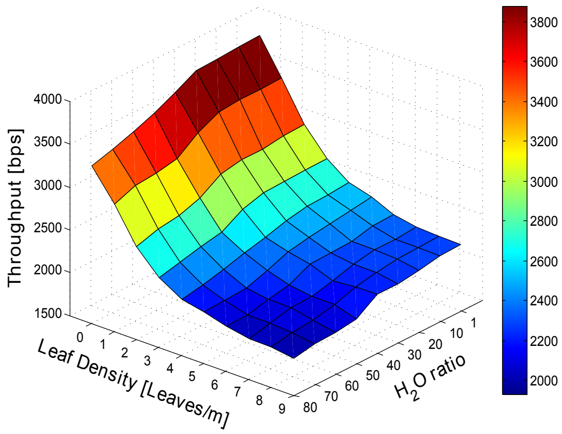

(b) 100 nano-devices.

Fig. 5.6 Throughput comparison for a nanonetwork of 5 micro-devices and various number of nano-devices.

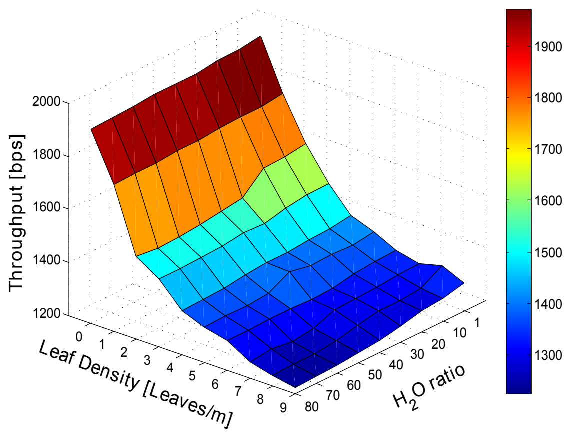

(a) 2 micro-devices.

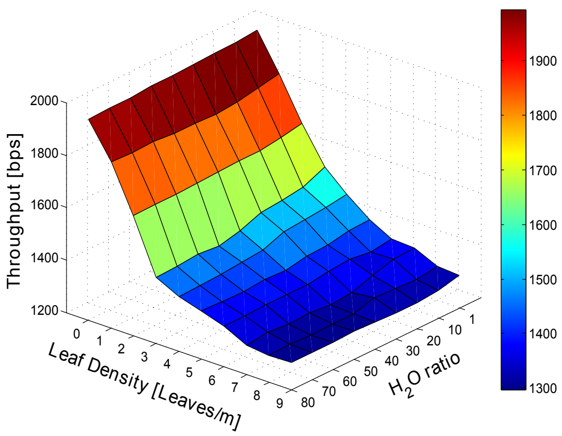

(b) 10 micro-devices.

Fig. 5.7 Throughput comparison for a nanonetwork of 50 nano-devices and various number of micro-devices.

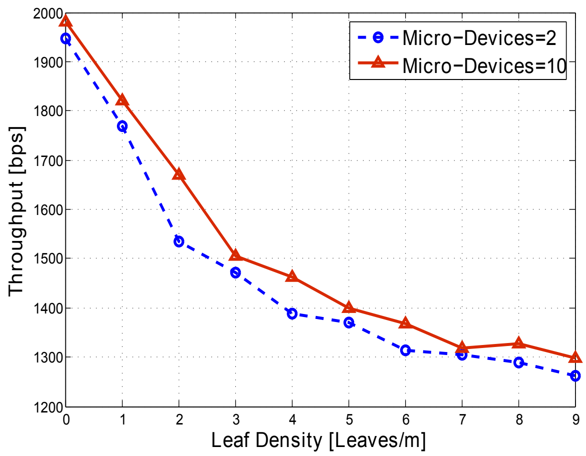

Fig. 5.8 Achievable throughput for different number of micro-devices and a moisture content of 30%.

We can also see that for all moisture levels, an increase in the leaf density can decrease the throughput drastically, specifically for the leaf ratios in the range of 0 – 5 [leaves/m]. Furthermore, it can be observed that an increase in moisture level decreases the throughput, however at a much slower pace compared to when the leaf density changes.

Next, we investigate the effect of the number of micro-devices on the achievable throughput. Considering the same configuration as in the previous experiment, and by deploying 50 nano-devices and 2/10 micro-devices, the resulting throughput is shown in Fig.5.7. Once again the significant degradation of the throughput as a function of the increased leaf density can be observed in these plots. To infer the effect of the number of micro-devices on the throughput more precisely, this parameter is compared in Fig.5.8 for both numbers of micro-devices and a moisture content of 30%. It can be concluded that increasing the number of micro-devices is slightly improving the throughput, due to the decreased average distance between nano-devices and their sink nodes.

5.3.3 Plant Structure for Non-Line of Sight Communications

For simulations based on scenario 2, i.e., communications in a hybrid channel and for a refined plant model, we consider a coffee plant. We assume that such a plant is a 1m single stem with the radius of 0.01m and two classes of leaf lengths equal to 0.2m and 0.3m, and a leaf angle equal to 60°. The height of the plant can be divided into three equal regions with different moisture levels. According to the provided refined plant model in §4.1.2, this plant can be modeled as two concentric cylinders with the following related parameters: h=1m, I=2, J=3, L_1=0.2m, L_2=3m and θ_1=θ_2=60°. The total attenuation due to absorption and

scattering of a fresh leaf are set based on the measured data in [52].
According to the radius of the stem, i.e., r_s=0.01m, and by assuming the depth of a micro-device as h_m=0.01m, the field of view for micro-devices, ω, can be calculated based on equation (4.13), as follows:

$$\tan(\frac{\varphi}{2}) = \frac{1}{\sqrt{(1+1)^2-1^2}} = 0.57 \longrightarrow \varphi = \arctan\left(\frac{2\times 0.57}{1-(0.57)^2}\right) \approx \frac{\pi}{3} \tag{5.17}$$

Therefore,

$$\omega = 2\pi - \varphi = \frac{5\pi}{3} = 300^\circ \tag{5.18}$$

It should be highlighted, as our simulations are coordinate based, the coordinates of the nano-nodes and micro-devices and also the field of view for micro-devices can determine whether the nano-nodes are capable to communicate with their sink nodes or not.

5.3.3.1 Probability of Successful Transmission in Non-Line of Sight Communications

We now study the probability of successful NLoS transmissions based on equation 4.11, which was defined in chapter 4. We assume that the humidity regions of the plant contain 10%, 40% and 80% moisture, from the top to the bottom of plant. We also consider the deployment of 4 micro-devices and 100 nano-devices, which are evenly distributed between the horizontal and vertical structural regions of the plant. In such a model, the average number of leaves in the internal and external cylinders are set as $\lambda_1 = 10$ and $\lambda_2 = 15$ [leaves/m], respectively. For the channel allocation to nano-nodes, the Two-phase strategy is used as it shows a more efficient performance compared with the rest of the proposed approaches.

We compare the performance of communications for the nano-nodes located in the internal cylinder against those located in the external cylinder. In this regard, we consider average leaf thickness values of 100μm and 200μm; and also path-loss threshold values of 110dB and 140dB. The probability of successful transmissions is presented in Fig. 5.9, based on the mentioned simulation settings. The provided results are averaged over 10 second periods. It is worth noting that, equation (4.11) is a function of time and it varies based on the number of active nano-nodes and their channel conditions. We assume after depleting the energy, it takes nano-devices a random time in the range of 50–60sec to be fully charged and capable to communicate again. Therefore, at any given time, there will be only a subset of active nano-nodes in the network.

First, a comparison between all the presented plots shows a higher probability of success in transmissions for the nano-devices located in the internal cylinder, due to a lower ratio of leaves in this region. In addition, it can be observed that for a certain value of the leaf thickness, increasing the path-loss threshold results in a greater increase in the successful transmission probability of the nano-nodes located in the external cylinder, compared with those which are located in the internal cylinder. This observation is due to a shorter distance between nano-nodes located in the internal cylinder and their sink nodes, as well as the lower ratio of the leaves in the internal cylinder.
Following the same reason, for a given path-loss threshold, increasing the average leaf thickness affects communications in the external cylinder more considerably compared to the communications of nano-nodes located in the internal cylinder.

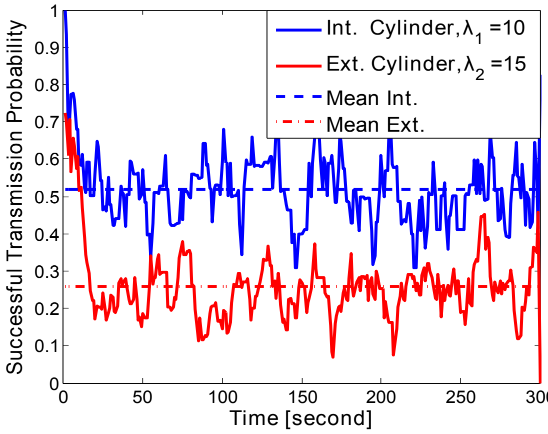

(a) Leaf thickness= 100μm,
Path-loss threshold = 110dB

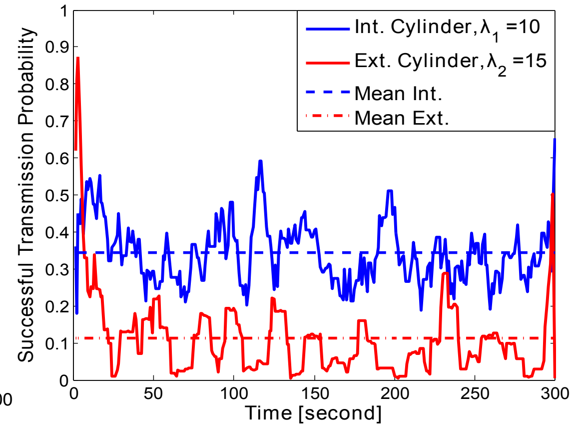

(b) Leaf thickness= 200μm,
Path-loss threshold = 110dB

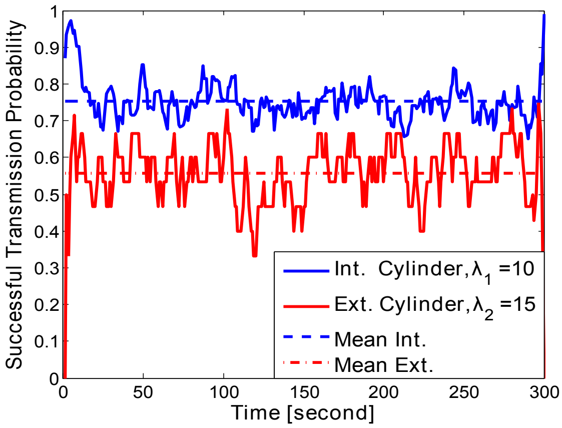

(c) Leaf thickness= 100μm,
Path-loss threshold = 140dB

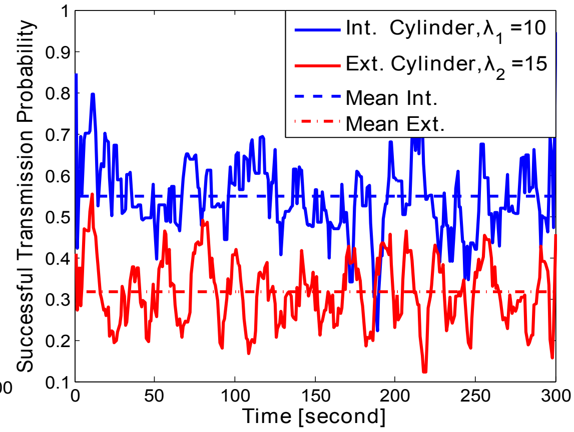

(d) Leaf thickness= 200μm,
Path-loss threshold = 140dB

Fig. 5.9 Successful transmission probability in NLoS communications, for nano-nodes located in different cylindrical regions of a plant.

5.4 Summary and Conclusions

In this chapter, we proposed several frequency allocation strategies for a hierarchical nanonetwork deployed within a plant environment. These strategies, which are accompanied by a basic sink node assignment algorithm, seek to decrease the attenuation and noise effects in the channel, through locating the clearest transmission frequencies.
In order to evaluate the performance of the proposed approaches, we used our previously introduced framework. This framework can be modified to analyze the performance under a variety of transmission scenarios, including different plant types as well as LoS and NLoS communications.

Our analysis highlights the following conclusions. Firstly, our proposed strategies can approximate the results of the exhaustive search of the desired channel to define the most appropriate frequencies. Secondly, these strategies improve the performance of the nano-communications in several contexts, as opposed to transmission at random frequencies. Among all the introduced approaches, the Two-phase strategy, which is based on the pre-stored data, has the most efficient performance regarding the spectrum usage and energy consumption. Thirdly, leaf density has a greater impact on degrading the performance of LoS transmissions, compared to the effect of moisture ratio. This conclusion is based on the increased probability of signal loss due to the increased probability of obstruction in LoS communications. It is also shown that increasing the number of nano-devices improves the network throughput considerably, as the number of observations is increased, offsetting the probability of obstruction in LoS transmissions. On the other hand, increasing the number of micro-devices leads to only a marginal improvement of the performance, which is due to a decrease in the average distances between transmitters and their sink nodes. Finally, the drastic effect of the path-loss threshold on the probability of success in NLoS transmissions was studied. The obtained results show that the desired performance can be achieved through the efficient selection of the path-loss threshold value based on the plant attributes.

Chapter 6

Conclusions and Future Work

In this thesis, we aimed to contribute to the area of THz nanonetworking through the definition and evaluation of our research hypothesis. This hypothesis states that a cross-layer communications framework, which includes frequency allocation strategies combined with medium-specific path-loss models will be viable for nanonetwork communications in a vegetation environment. In the following, we discuss how the structure of this document addresses such a hypothesis.

In chapter 3, we introduced path-loss models for THz communications in vegetation environments, which can accommodate different types of plants. We also reviewed a THz channel capacity model to evaluate the achievable data rates in nano-communications. The proposed path-loss models are basic as they only account for the attenuative effects of air and plant leaves on THz radiation. However, as the current literature does not contain any similar work in this area, these models can be considered as base lines for an analysis on the THz propagation in such scenarios.

We studied the total encountered path-loss under different assumptions of the transmission channel, with respect to its composition and also leaves attributes. The provided results demonstrated that air constituents, especially moisture, create attenuation peaks across the entire THz band. These peaks divide the spectrum into narrower transmission windows, where their widths are a function of the frequency, distance and also the relative humidity. On the other hand leaves loss behavior is linear and it has a much higher degree compared to air.

It can be concluded that the magnitude of signal loss in such hybrid channels depends on the specific composition of the medium and also attributes of leaves. The resulting loss can in turn greatly reduce the effective transmission distance and channel capacity. Therefore, in order to make THz nano-communications resilient to loss, the transmission windows need to be located based on the specific channel conditions. Then, in order to improve the performance of nanonetworks, advanced communication protocols need to be developed for the allocation of those clear channels to nano-nodes.

In chapter 4, we introduced a framework for the evaluation of nano-communications performance in the proximity of plants. As the research on this topic is still at an early stage, it is not feasible to deploy nanonetworks in actual plant environments and perform real performance measurements. In this regard, our proposed framework includes primitive models of a plant, which can be considered as the host environment for a monitoring nanonetwork. The proposed models can be modified based on plant characteristics to take different species into account. In addition, this framework includes definitions for performance evaluations in terms of probability of success in transmissions. The proposed benchmarks are specified for LoS and NLoS nano-communications. The probability model for LoS transmissions is basic as it assumes that THz radiation cannot pass through leaves. Hence, the signal loss is mainly considered due to the obstruction caused by leaves and also the limited THz channel capacity to relay the generated traffic. However, in a real transmission scenario, THz waves can pass through leaves, where the proportion of the transmitted signal depends on the properties of leaves. Therefore, the probability model for NLoS transmissions was introduced to take such an issue into account.

In the rest of the chapter, first, we approximated the total path-loss by considering extreme transmission conditions for vegetation monitoring nanonetworks, i.e., transmission in the vicinity of a sparse/dense plant and in a medium with low/high humidity ratios. Once again, we observed the great effect of moisture, leaves and distance on the level of signal degradation.

Then, by focusing on a subset of transmission frequencies and distances and also the best/-worst channel conditions, we defined boundaries for the path-loss threshold. Those boundaries, which are defined as a function of the vegetation attributes, can specify the maximum acceptable path-loss threshold for proper reception of a signal. As the path-loss threshold definition can be modified based on the specific transmission condition, it can provide guidelines for transceiver design purposes.

In the later discussion, we analyzed the effect of the channel attributes and the path-loss threshold on the maximum number of leaves that can obstruct the transmission path. There it was shown that for lower moisture ratios, the maximum number of leaves linearly decreases with an increase of distance/frequency. However, for a high level of moisture content, such a parameter had a non-linear behavior across the frequency band, i.e., rapid increase/decrease at various frequencies; which is due to the high absorption peaks at specific frequencies.

Finally, based on such an analysis, we studied the loss probability for single radio links. It is worth to note, that our introduced performance benchmarks, approximate the overall probability of success in transmissions as a product of the loss probability for single radio links. It was shown that the efficient selection of the path-loss threshold can reduce the probability of loss and consequently improve the achievable transmission distance.

In chapter 5, we defined several frequency allocation strategies, which are combined with an initial sink node selection algorithm, for hierarchical nanonetworks. These approaches rely on physical channel models, introduced in chapter 3, for the most efficient channel assignment to the network components. In fact, such mechanisms are implemented in order to optimize several performance metrics, including the aggregated channel capacity, total consumed energy in the frequency tuning process and distribution of nano-devices between sink nodes. As there are several parameters to be optimized, we used a multi-objective GA to find the best communication settings for nano-nodes, given specific transmission conditions, e.g., distance, medium composition and so on. In addition, we deployed swarming techniques to control the spread of the allocated frequencies across the THz channel.

We demonstrated that the proposed approaches can approximate the results of exhaustive search, by locating the global optimal frequencies. In addition, it was shown that they outperform a random frequency/sink node assignment approach, in order to optimize the channel capacity and power consumption. However, in terms of the fair distribution of nano-nodes among sink nodes, their performance is almost similar to a random approach. Among all the proposed strategies, those which allow the frequency duplication, result in a more efficient use of the spectrum.

Then, based on the proposed communications framework in chapter 4 and also deploying the most efficient channel assignment approach, we analyzed the performance of LoS and NLoS nano-communications in a vegetation environment. There we observed the significant effect of plant leaves and moisture on reducing the probability of successful transmissions, especially for LoS communications. It was concluded that a higher performance can be achieved through deploying a larger number of nano- or micro-devices in the network as well as an efficient selection of the path-loss threshold value.

6.1 Future Work

In this section, we address some of the potential future work that can emerge as the continuation of this research project. In this regard, we consider short term and long term research goals. By focusing on the physical channel specifications, our short term research plans center around more refined THz channel models for communication through vegetation. However, in the long term plans, we will consider the higher layer communication protocols for nanonetworks, given their communication constraints.

6.1.1 Short Term Plans

The initial THz path-loss models presented in chapter 3, can be used for an estimation of the total loss due the presence of air and also plant leaves along the transmission path. These models consider the introduced absorption by the air and leaves, and also the surface roughness scattering of leaves as the main sources of the THz signal loss.

Despite the proposed path-loss models are based on measured data available in the literature, for individual leaves and leaf types, we wish to validate them through comparison with some real measurements involving links operating in the vicinity of a variety of plants. The measurements can be carried out by deploying the introduced THz-TDS system in Chapter 3. Such an approach is based on the radiation of a broadband THz pulse through a leaf or several leaves and then comparing the magnitude and the phase of the received signal with the free-space transmissions [37].

In addition to the above mentioned points, in a realistic wireless communication scenario, there are other factors which can contribute to the total loss, such as reflections from surfaces. For nano-communications in the vicinity of plants, one avenue of research that needs to be explored is the effect of reflections on the total received signal power, for single leaf and multiple leaves transmission scenarios.

For example, it is known that once a propagating wave encounters a slab, a proportion of the signal can pass through the slab, while the rest is reflected back [14, 88]. In this case, the transmitted signal can get trapped inside the slab and undergo a series of forward/backward reflections (Fig. 6.1a). The ratio of the transmitted/reflected signal depends on several parameters, including the electrical properties of the slab and its thickness and also the transmission frequency. For a transmission path which is composed of several slabs, this behavior can be observed within the individual slabs as well as among the consecutive layers (Fig. 6.1b). Such phenomenons can have constructive/destructive effects, so they can influence the total signal level at the receiver.

As stated, the proposed models can approximate the signal loss due to the absorption by plant leaves. This issue can affect the validity of these models for THz communications through plant foliage. Therefore, another refinement to the proposed models is the investigation of the encountered loss due to other parts of the vegetation, e.g., fruits, stalks, stems and so on. The provision of loss models for various parts of plants can lead to generic loss models, which can predict the total signal degradation level in a plant canopy, given its general properties.

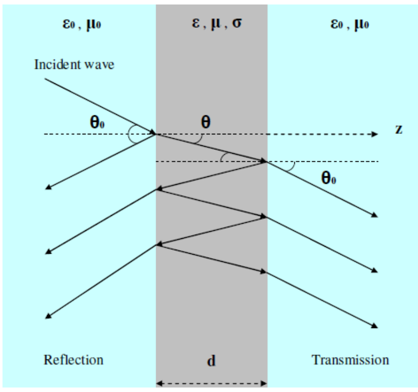

(a)

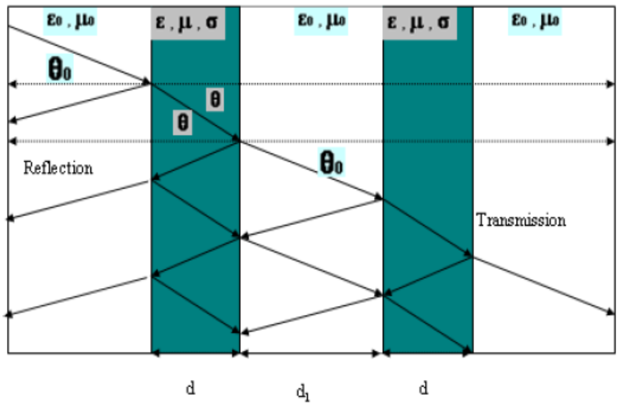

(b)

Fig. 6.1 The resulting reflections for transmission through a single slab (a); and multiple slabs (b) [112].

6.1.2 Long Term Plans

Similar to traditional WSNs, nanonetwork communications will deal with different challenges regarding rough environmental conditions, in which they will be deployed in. The vegetation monitoring nanonetworks will be exposed to a variety of harsh natural factors, including heavy rain, hail or snowfall, sandstorms and so forth, which can cause nano-nodes to be blown/washed away [12]. They can also be physically destroyed or relocated by animals. In addition, nano-nodes can fail due to hardware/software malfunctioning. All these points can cause a high degree of disconnectivity for nanonetworks, which in turn can degrade different aspects of the performance, e.g., the accuracy of observations.

Therefore, developing fault-tolerant and environmental-aware communication protocols can tackle those challenges. Such protocols can be proposed in a cross-layer fashion, while satisfying various strategies at different layers of the network. For example, they can include topology reformation mechanisms for communications in an environment with rapid climate changes. At a more advanced level, such protocols can also determine specifications for the number of the deployed nano-devices and also their refreshment rate based on several criteria, such as nodes failure rate, geographical and climate conditions or the desired level of observations. Further research around the above mentioned points is considered as our future and long term objective.

Bibliography

[1] S. Abadal, M. Iannazzo, M. Nemirovsky, A. Cabellos-Aparicio, H. Lee, and E. Alarcon. On the area and energy scalability of wireless network-on-chip: A model-based benchmarked design space exploration. *IEEE/ACM Transactions on Networking*, 23 (5):1501–1513, 2015.

[2] Q.H. Abbasi, L. Ali, M. Ur Rehman, S. Liaqat, and A. Alomainy. Numerical radio propagation characterisation and system level modelling for ultra wideband on-body communications. In *IEEE International RF and Microwave Conference (RFM)*, pages 129–132, 2013.

[3] Q.H. Abbasi, S. Liaqat, L. Ali, and A. Alomainy. An improved radio channel characterisation for ultra wideband on-body communications using regression method. In *International Symposium on Future Information and Communication Technologies for Ubiquitous HealthCare (Ubi-HealthTech)*, pages 1–4, 2013.

[4] N. Akkari, J.M. Jornet, P. Wang, E. Fadel, L. Elrefaei, MGA Malik, S. Almasri, and I.F. Akyildiz. Joint physical and link layer error control analysis for nanonetworks in the terahertz band. *Wireless Networks*, pages 1–13, 2015.

[5] I. F. Akyildiz and J.M. Jornet. The internet of nano-things. *IEEE Wireless Communications*, 17(6):58, 2010.

[6] I. F. Akyildiz, J. M. Jornet, and M. Pierobon. Propagation models for nanocommunication networks. In *European Conference on Antennas and Propagation (EuCAP)*, pages 1–5, 2010.

[7] I.F. Akyildiz and J.M. Jornet. Electromagnetic wireless nanosensor networks. *Nano Communication Networks*, 1(1):3–19, 2010.

[8] I.F. Akyildiz, W. Su, Y. Sankarasubramaniam, and E. Cayirci. A survey on sensor networks. *IEEE Communications Magazine*, 40(8):102–114, 2002.

[9] I.F. Akyildiz, F. Brunetti, and C. Blázquez. Nanonetworks: A new communication paradigm. *Computer Networks*, 52(12):2260–2279, 2008.

[10] I.F. Akyildiz, J.M. Jornet, and M. Pierobon. Nanonetworks: A new frontier in communications. *ACM Communications*, 54(11):84–89, 2011.

[11] I.F. Akyildiz, M. Pierobon, S. Balasubramaniam, and Y. Koucheryavy. The internet of bio-nano things. *IEEE Communications Magazine*, 53(3):32–40, 2015.

[12] F. M. Al-Turjman, A. E. Al-Fagih, H. S. Hassanein, and M. A. Ibnkahla. Deploying fault-tolerant grid-based wireless sensor networks for environmental applications. In *IEEE Conference on Local Computer Networks (LCN)*, pages 715–722, 2010.

[13] B. Atakan and O.B. Akan. Carbon nanotube-based nanoscale ad hoc networks. *IEEE Communications Magazine*, 48(6):129–135, 2010.

[14] C. A. Balanis. *Advanced engineering electromagnetics*. New York: Wiley, 1989.

[15] S. Balasubramaniam and J. Kangasharju. Realizing the internet of nano things: challenges, solutions, and applications. *Computer*, (2):62–68, 2013.

[16] R. Bennewitz, J.N. Crain, A. Kirakosian, J.L. Lin, J.L. McChesney, D.Y. Petrovykh, and F.J. Himpsel. Atomic scale memory at a silicon surface. *Nanotechnology*, 13(4): 499, 2002.

[17] K. Bhargava, S. Ivanov, and W. Donnelly. Internet of nano things for dairy farming. In *ACM International Conference on Nanoscale Computing and Communication (Nanocom)*, pages 1–2, 2015.

[18] P. Bondavalli, P. Legagneux, and D. Pribat. Carbon nanotubes based transistors as gas sensors: state of the art and critical review. *Sensors and Actuators B: Chemical*, 140 (1):304–318, 2009.

[19] N. Born, R. Gente, D. Behringer, M. Schwerdtfeger, S. Busch, S. Liepelt, B. Ziegenhagen, and M. Koch. Monitoring the water status of plants using thz radiation. In *International Conference on Infrared, Millimeter, and Terahertz waves (IRMMW-THz)*, pages 1–2, 2014.

[20] P. Boronin, V. Petrov, D. Moltchanov, Y. Koucheryavy, and J. M. Jornet. Capacity and throughput analysis of nanoscale machine communication through transparency windows in the terahertz band. *Nano Communication Networks*, 5(3):72–82, 2014.

[21] B. Breitenstein, M. Scheller, M. K. Shakfa, T. Kinder, T.and Müller-Wirts, M. Koch, and D. Selmar. Introducing terahertz technology into plant biology: A novel method to monitor changes in leaf water status. *Journal of Applied Botany and Food Quality*, 84(2):158, 2012.

[22] A. Brizzi, A. Pellegrini, L. Zhang, and Y. Hao. Statistical path-loss model for on-body communications at 94 ghz. *Antennas and Propagation, IEEE Transactions on*, 61(11): 5744–5753, 2013.

[23] H. Chen and R. Yada. Nanotechnologies in agriculture: New tools for sustainable development. *Trends in Food Science & Technology*, 22(11):585–594, 2011.

[24] A. Chipperfield, P. Fleming, H. Pohlheim, and C. Fonseca. Genetic algorithm toolbox for use with matlab. *Department of Automatic Control and Systems Engineering, University of Sheffield, Users Guide, Version 1.2*, 1994.

[25] Y. Cui, Q. Wei, H. Park, and C. M. Lieber. Nanowire nanosensors for highly sensitive and selective detection of biological and chemical species. *Science*, 293(5533):1289–1292, 2001.

[26] M. Dicke and I. T. Baldwin. The evolutionary context for herbivore — induced plant volatiles: beyond the 'cry for help'. *Trends in plant science*, 15(3):167–175, 2010.

[27] M. Donohoe, S. Balasubramaniam, B. Jennings, and J.M. Jornet. Powering in-body nanosensors with ultrasounds. *IEEE Transactions on Nanotechnology*, PP(99):1–1, 2015.

[28] M. Dragoman and D. Dragoman. Graphene-based quantum electronics. *Progress in Quantum Electronics*, 33(6):165–214, 2009.

[29] M. Dragoman, A. A. Muller, D. Dragoman, F. Coccetti, and R. Plana. Terahertz antenna based on graphene. *Journal of Applied Physics*, 107(10):104313–104313, 2010.

[30] F. Dressler and S. Fischer. Connecting in-body nano communication with body area networks: challenges and opportunities of the internet of nano things. *Nano Communication Networks*, 6(2):29–38, 2015.

[31] Zheyu Fang, Yumin Wang, Zheng Liu, Andrea Schlather, Pulickel M Ajayan, Frank HL Koppens, Peter Nordlander, and Naomi J Halas. Plasmon-induced doping of graphene. *Acs Nano*, 6(11):10222–10228, 2012.

[32] R. Filter, M. Farhat, M. Steglich, R. Alaee, C. Rockstuhl, and F. Lederer. Tunable graphene antennas for selective enhancement of THz-emission. *Optics Express*, 21: 3737–3745, 2013.

[33] M. Gagliano, M. Renton, N. Duvdevani, M. Timmins, and S. Mancuso. Acoustic and magnetic communication in plants. *Plant Signaling & Behavior*, 7(10):1346–1348, 2012.

[34] M. Gagliano, M. Renton, N. Duvdevani, M. Timmins, and S. Mancuso. Out of sight but not out of mind: alternative means of communication in plants. *PLoS One*, 7(5): e37382, 2012.

[35] V. Gazi and K. M. Passino. A class of attractions/repulsion functions for stable swarm aggregations. *International Journal of Control*, 77(18):1567–1579, 2004.

[36] V. Gazi and K. M. Passino. Stability analysis of social foraging swarms. *IEEE Transactions on Systems, Man, and Cybernetics,*, 34(1):539–557, 2004.

[37] R. Gente and M. Koch. Monitoring leaf water content with thz and sub-thz waves. *Plant methods*, 11(1):1–9, 2015.

[38] R. Gente, N. Born, N. Voß, W. Sannemann, J. Léon, M. Koch, and E. Castro-Camus. Determination of leaf water content from terahertz time-domain spectroscopic data. *Journal of Infrared, Millimeter, and Terahertz Waves*, 34(3-4):316–323, 2013.

[39] S. S. Ghassemzadeh, L. J. Greenstein, A. Kavcic, T. Sveinsson, and V. Tarokh. An empirical indoor path loss model for ultra-wideband channels. *Journal of Communications and Networks*, 5(4):303–308, 2003.

[40] A. Goldsmith. *Wireless communications*. Cambridge university press, 2005.

[41] B. Guo, L. Fang, B. Zhang, and J. Gong. Graphene doping: a review. *Insciences J.*, 1 (2):80–89, 2011.

[42] H. Guo, P. Johari, J. Jornet, and Z. Sun. Intra-body optical channel modeling for in-vivo wireless nanosensor networks. *IEEE Transactions on NanoBioscience*, PP (99):1–1, 2015.

[43] A. Gupta and P. Mohapatra. A survey on ultra wide band medium access control schemes. *Computer Networks*, 51(11):2976–2993, 2007.

[44] C. Han and I.F. Akyildiz. Distance-aware multi-carrier (damc) modulation in terahertz band communication. In *IEEE International Conference on Communications (ICC)*, pages 5461–5467, 2014.

[45] C. Han, A.O. Bicen, and I.F. Akyildiz. Multi-ray channel modeling and wideband characterization for wireless communications in the terahertz band. *IEEE Transactions on Wireless Communications*, 14(5):2402–2412, 2015.

[46] M. Heil and J. C. S. Bueno. Within-plant signaling by volatiles leads to induction and priming of an indirect plant defense in nature. *Proceedings of the National Academy of Sciences*, 104(13):5467–5472, 2007.

[47] M. Heil and J. Ton. Long-distance signalling in plant defence. *Trends in Plant Science*, 13(6):264–272, 2008.

[48] R. Jain. Channel models a tutorial. *WiMAX Forum AATG*, 2007.

[49] C. Jansen, S. Priebe, C. Möller, M. Jacob, H. Dierke, M. Koch, and T. Kürner. Diffuse scattering from rough surfaces in thz communication channels. *IEEE Transactions on Terahertz Science and Technology*, 1(2):462–472, Nov 2011.

[50] I.T. Javed and I.H. Naqvi. Frequency band selection and channel modeling for wnsn applications using simplenano. In *IEEE International Conference on Communications (ICC)*, pages 5732–5736, 2013.

[51] J. H Jiang and D. L. Wu. Ice and water permittivities for millimeter and sub-millimeter remote sensing applications. *Atmospheric Science Letters*, 5(7):146–151, 2004.

[52] C. Jördens, M. Scheller, B. Breitenstein, D. Selmar, and M. Koch. Evaluation of leaf water status by means of permittivity at terahertz frequencies. *Journal of biological physics*, 35(3):255–264, 2009.

[53] J. M. Jornet. A joint energy harvesting and consumption model for self-powered nano-devices in nanonetworks. In *IEEE International Conference on Communications (ICC)*, pages 6151–6156, 2012.

[54] J. M. Jornet. Low-weight error-prevention codes for electromagnetic nanonetworks in the terahertz band. *Nano Communication Networks*, 5(1):35–44, 2014.

[55] J. M. Jornet and I. F. Akyildiz. Channel capacity of electromagnetic nanonetworks in the terahertz band. In *IEEE International Conference on Communications (ICC)*, pages 1–6, 2010.

[56] J. M. Jornet and I. F. Akyildiz. The internet of multimedia nano-things. *Nano Communication Networks*, 3(4):242–251, 2012.

[57] J. M. Jornet, J.C. Pujol, and J. Solé Pareta. Phlame: a physical layer aware mac protocol for electromagnetic nanonetworks in the terahertz band. *Nano Communication Networks*, 3(1):74–81, 2012.

[58] J.M. Jornet and I. F. Akyildiz. Femtosecond-long pulse-based modulation for terahertz band communication in nanonetworks. *IEEE Transactions on Communications*, 62 (5):1742–1754, 2014.

[59] J.M. Jornet and I.F. Akyildiz. Graphene-based nano-antennas for electromagnetic nanocommunications in the terahertz band. In *IEEE European Conference on Antennas and Propagation (EuCAP)*, 2010.

[60] J.M. Jornet and I.F. Akyildiz. Channel modeling and capacity analysis for electromagnetic wireless nanonetworks in the terahertz band. *IEEE Transactions on Wireless Communications*, 10(10):3211–3221, 2011.

[61] J.M. Jornet and I.F. Akyildiz. Information capacity of pulse-based wireless nanosensor networks. In *IEEE Communications Society Conference on Sensor, Mesh and Ad Hoc Communications and Networks (SECON)*, pages 80–88, 2011.

[62] J.M. Jornet and I.F. Akyildiz. Low-weight channel coding for interference mitigation in electromagnetic nanonetworks in the terahertz band. In *IEEE International Conference on Communications (ICC)*, pages 1–6, 2011.

[63] J.M. Jornet and I.F. Akyildiz. Joint energy harvesting and communication analysis for perpetual wireless nanosensor networks in the terahertz band. *IEEE Transactions on Nanotechnology*, 11(3):570–580, 2012.

[64] J.M. Jornet and I.F. Akyildiz. Graphene-based plasmonic nano-antenna for terahertz band communication in nanonetworks. *IEEE Journal on Selected Areas in Communications*, 31(12):685–694, 2013.

[65] M. Kocaoglu and O.B. Akan. Minimum energy coding for wireless nanosensor networks. In *IEEE INFOCOM Proceedings*, pages 2826–2830, 2012.

[66] M. Kocaoglu and O.B. Akan. Minimum energy channel codes for nanoscale wireless communications. *IEEE Transactions on Wireless Communications*, 12(4):1492–1500, 2013.

[67] M. Kocaoglu and D. Malak. On the node density limits and rate-delay-energy tradeoffs in ad hoc nanonetworks with minimum energy coding. In *IEEE International Conference on Communications (ICC)*, pages 6157–6161, 2012.

[68] J. Kokkoniemi, J. Lehtomaki, and M. Juntti. Frequency domain scattering loss in thz band. In *Global Symposium On Millimeter Waves (GSMM)*, pages 1–3, May 2015. doi: 10.1109/GSMM.2015.7175457.

[69] J. Kokkoniemi, J. Lehtomäki, and M. Juntti. Energy detection in thz nanonetworks in scattering environment. In *ACM International Conference on Nanoscale Computing and Communication (Nanocom)*, pages 1–6, 2015.

[70] J. Kokkoniemi, J. Lehtomaki, K. Umebayashi, and M. Juntti. Frequency and time domain channel models for nanonetworks in terahertz band. *IEEE Transactions on Antennas and Propagation*, 63(2):678–691, 2015.

[71] A. Konak, D. W. Coit, and A. E. Smith. Multi-objective optimization using genetic algorithms: a tutorial. *Reliability Engineering & System Safety*, 91(9):992–1007, 2006.

[72] J. Lee and S. Kim. Manufacture of a nanotweezer using a length controlled cnt arm. *Sensors and Actuators A: Physical*, 120(1):193–198, 2005.

[73] H. J. Liebe, G. A. Hufford, and T. Manabe. A model for the complex permittivity of water at frequencies below 1 thz. *International Journal of Infrared and Millimeter Waves*, 12(7):659–675, 1991.

[74] I. Llatser, C. Kremers, A. Cabellos-Aparicio, J. JoJornet, E. Alarcón, and D. N. Chigrin. Graphene-based nano-patch antenna for terahertz radiation. *Photonics and Nanostructures-Fundamentals and Applications*, 10(4):353–358, 2012.

[75] I. Llatser, C. Kremers, D. N. Chigrin, J. M. Jornet, M. C. Lemme, A. Cabellos-Aparicio, and E. Alarcon. Radiation characteristics of tunable graphennas in the terahertz band. *Radioengineering*, 21(4):946–53, 2012.

[76] I. Llatser, C. Kremers, D.N. Chigrin, J.M. Jornet, M.C. Lemme, A. Cabellos-Aparicio, and E. Alarcón. Characterization of graphene-based nano-antennas in the terahertz band. In *European Conference on Antennas and Propagation (EUCAP)*, pages 194–198, 2012.

[77] I. Llatser, S. Abadal, A. M. Sugranes, A. Cabellos-Aparicio, and E. Alarcon. Graphene-enabled wireless networks-on-chip. In *International Black Sea Conference on Communications and Networking (BlackSeaCom)*, pages 69–73, 2013.

[78] H. Looyenga. Dielectric constants of heterogeneous mixtures. *Physica*, 31(3):401–406, 1965.

[79] P. Di Lorenzo and S. Barbarossa. A bio-inspired swarming algorithm for decentralized access in cognitive radio. *IEEE Transactions on Signal Processing*, 59(12):6160–6174, 2011.

[80] V. Manzella, C. Gaz, A. Vitaletti, E. Masi, L. Santopolo, S. Mancuso, D. Salazar, and J. J. de las Heras. Plants as sensing devices: The pleased experience. In *ACM Conference on Embedded Networked Sensor Systems (SenSys)*, pages 76:1–76:2, 2013.

[81] S. Mohrehkesh and M. C. Weigle. Rih-mac: Receiver-initiated harvesting-aware mac for nanonetworks. In *ACM International Conference on Nanoscale Computing and Communication (Nanocom)*, pages 6:1–6:9, 2014.

[82] S. R. Mousavi and M. Rezaei. Nanotechnology in agriculture and food production. *Journal of Applied Environmental and Biological Sciences*, 1(10):414–419, 2011.

[83] T. Nakano, T. Suda, M. Moore, R. Egashira, A. Enomoto, and K. Arima. Molecular communication for nanomachines using intercellular calcium signaling. In *IEEE Conference on Nanotechnology*, pages 478–481, 2005.

[84] T. Nakano, M.J. Moore, F. Wei, A.V. Vasilakos, and J. Shuai. Molecular communication and networking: Opportunities and challenges. *IEEE Transactions on NanoBioscience*, 11(2):135–148, 2012.

[85] T. Nakano, S. Kobayashi, T. Suda, Y. Okaie, Y. Hiraoka, and T. Haraguchi. Externally controllable molecular communication. *IEEE Journal on Selected Areas in Communications,*, 32(12):2417–2431, 2014.

[86] Y. Ohno, K. Maehashi, and K. Matsumoto. Chemical and biological sensing applications based on graphene field-effect transistors. *Biosensors and Bioelectronics*, 26(4): 1727–1730, 2010.

[87] Y. Okaie, T. Nakano, T. Hara, T. Obuchi, K. Hosoda, Y. Hiraoka, and S. Nishio. Cooperative target tracking by a mobile bionanosensor network. *IEEE Transactions on NanoBioscience*, 13(3):267–277, 2014.

[88] S. J. Orfanidis. *Electromagnetic waves and antennas*. Rutgers University New Brunswick, NJ, 2002.

[89] J.D. Owens, W.J. Dally, R. Ho, D.N. Jayasimha, S.W. Keckler, and L. Peh. Research challenges for on-chip interconnection networks. *IEEE Micro*, 27(5):96–108, 2007.

[90] P.W. Paré and J. H. Tumlinson. Plant volatiles as a defense against insect herbivores. *Plant Physiology*, 121(2):325–332, 1999.

[91] F. Peper, K. Leibnitz, J.-N. Teramae, T. Shimokawa, and N. Wakamiya. Low-complexity nanosensor networking through spike-encoded signaling. *IEEE Internet of Things Journal*, 3(1):49–58, 2016.

[92] J. Perruisseau-Carrier. Graphene for antenna applications: Opportunities and challenges from microwaves to thz. In *Loughborough Antennas and Propagation Conference (LAPC)*, pages 1–4, 2012.

[93] R. Piesiewicz, T. Kleine-Ostmann, N. Krumbholz, D. Mittleman, M. Koch, J. Schoebel, and T. Kürner. Short-range ultra-broadband terahertz communications: Concepts and perspectives. *IEEE Antennas and Propagation Magazine*, 49(6):24–39, 2007.

[94] C. M. J. Pieterse and M. Dicke. Plant interactions with microbes and insects: from molecular mechanisms to ecology. *Trends in Plant Science*, 12(12):564–569, 2007.

[95] S. Rasmann and T. Turlings. Simultaneous feeding by aboveground and belowground herbivores attenuates plant-mediated attraction of their respective natural enemies. *Ecology Letters*, 10(10):926–936, 2007.

[96] M. M. F. Ribas, V. Cereda, M. P.and Bôas, and R. Lyra. Use of cassava wastewater treated anaerobically with alkaline agents as fertilizer for maize (zea mays l.). *Brazilian Archives of Biology and Technology*, 53(1):55–62, 2010.

[97] L. S. Rothman, I. E. Gordon, A. Barbe, D. C. Benner, P. F. Bernath, M. Birk, V. Boudon, L. R. Brown, A. Campargue, J. P. Champion, et al. The hitran 2008 molecular spectroscopic database. *Journal of Quantitative Spectroscopy and Radiative Transfer*, 110(9):533–572, 2009.

[98] S. Roundy, P. K. Wright, and J. Rabaey. A study of low level vibrations as a power source for wireless sensor nodes. *Computer communications*, 26(11):1131–1144, 2003.

[99] M. Scheller, C. Jordens, B. Breitenstein, D. Selmar, and M. Koch. Effective permittivity and scattering model for the evaluation of the leaf water status. In *IEEE International Conference on Infrared, Millimeter and Terahertz Waves (IRMMW-THz)*, pages 1–2, 2008.

[100] T. Schneider, A. Wiatrek, S. Preussler, M. Grigat, and R. Braun. Link budget analysis for terahertz fixed wireless links. *IEEE Transactions on Terahertz Science and Technology*, 2(2):250–256, 2012.

[101] F. Schwierz. Graphene transistors. *Nature nanotechnology*, 5(7):487–496, 2010.

[102] O. Sener, H. Gozubenli, O. Konuskan, and M. Kilinc. The effects of intra-row spacings on the grain yield and some agronomic characteristics of maize. *Asian Journal of Plant Sciences*, 3(4):429–432, 2004.

[103] R. Sheldon. *A first course in probability*. Pearson Education India, 2002.

[104] M. Tamagnone, J. S. Gómez-Díaz, J. R. Mosig, and J. Perruisseau-Carrier. Reconfigurable terahertz plasmonic antenna concept using a graphene stack. *Applied Physics Letters*, 101:214102, 2012.

[105] F. T. Ulaby and R. P. Jedlicka. Microwave dielectric properties of plant materials. *IEEE Transactions on Geoscience and Remote Sensing*, (4):406–415, 1984.

[106] N. Wang, N. Zhang, and M. Wang. Wireless sensors in agriculture and food industry — recent development and future perspective. *Computers and electronics in agriculture*, 50(1):1–14, 2006.

[107] P. Wang, J. M. Jornet, M. G. A. Malik, N. Akkari, and I. F. Akyildiz. Energy and spectrum-aware mac protocol for perpetual wireless nanosensor networks in the terahertz band. *Ad Hoc Networks*, 11(8):2541–2555, 2013.

[108] Z.L. Wang. Towards self–powered nanosystems: From nanogenerators to nanopiezotronics. *Advanced Functional Materials*, 18(22):3553–3567, 2008.

[109] R. Wilk, I. Pupeza, R. Cernat, and M. Koch. Highly accurate thz time-domain spectroscopy of multilayer structures. *IEEE Journal of Selected Topics in Quantum Electronics*, 14(2):392–398, 2008.

[110] G. Witzany. Plant communication from biosemiotic perspective: differences in abiotic and biotic signal perception determine content arrangement of response behavior. context determines meaning of meta-, inter-and intraorganismic plant signaling. *Plant signaling & behavior*, 1(4):169–178, 2006.

[111] S. Xu, B.J. Hansen, and Z.L. Wang. Piezoelectric-nanowire-enabled power source for driving wireless microelectronics. *Nature communications*, 1:93, 2010.

[112] A. Yahalom, Y. Pinhasi, E. Shifman, and S. Petnev. Transmission through single and multiple layers in the 3-10 ghz band and the implications for communications of frequency varying material dielectric constants. *WSEAS Transactions on Communications*, 9(12):759–772, 2010.

[113] O. Yalgashev, M. Bakhouya, J. Gaber, and M. A. Manier. Adaptive transmission range control for electromagnetic-based broadcasting in nanonetworks. *Procedia Computer Science*, 52:1077–1082, 2015.

[114] K. Yang, A. Alomainy, and Y. Hao. In-vivo characterisation and numerical analysis of the thz radio channel for nanoscale body-centric wireless networks. In *Radio Science Meeting (Joint with AP-S Symposium)*, pages 218–219, 2013.

[115] K. Yang, A. Pellegrini, A. Brizzi, A. Alomainy, and Y. Hao. Numerical analysis of the communication channel path loss at the thz band inside the fat tissue. In *IEEE MTT-S International Microwave Workshop Series on RF and Wireless Technologies for Biomedical and Healthcare Applications (IMWS-BIO)*, pages 1–3, 2013.

[116] K. Yang, Q. H. Abbasi, K. Qaraqe, A. Alomainy, and Y. Hao. Body-centric nanonetworks: Em channel characterisation in water at the terahertz band. In *Asia-Pacific Microwave Conference (APMC)*, pages 531–533, 2014.

[117] K. Yang, A. Pellegrini, M.O. Munoz, A. Brizzi, A. Alomainy, and Y Hao. Numerical analysis and characterization of thz propagation channel for body-centric nano-communications. *IEEE Transactions on Terahertz Science and Technology*, 5(3): 419–426, 2015.

[118] N. Yazdani. Multi-frequency time-division multiple-access (mf-tdma) resource packing. In *IEEE Military Communications Conference (MILCOM)*, pages 1–8, 2008.

[119] Y. YHao, S. Wang, Y. Zhang, and Z. L. Wang. Pyroelectric nanogenerators for driving wireless sensors. *Nano letters*, 12(12):6408–6413, 2012.

[120] E. Zarepour, M. Hassan, C.T. Chou, and A.A. Adesina. Frequency hopping strategies for improving terahertz sensor network performance over composition varying channels. In *IEEE International Symposium on a World of Wireless, Mobile and Multimedia Networks (WoWMoM)*, pages 1–9, 2014.

[121] E. Zarepour, M. Hassan, C. T. Chou, and A. A. Adesina. Remote detection of chemical reactions using nanoscale terahertz communication powered by pyroelectric energy harvesting. In *ACM International Conference on Nanoscale Computing and Communication (Nanocom)*, pages 1–8, 2015.

[122] A. I. Zygielbaum, A. A. Gitelson, T. J. Arkebauer, and D. C. Rundquist. Non-destructive detection of water stress and estimation of relative water content in maize. *Geophysical Research Letters*, 36(12):L12403, 2009.

List of Acronyms

cdf cumulative distribution function.
CNTs Carbon Nanotubes.

EM Electromagnetic.
EMT Effective Medium Theory.

GA Genetic Algorithm.
GNRs Grephene Nanoribbon.

HITRAN High Resolution Transmission.

IoBNT Internet of Bio-NanoThings.
IoMNT Internet of Multimedia-NanoThings.
IoNT Internet of NanoThings.
IoT Internet of Things.

LLC Logical Link Control.
LLL Landau, Lifshitz, Looyenga.
LoS Line of Sight.

MAC Media Access Control.

NLoS Non-Line of Sight.
NoC Network on Chip.

pdf probability distribution function.
psd power spectral density.

SNR Signal to Noise Ratio.
SPP Surface Plasmon Polaritons.

Tbps Terabit per second.
THz-TDS THz Time-Domain Spectroscopy.

TS-OOK Time Spread On-Off Keying.

UWB Ultra Wide Band.

VOCs Volatile Organic Compounds.

WNoC Wireless Network on Chip.

WNSNs Wireless Nanosensor Networks.

Appendix A

Among the existing approaches, we deploy a GA as on optimization solution in this thesis. In the following, we describe more details about this technique and its implementation in our work. Such a description includes the main principals of the algorithm and also its most fundamental operators and functions.

A.1 Genetic Algorithm

GA refers to a class of adaptive and heuristic search techniques, which resemble the natural biological evolution. The main idea of this approach is to find the most optimized solutions of a certain problem, based on the principle of survival of the fittest generation [24].
Next, we review the principle and components of such a technique.

A.1.1 Principle

The main principle of a GA, is to map the solution space of a given problem into natural individual entities, i.e., chromosomes. Therefore, the population of potential solutions can be mapped into a population of chromosomes. In this mapping, each solution, which can be composed of a single or multiple decision variables, will be presented as genes in the structure of individual chromosomes.
Then, in a population of chromosomes, the fitness of individuals can be evaluated based on the definition of single or multiple objectives in the problem domain. The most fitted individuals of a population will be selected as the parents to reproduce the next generation, through biological mechanisms, i.e., crossovers and mutations. In such a way, highly fitted individuals relative to the whole population have a high probability of being selected for mating; whereas those which are less fit will have a lower chance to be selected.
After the mating process of parents, performance of the resulting offspring to satisfy the objectives will be evaluated. Then, a subset of the most efficient individuals will be reinserted

to the primary population. The reinsertion of the offspring to their parents population is based on the replacement of less efficient parents with their more efficient offspring. Therefore, the new generation is supposed to be better suited to the environment, in the context of solving the problem, compared to their primary parents generation.
The selection of the most fitted individuals and reproduction of the new generations, as well as the evaluation and reinsertion of the resulting offspring will continue iteratively up to the stage that certain criteria are satisfied, e.g. for a certain number of generations, or when a particular point in the search space is encountered.
There are certain terminologies and operators employed in the GA, such as individuals, population, objective and fitness functions, crossover and mutation and also reinsertion, which are discussed next.

A.1.2 Individuals and Population

The combination of decision variables of a problem form an individual, or a chromosome, which is the main entity for the GA operations. In such a structure, each decision variable acts as a gene or the most basic component of a chromosome. One of the most common formats to present an individual is the integer presentation, where the genes of a chromosome are represented by integer values. A number of individuals, or the potential solutions of a problem, form a GA population. The individuals of a population can be initialized by using a uniformly distributed random number generator. For such a purpose a maximum number of individuals can be generated, with their genes being random values selected in a predefined range. An individual can be presented based on the following format:

$$Chr = \begin{bmatrix} g_1 & \dots g_i \end{bmatrix} \quad for \quad i = 1, 2, \cdots N_{var} \tag{A.1}$$

where g_i is an integer value representing the ith decision variable/gene of a potential solution/chromosome and N_{var} is the chromosome length or the number of genes in an individual. In a similar approach a population can be defined as:

$$Pop = \begin{pmatrix} Chr_1 \\ \vdots \\ Chr_j \end{pmatrix} \quad for \quad j = 1, 2, \cdots N_{ind} \tag{A.2}$$

where Chr_j is the chromosome structure defined in equation (A.1) and N_{ind} is the maximum number of individuals of the population.

A.1.3 Objective Function

The objective function in a GA determines the performance of individuals of a population in the problem domain. Such a function can be implemented in a single-objective or multi-objective fashion. The purpose of an objective function with a single objective is minimizing/maximizing a single value, e. g, minimizing the power consumption of wireless nodes across a network. Whereas, the purpose of a multi-objective function is to optimize several parameters, which can be considered as maximization of a set of values and minimization of the rest. It should be noted, that a multi-objective function can represent conflicting goals. For example, defining an objective as maximizing the duty cycles of wireless nodes in a network can disturb the energy consumption minimization as another objective. One of the most common implementations of a GA with several objectives is the weighted-sum multi-objective GA [71], in which the final objective function is constructed based on a weighted sum of the several objective functions. Therefore, the final objective function can be presented as:

$$Obj_f = W_1.Obj_1 + \cdots + W_t.Obj_t \quad for \quad t = 1, 2, \cdots N_{obj} \tag{A.3}$$

where Obj_t is a single normalized objective function with its relevant weight as W_t, and N_{obj} represents the total objectives that need to be satisfied.

A.1.4 Fitness Function

The relative performance of an individual within a population can be evaluated according a fitness function. In fact, the fitness function transforms the value of the objective function into a non-negative scalar value in an arbitrary range, e.g., [0, F_{val}], which represents the relative fitness of individuals. In an optimization problem, the most fitted individuals are assigned values closer to F_{val}; whereas, the least fitted solutions are assigned values closer to 0. The resulting fitness values are the basis for selecting an individual for the reproduction process of the next generations.

A.1.5 Operators

In the following, the main GA operators which contribute to the creation of generations are discussed:

1. Selection: This is the operation in which a certain number of individuals are selected based on their relative fitness, for mating purposes, or for reinsertion into the current population and formation of the next generations. Among different selection

approaches, stochastic universal sampling is a common technique, where the samples are chosen by deploying a set of selection pointers. In this approach, the sum of the raw fitness values of all the individuals is defined by a real-value as *Sum*, and individuals are mapped one-to-one into continuous intervals in the range of [0, *Sum*]. Then, S_{ind} pointers which are equally spaced will be used to select the samples, where S_{ind} denotes the number of the required individuals. In this regard, the population is shuffled and a number in the range of [0 Sum/S_{ind}] is randomly chosen, which represents the location of the first selection pointer. Finally, the required samples are chosen by generating S_{ind} equally spaced pointers, and selecting the individuals whose fitness span the positions of the pointers. The number of individuals to be selected from an initial population is determined according to the population size, N_{ind}, and also the generation gap, G_{gap}, as: $S_{ind} = G_{gap}.N_{ind}$. In fact, the generation gap specifies the fraction of the population that need to be regenerated.

2. Crossover (Recombination): Crossover or recombination refers to the process in which the selected individuals are combined to produce a subset of offspring. Through such a process, which resembles the natural mating of chromosomes, the resulting individuals inherit some of their parents biological characteristics. In the most basic type of crossover, a random point along chromosomes is selected, then, all genes located after the selected point will be swapped between chromosomes. An extension to this algorithm is known as the uniform crossover, where a crossover mask is applied to the parent chromosomes to determine their contribution in the mating process. In fact, the crossover mask is a matrix with the same length as the parents, where each entry is a random parity value that acts as a mask to define the donating parent and genes to reproduce an offspring.

3. Mutation: The mutation operand alters the elements of the chromosome structure with a very low probability, P_{mut}. This process guarantees that a diverse range of variables from the search space are selected; hence, it avoids the convergence of individuals to a local optimum. There exists a variety of mutation operands based on the encoding type of individuals. Among all, uniform mutation is one of the most common mutation operators which replaces the selected gene with a random value taken from a predefined range. This type of mutation is applicable to integer value individuals.

4. Reinsertion: Following the crossover and mutation operations, the generated offspring should be reinserted into the initial parent population. One of the widely used reinsertion categories are generational algorithms, where all or a ratio of the generated individuals will be inserted into the old population to form the next generation. The

replacement process can be accomplished based on the fitness of the offspring and a replacement/deletion strategy. One of the most well-known replacement strategies is replacement with the worst individuals, in which the least fit parents will be replaced with their most fit offspring. To guarantee the propagation of the most efficient individuals to the next generations, an elitism mechanism can be employed. Such a technique retains a ratio of the best solutions from any generation, E_{rate}, to be carried across the new population, in order to allow them to sustain. The elitism mechanism can significantly improve the convergence time and computational cost of GA.

A.1.6 Termination

As GA-based techniques are stochastic, they do not provide a single solution, but rather a class of best fitted alternatives. For the definition of such solutions, the algorithm needs to terminate upon satisfying certain conditions. Termination of the algorithm based on the generation number is one of the most common techniques in GA, where the algorithm runs for a certain number of generations defined by the user. Another alternative to terminate a GA is the convergence of the population based on a predefined threshold.